Zwitterion-Containing Ionogel Electrolytes

A thesis submitted by

Fatin Marzooq

in partial fulfilment of the requirements for the degree of

Master of Science

in

Chemical Engineering

Tufts University

August 2016

Advisor: Professor Matthew J. Panzer

Abstract

Ionic liquids (ILs) are promising next-generation electrolytes featuring negligible vapour pressures, high thermal and electrochemical stability, and high ionic conductivities. Supporting ILs with a polymer matrix to form solid-state ionogels can yield safer electrolytes that prevent IL leakage. It is presently accepted that some fraction of the ions comprising an IL are not fully dissociated, and thus unable to migrate freely in an electric field. In this work, zwitterions were used to promote ion pair dissociation in a well-studied hydrophobic IL with the goal of obtaining a novel class of ionogels. Zwitterion-containing ionogels were successfully synthesised using two different zwitterionic molecules, one of which was polymerisable. Compression testing led to observations of increased elastic moduli with increasing zwitterionic content, indicating the presence of ordered zwitterionic domains. The non-polymerisable zwitterion-containing ionogels exhibited tunable mechanical properties and moderate ionic conductivities; the polymerised zwitterion-containing ionogels displayed even more promising results. Remarkably, increasing zwitterion concentration for fixed total polymer content resulted in nearly equivalent ionic conductivity in spite of increased elastic modulus. Evidence for enhanced ion dissociation due to strong charge-dipole interactions between the IL ions and zwitterionic molecules was observed. Cyclic voltammetry testing showed that the electrochemical stability of the zwitterion-containing ionogels was

essentially unchanged from that of the neat IL. Additionally, zwitterion-containing ionogels exhibited high thermal stability, up to $310\,^{o}C$.

Table of Contents

List of Figures

List of Tables

Zwitterion-Containing Ionogel Electrolytes

Chapter 1: Introduction

1.1 Motivations

The concept of energy storage has been one of the biggest drivers and challenges of technological progress. Our ability to advance current technologies is limited by our inability to generate and store vast quantities of energy. With human development reaching for new heights in space exploration, industrial output, and data storage, global energy demands are ever increasing.[1, 2] Furthermore, the shift in world culture toward energy production and the sustainability of the environment has necessitated the transition from fossil fuels to more renewable forms of energy.[3]

Alternative forms of energy, while greatly reducing carbon emissions, require the development of more advanced forms of energy storage, due to the sporadic nature of the renewable energy collection systems.[4] Electrical energy storage, in particular, has emerged as an especially important field of study due to the necessity of storing energy from renewable sources and converting it to electrical energy when needed. This prevents instability within the grid and ensures a constant supply of electricity despite inconsistencies in the supply of renewable energy.[4] Thus far, advanced electrical energy storage systems have allowed for the development of hybrid vehicles, high-performance portable smartphones and constantly

shrinking devices, such as the Apple Watch and Google Glass, as well as numerous aerospace applications.[5]

Increases in world population also place a larger burden on energy requirements in order to maintain current lifestyles.[2, 3, 6] As solar and wind energy resources become more popular alternatives to fossil fuels, developing efficient and sustainable energy storage technologies becomes imperative. Electrochemical energy storage techniques have been marked by the field as having the potential for great impact in the device industry, resulting in the manufacture of smaller, portable, and even flexible products. Creating lithium metal batteries that can avoid dendrite growth, or supercapacitors with optimised energy and power densities whilst maintaining good mechanical properties will allow for further advancements on the technology platform. With new research in electrochemical energy storage evolving every day, progress in space exploration and global connectivity become sure possibilities.

While electrochemical energy storage is a very broad field, there has been substantial research concerning the use of ionic liquids (ILs) –room temperature molten salts- as electrolytes in supercapacitors.[6-8] There has also been some research conducted showing the use of zwitterions as additives to primarily ionic liquid-lithium salt mixtures for lithium ion battery applications.[9-12] Few publications have delved into the use of zwitterions in a pure ionic liquid (or gel) system, however. Furthermore, the

nature of the interactions between the ionic liquids and the zwitterionic additives have not been fully characterised to date. Thus, there is a need for a comprehensive evaluation of the incorporation of zwitterions in ionic liquids for energy storage applications.

1.2 The State of the Art in the Field of Ionogel Electrolytes

1.2.1 How Ionogels Are Made

Ionic liquids have gained traction in the field of electrochemical energy storage, primarily due to their negligible vapour pressure and their wide electrochemical window.[8, 13-16] Recently, the field has looked to address the challenge of creating a solid device containing ionic liquids while maintaining the promising properties of these materials. Immobilising the ionic liquid in a solid-state structure is an important problem to solve as it has great potential to advance the field of flexible and safe electronics.

Ionogels fall under two different classes of gel: physical, or chemical. A physical gel is held together through a three-dimensional network of weak interactions which include Van der Waals forces, London forces, hydrogen bonding, and dipole-dipole interactions, to name a few.[16] Conversely, chemical gels are supported by a covalently bonded scaffold or matrix.

Often, physical gels are formed through the addition of low molecular weight gelators, inorganic nanoparticles, carbon nanotubes, or physically entangled polymers. Low molecular weight gelators are organic compounds

that can form aggregates in a solvent through molecular stacking, or other reversible interactions. The network formed by molecular aggregation eventually leads to the gelation of the ionic liquid.[17] Low molecular weight gelators are usually added to a liquid in small quantities. Upon dissolution of the organic molecules in the liquid at high temperatures, the solution is cooled which induces gelation. Organic gelators have been shown to successfully gel ionic liquids while allowing for a high thermal stability and a wide electrochemical window.[16-18] Where gels formed using low molecular weight gelators fall short, however, is in their mechanical properties. Gels formed in this manner tend to be more akin to viscous liquids, pastes, or slurries than palpable solids.

Nanoparticles may also be used as fillers in ionic liquids to immobilise the liquid and prevent the leakage of devices. Inorganic nanoparticles may be incorporated into a gel in two ways. The first method is the simple addition of particles such as silica or alumina directly into the liquid to form a suspension which prevents liquid flow. The second method by which nanoparticles may be added is via the *sol-gel* reaction to form silica nanoparticle derivatives *in-situ*.[19] One advantage of using a nanoparticle gel matrix is that only a small percentage of the gel structure by mass is non-conductive. This allows for the retention of high ionic conductivities while also ensuring that the resulting gel is mechanically compliant.[19, 20] Additionally ionogels confined by a nanoparticle matrix have very high

thermal stabilities as the nanoparticles are often more thermally stable than the ionic liquid.

In addition to nanoparticles and small organic molecules, polymers are a viable option for gelation when added to an ionic liquid. Incorporating a polymer into an ionic liquid to form an ionogel causes the gel composite to exhibit properties from both the polymeric compound and the ionic liquid. So, the overall properties of the composite material may be tuned by using an apt ionic liquid for the desired application, as well as a suitable polymer.

One method by which ionic liquid gels may be formed is IL uptake in a polymer scaffold or membrane.[16, 21-23] To achieve this, polymer films are primarily solution cast, whereupon, they are immersed in ionic liquids for a specified period of time.[21, 22] Ionic liquids have been shown to modify the properties of polymers as they can act as plasticisers, lowering the glass transition temperature, T_g, or may affect the morphology of the film or membrane.[23, 24]

Polymer-based ionogels may also be fabricated by mixing a prepared polymer with an ionic liquid and a cosolvent which is then evaporated slowly.[16, 23, 25-27] Alternatively, monomers with a single polymerisable group may be polymerised *in-situ*, using the ionic liquid as the solvent.[16, 23] The resulting gels are held together through the physical entanglement of the polymer chains, as opposed to chemical cross-links. In addition to physical entanglement, polymers like poly(ethylene oxide) (PEO) are crystalline and

can form a matrix through stacking of the ether groups which leads to increased mechanical stability, albeit decreased ionic conductivity due to slower ion transport.[28]

Chemically cross-linked gels may be attained through the addition of a chemical cross-linker such as pentaerythritol tetraacrylate (PETA-4), **Figure 1.5c** in Section 1.4. The four functional groups in PETA-4 allow multiple chains to be covalently linked together in the overall scaffold. In the case of polymer-supported ionogel electrolytes, the polymer architecture may affect the mechanical properties of the gel composite, causing it to be elastic and flexible, or glassy and brittle, depending on the polymer used. In addition, the cross-link density may greatly influence the stiffness and elasticity of the resulting material.

In many cases, chemically cross-linked polymers are formulated *in-situ*. The monomers (predominantly acrylate, methacrylate, or vinyl-functionalised) are added to the ionic liquid directly and then polymerised using thermal or photoinitiators in a free-radical polymerisation reaction.[29-31] Aside from free-radical polymerisation, ionic liquids have been successfully employed as solvents in reversible addition fragmentation transfer (RAFT) polymerisation, atom transfer radical polymerisation (ATRP), and reverse ATRP of styrene and acrylate monomers.[29, 32-34]

Due to their tunability, ionic liquids may be designed to solvate many different materials including (incredibly) cellulose.[7, 15] One of the major

challenges associated with creating cross-linked polymer gels, however, is the solubility or miscibility of monomers and their polymers in ionic liquids. Due to the myriad of ionic liquids available, solubility trends in ionic liquid solvents cannot be painted with a single brush.

Generally, composite gel electrolytes containing ionic liquids and polymers can be thought of as salt-in-polymer, or polymer-in-salt materials.[35] It is not yet understood whether polymer-IL composites can be considered to be homogeneous materials, or should be viewed as a polymer scaffold with distinct ionic liquid domains. In any case, high conductivity materials can be produced by combining ionic liquids and polymers. Watanabe has previously ascribed this result to the plasticisation of the polymer by the ionic liquid.[35, 36] So, not only does the ionic liquid introduce charge carriers into the system, but through plasticization, it can increase the mobility of said ions within the gel.

There is also evidence that *in-situ* polymerisation in ionic liquids can lead to a change in polymer properties such as the composition, and the density, thus changing the polymer architecture.[36, 37] This may, in turn, affect the molecular interactions between the ionic liquid and the scaffold, and mobility of ions within the scaffold. Changing the nature of the interactions between the ionic liquid and the polymer could potentially lead to improved mechanical and electrochemical properties of the gel composite material.

1.2.2 Zwitterions in Ionic Liquids and Ionogels

Zwitterions are molecules that bear the same number of anionic and cationic groups, and are, therefore, net neutral despite containing multiple charged moieties. The Ohno and MacFarlane groups have pioneered the field of zwitterions for electrochemical purposes. They have postulated that zwitterions and their derivatives could be used as additives in lithium salt mixtures in order to promote ion-dissociation through their interactions with ionic liquids, thereby increasing the ionic conductivity. Typically, zwitterions used in electrochemical research are carboxy- or sulfobetaines.[5, 9, 10, 25, 38, 39]

Zwitterionic molten salts have been explored as a solvent for lithium ion batteries.[9, 10, 12, 38] Due to the tethering of the anion to the cation, zwitterions are unable to migrate in an electric field. So, the conductivity of liquid zwitterions is very low. It has been shown, however, that these liquid zwitterions can act as a conductive matrix for lithium ions to flow through, resulting in a boost in conductivity.[38]

Byrne *et al.* have confirmed in their work that incorporating sulfonate-based zwitterionic additives into dissolved lithium bis(trifluoromethylsulfonyl)imide (Li TFSI) salt solutions leads to improved ionic conductivities due to an increase in lithium mobility, as shown by pulsed-field gradient spin-echo (PGSE) Nuclear Magnetic Resonance (NMR) diffusion experiments.[9, 10, 12]

Most explorations of the use of zwitterions in conductive electrolytes concerned the development of lithium ion or lithium metal batteries.[5, 9-12, 38-41] Additionally, in these various studies, zwitterions were used as solid additives dissolved in a liquid solution, not in a gel electrolyte. Moreover, these zwitterions are not incorporated into the gel scaffold.

It has been suggested that zwitterions offer a favourable path for lithium ions to travel through within the solvent.[9] Alternatively, data have shown that zwitterions may be affecting the ion concentration at the solid-electrolyte interphase (SEI) in lithium ion batteries. This causes lithium ions to be readily available to undergo redox at the electrode interface.[10, 12] There have been very few studies focusing on the nature of the interactions between the ionic liquid itself and the zwitterions.

Furthermore, there have also been few studies where zwitterions have been employed in gelled electrolytes and in the polymer scaffold of gel electrolytes. The Ohno group has previously reported on the polymerisation of polyimide in a zwitterion/imidazolium-based ionic liquid mixture to form a gel.[40] These gels, however, exhibited very low ionic conductivities. Recently, the group has also successfully fabricated gels through the use of a highly branched phosphonium type zwitterion additive in an amino acid ionic liquid.[25] In this case, the branches on the zwitterion led to the formation of ionophobic domains governed by the long alkyl chains, and hydrophilic domains populated by the zwitterionic portions of the molecules. This

suggests that zwitterions may be used to create materials containing varying micro- or nanodomains. In the above-mentioned study, however, the incorporation of phosphonium type zwitterions led to a threefold decrease in ionic conductivity.

So, there is a need for a comprehensive study focusing on the nature of the molecular interactions occurring between ionic liquids and zwitterions. To date, zwitterions have not been successfully employed to make mechanically robust ionogels with high ionic conductivities.

1.2.3 Electrochemical Applications for Ionogels

Ionogel applications range from drug delivery to separation membranes to a myriad of electrochemical uses.[16] In terms of electrochemical applications, ionogels may be used in fuel cells, dye-sensitised solar cells, lithium ion batteries, and electric double layer capacitors (EDLCs), to name a few.[8, 16]

Fuel cells can be categorised based on the type of electrolyte they use and the temperature at which they are operated. Proton exchange membrane fuel cells (PEMFC) use ionogels in the membrane electrode assembly (MEA). The MEA consists of a proton exchange membrane sandwiched between two electrodes. Protic ionic liquids have been used as electrolytes in PEMFCs within the PEM as they may be operated at temperatures above $100^{\circ}C$ and exhibit high ionic conductivities under anhydrous conditions.[8, 42]

Immobilized ionic liquids are highly sought after for fuel cell applications as polymer-based ionogels may be formed into thin films, resulting in more mechanically stable membranes with high conductivities.

Dye-sensitised solar cells employ ionic liquid gels in order to improve their long-term stability. This is achieved due to the negligible vapour pressures of ILs. Ionogels are used in order to eliminate the possibilities of electrolyte leakage.[8] Both solar and fuel cells require ongoing investigation as to how ionic liquids may be incorporated into the technology to ensure long-term stability.

Lithium ion batteries have been explored as a means of eliminating dendrite formation on electrode surfaces. Lithium ion batteries, however, exhibit low ionic conductivities and lithium transference numbers, in part due to the high viscosity associated with lithium salt systems. Ionic liquid electrolytes have been used as plasticisers, lowering the viscosity of the electrolyte solutions, and to encourage stable cycling of the batteries.[8, 43] Hybrid ionogel electrolytes have also been formed using a condensation polymerisation reaction involving alkoxysilanes. The resulting SiO_2 based ionogel retained the promising electrical properties of the ionic liquid used, and also displayed good mechanical stability.[44]

In addition to the many other electrochemical uses outlined above, ionogels have been widely used in electric double-layer capacitors (EDLCs). EDLCs, otherwise known as supercapacitors, or ultracapacitors consist of

ionic liquid electrolytes in place of the insulating dielectric more commonly found in conventional capacitors. Confining the ionic liquid in an EDLC eliminates the need for a protective casing and prevents the possibility of electrolyte leakage, resulting in safer devices. Additionally, ionic liquids are highly electrochemically stable, leading to a high energy density.[8, 14] The high specific energy of supercapacitors also allows them to compete with batteries due to the large ion concentration characteristic of ionic liquids.[8, 45]

1.3 Solid-State Ionic Liquid/Ionogel Supercapacitors Bridging the Gap in Energy Storage

Electric double-layer capacitors (EDLCs) have generated much interest as their energy and power densities are able to bridge the gap between conventional capacitors and electrochemical cells or batteries. This can be seen in the Ragone plot shown in **Figure 1.1**.

An electrochemical cell relies on the progression of a chemical reaction undergoing redox at the anode and cathode, allowing for large quantities of energy to be stored and discharged over a long period of time. Although the electrochemical reactions occurring should be reversible, typically, batteries may only be charged and discharged for hundreds to a few thousand cycles before experiencing a significant capacity loss and an increase in internal resistance due to the volume changes associated with redox.[46, 47]

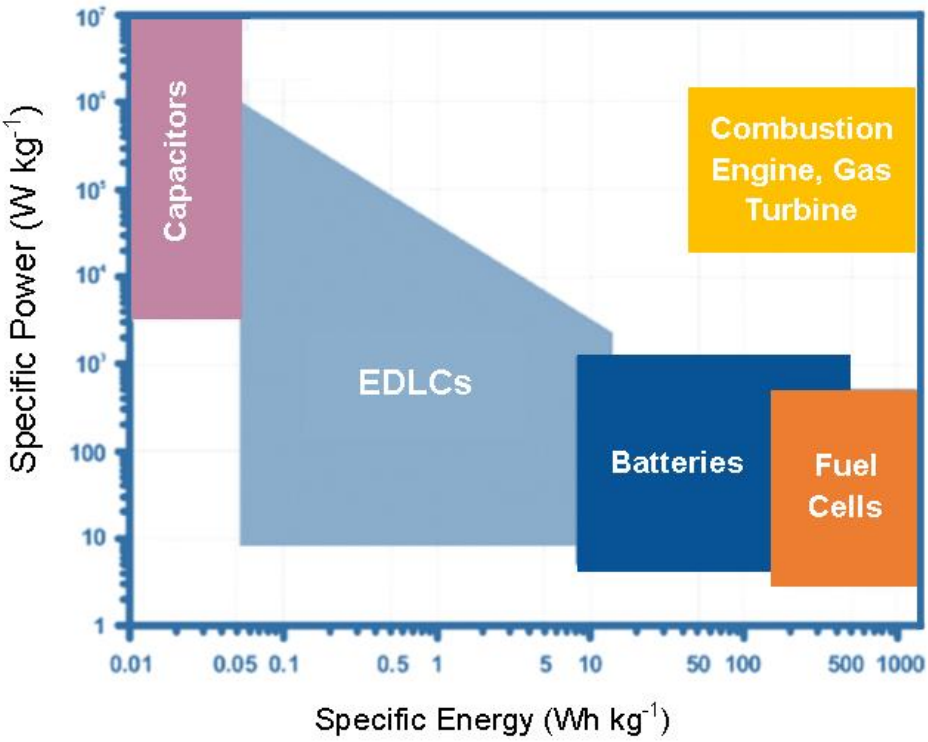

Figure 1.1: Ragone plot showing power and energy densities for various modes of energy storage. Electric double layer capacitors (EDLCs) fall between conventional capacitors and batteries in terms of their storage capabilities. Adapted from Winter and Brodd.[48]

Converse to electrochemical cells, conventional capacitors may be operated for a nearly infinite number of cycles, provided they are being used within their initial design parameters.[47] A conventional capacitor consists of two electrodes, separated by an insulating dielectric material, connected to an electric load, **Figure 1.2a**. Upon charging, a voltage is applied to the capacitor causing electrons to be deposited onto one electrode. Due to the insulating dielectric material separating the two electrodes, electrons are unable to flow from one electrode to the other, resulting in the accumulation of charges. Once the capacitor is charged, the electrodes remain polarised,

storing charge as electrostatic potential energy. The energy stored in a capacitor may be described as follows:

$$E = \frac{1}{2} CV^2 \qquad (1.1)$$

where V is the potential difference across the electrodes, and C is the capacitance with units of Farads, (F). Capacitance is a measure of the amount of electric charge that is able to be stored within a body, given a voltage, Equation (1.2), where Q is the charge, measured in Coulombs.[49]

$$C = \frac{Q}{V} \qquad (1.2)$$

Since the capacitance is a function of the amount of charge that may be stored on the electrode, it is dependent upon the surface area of the electrode. Additionally, as the distance between electrodes or plates decreases, the electrostatic forces increase, provided the dielectric material remains stable. This results in the following expression for capacitance:

$$C = \frac{\varepsilon \mathrm{A}}{d} \qquad (1.3)$$

where ε is the dielectric constant, an inherent property of a given material, A is the surface area of the electrodes, and d is the distance between the two electrodes.

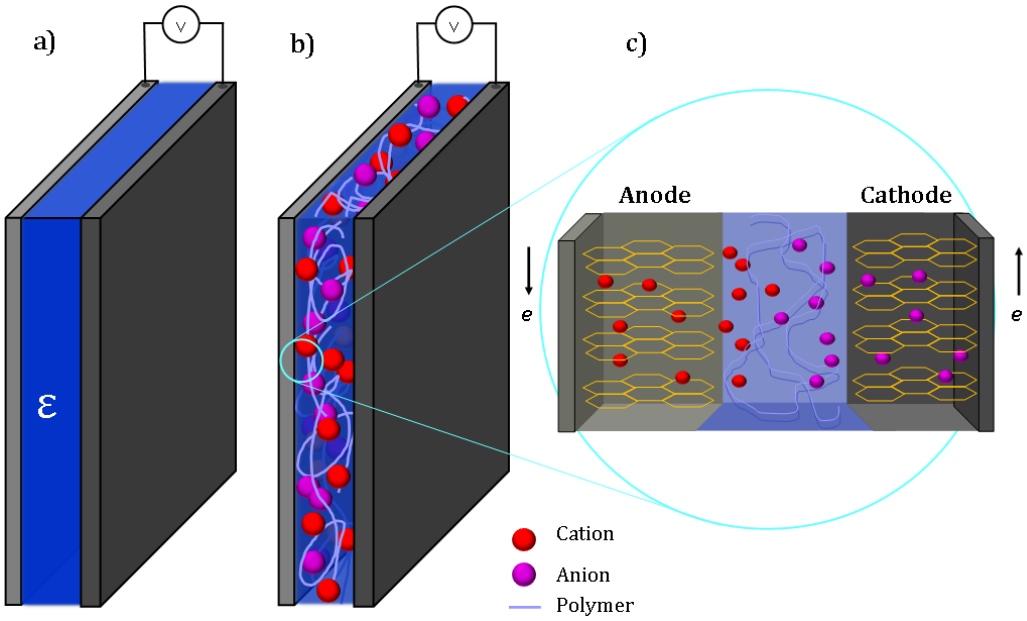

Figure 1.2: Schematics of conventional and electric double layer capacitors. (a) conventional parallel-plate capacitor, (b) electric double layer capacitor with high surface area graphite electrodes separated by an ionic liquid gel electrolyte, and (c) formation of the double layers within the electrodes of the supercapacitor.

Similar to conventional capacitors, electric double layer capacitors, or supercapacitors as they are more widely known, consist of electrodes separated by an ion-conducting electrolyte as opposed to an insulating dielectric, **Figure 1.2b**. Upon charging the plates, the electrolyte is polarised by the field created by the difference in potential between the electrode and the solvent, resulting in the formation of double layers, wherein ions distribute in the electrolyte towards the electrode of opposing charge, **Figure 1.2c**.[50, 51] So, for an electric double layer capacitor the capacitance is dependent upon the distance between the electrode and the layers of charges in the double layer, which is on the order of nanometres or sub-nanometres.

The surface area of concern is the specific surface area of the porous electrode accessible to the ions in the electrolyte.[47, 50, 51]

Typically, supercapacitors consist of a liquid electrolyte between the electrodes, necessitating the use of a rigid metal encasement to prevent leakage. This increases the weight and cost of the device whilst also limiting the device's use in flexible electronic applications. Some researched electrolytes include: aqueous solvents, organic electrolytes, and ionic liquids. Aqueous solvents used are typically acids, bases, or salt solutions. Organic electrolytes are predominantly organic salts dissolved in propylene carbonate due to its low flash point and lower toxicity relative to previously used anhydrous acetonitrile.[52] The ionic liquids that are generally used are either protic, aprotic, or zwitterionic.[47, 52]

Ionic liquids are organic molten salts at or below $100^{\circ}C$.[8, 14, 16] Ionic liquids are able to exist in their molten state at low temperatures due to the weak interactions between the typically large cation and charge-delocalised anion. Ionic liquids have previously been identified as promising safe alternatives to volatile organic electrolytes for electrochemical applications due to their negligible vapour pressure, high ionic conductivity, and high electrochemical and thermal stability.[8, 14, 15] Additionally, ionic liquids may be tuned to specific applications by changing the anion or cation. As such, they have often been hailed as "designer electrolytes".[7, 52, 53] The right combination of anion and cation could improve the electrochemical window

of the electrolytes, relative to their aqueous and organic counterparts. Aqueous and organic electrolytes have voltage windows of approximately 0.9 V and 2.5 V, respectively, whereas, many ionic liquids are stable up to 4.5 V, and some are stable up to even larger windows of 5 or 6 V.[52] Since the energy that may be stored in a capacitor is proportional to the square of the maximum voltage the device may be operated at, Equation(1.1), doubling the voltage stability window causes a factor of four increase in the energy storage capabilities when going from an organic electrolyte to an ionic liquid.

Confining the ionic liquid in a polymeric scaffold to create a solid-state electrolyte, however, has been shown to cause a change in the observed electrolyte properties. Namely, a reduction in ionic conductivity due to the physical barriers created by the polymer, as well as the substitution of non-conducting species for ionic liquid for the same device volume. This modification of favourable properties has driven research to create devices with higher ionic conductivities whilst maintaining good mechanical properties. One approach to doing this has been to introduce functional groups or additives that can promote ion dissociation or increase ion mobility.[9-12, 54] The ionic conductivity of an electrolyte is a function of the diffusion coefficients of mobile ions and the fraction of ions contributing to the ionic conductivity. So, increasing the mobility of the ions, or the fraction of ions dissociated in the electrolyte, may result in an increase in the ionic conductivity.

Zwitterions have been previously reported to be "ion-dissociating agents" –species that encourage the dissociation of lithium salts in ionic liquid solutions, thereby increasing the fraction of free ions present in the solution.[5, 10, 12, 41, 55] Additionally, it has been shown that certain polymer functional groups, such as the trifluoroethyl group, promote ionic liquid ion dissociation within ionogels due to interactions between the ionic liquid and the polymer backbone.[54] This work aims to address the challenge of producing solid-state ionogel electrolytes with high ionic liquid ion dissociation as well as good mechanical properties for use in electrochemical supercapacitors.

1.4 Thesis Work

In the present work, zwitterionic copolymers were explored as a potential strategy toward improving the electrochemical properties of ionogels. The primary ionic liquid used, 1-ethyl-3-methylimidazolium bis(trifluoromethylsulfonyl)imide (EMI TFSI), as shown in **Figure 1.3**, was chosen due to its favourable electrochemical properties: negligible vapour pressure and non-flammability; relatively low viscosity; high electrochemical stability; and moderate room temperature ionic conductivity –approximately 10 mS cm^{-1}.[8, 13, 56]

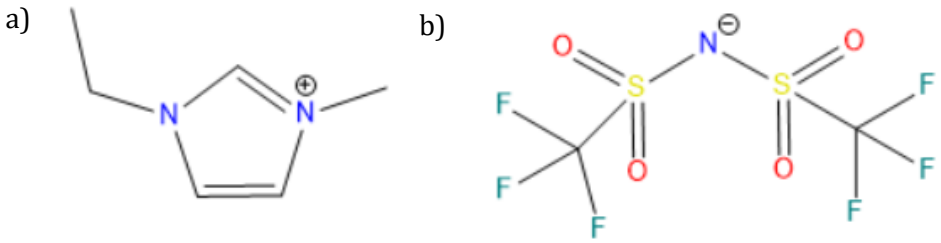

Figure 1.3: Chemical structures of a) 1-ethyl-3-methylimidazolium (EMI) cation and b) bis(trifluoromethylsulfonyl)imide anion.

Other hydrophobic ionic liquids containing the EMI cation are also currently being explored within our group in order to verify the zwitterion-effect across different systems, **Figure 1.4**. EMI FAP is the most hydrophobic of the three ILs investigated, while EMI TCB is the least hydrophobic.

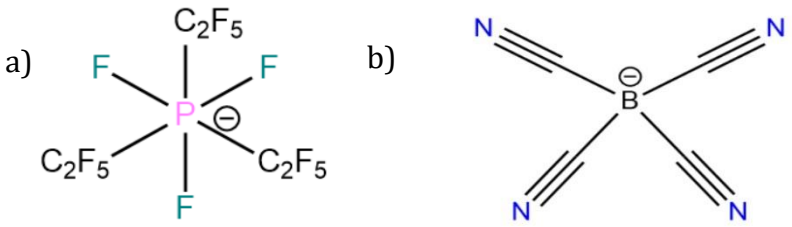

Figure 1.4: Chemical structures of ionic liquid anions: a) tris(perfluoroalkyl)trifluorophosphate (FAP), b) tetracyanoborate (TCB).

The copolymer that was synthesised consisted of a hydrophobic fluorinated monomer, a hydrophilic zwitterionic monomer, and a tetra-functional chemical cross-linking agent. The fluorinated monomer, 2,2,2-trifluoroethyl methacrylate (TFEMA) (**Figure 1.5b**) was chosen as a compatibilising agent in order to allow for the dissolution of the hydrophilic zwitterion in the hydrophobic ionic liquid.

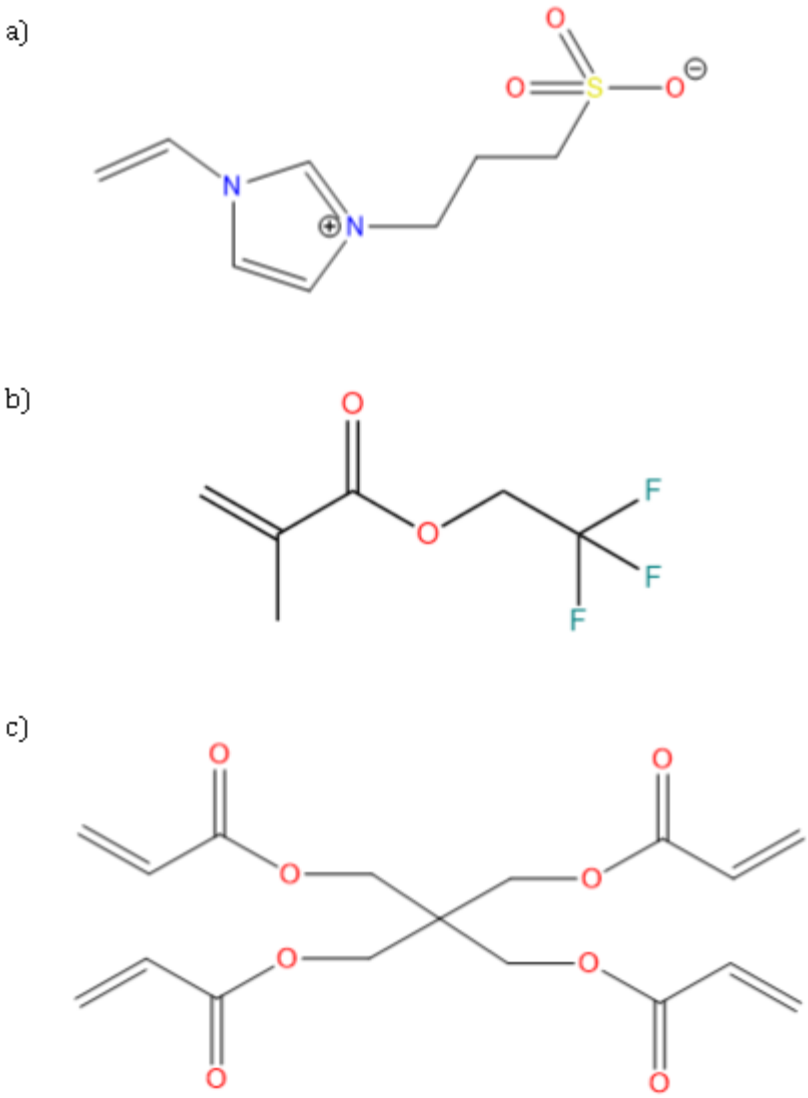

Figure 1.5: Structures of monomers used in zwitterion-containing ionogels. (a) sulfobetaine vinylimidazole (SBVI), (b) 2,2,2-trifluoroethyl methacrylate (TFEMA), and (c) pentaerythritol tetraacrylate (PETA-4).

Sulfobetaine methacrylate-*r*-trifluoroethyl methacrylate copolymer membranes have been synthesised previously in the literature. This polymer was synthesised via a thermally initiated free-radical polymerisation and was described as a statistical copolymer.[57] Given the similarities in the monomers used in this work and the polymerisation method used, it can be argued that

the copolymers being formulated are also statistical, despite the presence of the ionic liquid.

In order to analyse the effects of zwitterions in the polymer scaffold, a non-polymerisable zwitterion -sulfobetaine methylimidazole (SBMI)- was used as an additive in some ionogels. The data collected from these gels were used to isolate the effects of adding zwitterions to the polymer scaffold from the effects due to the presence of zwitterions in ionogels.

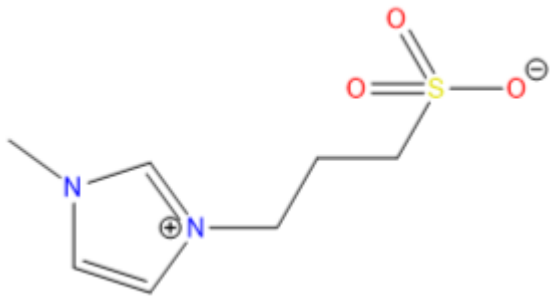

Figure 1.6: Chemical structure of sulfobetaine methylimidazole.

Sulfobetaine methylimidazole was chosen due to the similar chemical structure relative to SBVI. Due to the lack of polymerisable group on the molecule, SBMI may be added in place of SBVI during ionogel synthesis. So, the zwitterion effect may be more fully characterised by this approach.

This work aims to formulate high conductivity, mechanically stable zwitterion-containing ionogels, and evaluate the interactions occurring within these gels between the ionic liquid ions and the zwitterions present. To assess these ionogels, an arsenal of characterisation techniques was employed. The methods used include: thermogravimetric analysis,

compression testing, pulsed-field gradient spin-echo nuclear magnetic resonance spectroscopy, as well as various electrochemical characterisations such as ionic conductivity testing, and cyclic voltammetry.

Chapter 2 describes the synthesis methods used to produce the polymerisable and non-polymerisable zwitterions, as well as the zwitterion-containing ionogels. Additionally, this chapter includes some theoretical background of the experimental methods used and explains the various characterisation techniques.

Chapter 3 presents the results obtained concerning zwitterion-containing ionogels and offers some discussion to explain the experimental findings for each characterisation technique.

In Chapter 4, overall conclusions that may be gleaned from the results and discussion are summarised and related in order to offer one cohesive assessment of the zwitterion-containing ionogels discussed in this thesis. Additionally, ideas for future directions that build on this work are explored.

Appendix A contains the experimental data presented in the graphs displayed in this thesis, as well as standard deviations for some of the data.

Appendix B shows complete Arrhenius plots of zwitterion-containing ionogels that were not presented in the main text of the thesis.

1.5 References

1 Schmitt, H. H. *Return to the Moon: exploration, enterprise, and energy in the human settlement of space*. (Copernicus Books in association with Praxis Pub, 2006).

2 Chouhan, N. & Liu, R.-S. in *Electrochemical Technologies for Energy Storage and Conversion* Vol. 1&2 (eds Ru-Shi Liu *et al.*) 1-43 (Wiley-VCH Verlag GmbH & Co. KGaA, 2011).

3 Larcher, D. & Tarascon, J. M. Towards greener and more sustainable batteries for electrical energy storage. *Nature Chemistry* **7**, 19-29, doi:10.1038/NCHEM.2085 (2015).

4 Luo, X., Wang, J., Dooner, M. & Clarke, J. Overview of current development in electrical energy storage technologies and the application potential in power system operation. *Applied Energy* **137**, 511-536, doi:10.1016/j.apenergy.2014.09.081 (2015).

5 Wohde, F. *et al.* Li+ ion transport in ionic liquid-based electrolytes and the influence of sulfonate-based zwitterion additives. *Solid State Ionics* **284**, 37-44, doi:10.1016/j.ssi.2015.11.017 (2016).

6 Dunn, B., Kamath, H. & Tarascon, J.-M. Electrical energy storage for the grid: A battery of choices. *Science* **334**, 928-935, doi:10.1126/science.1212741 (2011).

7 Armand, M., Endres, F., MacFarlane, D. R., Ohno, H. & Scrosati, B. Ionic-liquid materials for the electrochemical challenges of the future. *Nat Mater* **8**, 621-629, doi:10.1038/nmat2448 (2009).

8 MacFarlane, D. R. *et al.* Ionic liquids and their solid-state analogues as materials for energy generation and storage. *Nature Reviews Materials* **1**, 15005, doi:10.1038/natrevmats.2015.5 (2016).

9 Byrne, N., MacFarlane, D. R. & Forsyth, M. Composition effects on ion transport in a polyelectrolyte gel with the addition of ion dissociators. *Electrochimica Acta* **50**, 3917-3921, doi:10.1016/j.electacta.2005.02.068 (2005).

10 Byrne, N. *et al.* Effect of zwitterion on the lithium solid electrolyte interphase in ionic liquid electrolytes. *Journal of Power Sources* **184**, 288-296, doi:10.1016/j.jpowsour.2008.04.094 (2008).

11 Tiyapiboonchaiya, C. *et al.* The zwitterion effect in high-conductivity polyelectrolyte materials. *Nat Mater* **3**, 29-32, doi:10.1038/nmat1044 (2004).

12 Byrne, N., Howlett, P. C., MacFarlane, D. R. & Forsyth, M. The Zwitterion Effect in Ionic Liquids: Towards Practical Rechargeable Lithium-Metal Batteries. *Advanced Materials* **17**, 2497-2501, doi:10.1002/adma.200500595 (2005).

13 Welton, T. Room-Temperature Ionic Liquids. Solvents for Synthesis and Catalysis. *Chemical Reviews* **99**, 2071-2084, doi:10.1021/cr980032t (1999).

14 Noda, A., Hayamizu, K. & Watanabe, M. Pulsed-Gradient Spin−Echo 1H and 19F NMR Ionic Diffusion Coefficient, Viscosity, and Ionic Conductivity of Non-Chloroaluminate Room-Temperature Ionic Liquids. *The Journal of Physical Chemistry B* **105**, 4603-4610, doi:10.1021/jp004132q (2001).

15 Zhang, S. *et al.* Beyond solvents and electrolytes: Ionic liquids-based advanced functional materials. *Progress in Materials Science* **77**, 80-124, doi:10.1016/j.pmatsci.2015.10.001 (2016).

16 Le Bideau, J., Viau, L. & Vioux, A. Ionogels, ionic liquid based hybrid materials. *Chemical Society reviews* **40**, 907-925, doi:10.1039/c0cs00059k (2011).

17 Ikeda, A. *et al.* Gelation of Ionic Liquids with a Low Molecular-Weight Gelator Showing <I>T</I>_{gel} above 100 °C. *Chemistry Letters* **30**, 1154-1155, doi:10.1246/cl.2001.1154 (2001).

18 Hanabusa, K., Fukui, H., Suzuki, M. & Shirai, H. Specialist Gelator for Ionic Liquids. *Langmuir* **21**, 10383-10390, doi:10.1021/la051323h (2005).

19 Horowitz, A. I. & Panzer, M. J. High-performance, mechanically compliant silica-based ionogels for electrical energy storage applications. *Journal of Materials Chemistry* **22**, 16534, doi:10.1039/c2jm33496h (2012).

20 Horowitz, A. I. *Ionogel Electrolytes through Sol-Gel Processing* Doctor of Philosophy thesis, Tufts University, (2015).

21 Izak, P., Hovorka, S., Bartovsky, T., Bartovska, L. & Crespo, J. Swelling of polymeric membranes in room temperature ionic liquids. *Journal of Membrane Science* **296**, 131-138, doi:10.1016/j.memsci.2007.03.022 (2007).

22 Brown, R. H. *et al.* Effect of Ionic Liquid on Mechanical Properties and Morphology of Zwitterionic Copolymer Membranes. *Macromolecules* **43**, 790-796, doi:10.1021/ma902028u (2010).

23 Laschewsky, A. Structures and Synthesis of Zwitterionic Polymers. *Polymers* **6**, 1544-1601, doi:http://dx.doi.org/10.3390/polym6051544 (2014).

24 Galin, M., Mathis, A. & Galin, J. C. Statistical n-butyl acrylate-(sulfopropyl)ammonium betaine copolymers. 5. Plasticization studies. *Macromolecules* **26**, 4919-4927, doi:10.1021/ma00070a028 (1993).

25 Taguchi, S., Matsumoto, T., Ichikawa, T., Kato, T. & Ohno, H. Gelation of an amino acid ionic liquid by the addition of a phosphonium-type zwitterion. *Chem Commun (Camb)* **47**, 11342-11344, doi:10.1039/c1cc14455c (2011).

26 Lee, J., Panzer, M. J., He, Y., Lodge, T. P. & Frisbie, C. D. Ion Gel Gated Polymer Thin-Film Transistors. *Journal of the American Chemical Society* **129**, 4532-4533, doi:10.1021/ja070875e (2007).

27 He, Y., Boswell, P. G., Bühlmann, P. & Lodge, T. P. Ion Gels by Self-Assembly of a Triblock Copolymer in an Ionic Liquid. *The Journal of Physical Chemistry B* **111**, 4645-4652, doi:10.1021/jp064574n (2007).

28 Croce, F., Appetecchi, G. B., Persi, L. & Scrosati, B. Nanocomposite polymer electrolytes for lithium batteries. *Nature* **394**, 456-458 (1998).

29 Susan, M. A. B. H., Kaneko, T., Noda, A. & Watanabe, M. Ion Gels Prepared by in Situ Radical Polymerization of Vinyl Monomers in an Ionic Liquid and Their Characterization as Polymer Electrolytes. *Journal of the American Chemical Society* **127**, 4976-4983, doi:10.1021/ja045155b (2005).

30 Tiruye, G. A. & Marcilla, R. in *Applications of Ionic Liquids in Polymer Science and Technology* (ed David Mecerreyes) 199-229 (Springer, 2015).

31 Visentin, A. F. *Advancing Polymer-Supported Ionogel Electrolytes Formed via Radical Polymerization* Doctorate of Philosophy thesis, Tufts University, (2014).

32 Biedroń, T. & Kubisa, P. Atom-Transfer Radical Polymerization of Acrylates in an Ionic Liquid. *Macromolecular Rapid Communications* **22**, 1237-1242, doi:10.1002/1521-3927(20011001)22:15<1237::AID-MARC1237>3.0.CO;2-E (2001).

33 Ma, H., Wan, X., Chen, X. & Zhou, Q.-F. Reverse atom transfer radical polymerization of methyl methacrylate in room-temperature ionic liquids. *Journal of Polymer Science, Part A: Polymer Chemistry* **41**, 143-151, doi:10.1002/pola.10558 (2002).

34 Perrier, S., Davis, T. P., Carmichael, A. J. & Haddleton, D. M. First report of reversible addition-fragmentation chain transfer (RAFT) polymerisation in room temperature ionic liquids. *Chemical Communications*, 2226-2227, doi:10.1039/B206534G (2002).

35 Winterton, N. Solubilization of polymers by ionic liquids. *Journal of Materials Chemistry* **16**, 4281-4293, doi:10.1039/B610143G (2006).

36 Watanabe, M., Yamada, S.-I., Sanui, K. & Ogata, N. High ionic conductivity of new polymer electrolytes consisting of polypyridinium, pyridinium and aluminium chloride. *Journal of the Chemical Society, Chemical Communications*, 929-931, doi:10.1039/C39930000929 (1993).

37 Visentin, A. F., Alimena, S. & Panzer, M. J. Influence of Ionic Liquid Selection on the Properties of Poly(Ethylene Glycol) Diacrylate-Supported Ionogels as Solid Electrolytes. *ChemElectroChem* **1**, 718-721, doi:10.1002/celc.201300205 (2014).

38 Yoshizawa, M., Hirao, M., Ito-Akita, K. & Ohno, H. Ion conduction in zwitterionic-type molten salts and their polymers. *Journal of Materials Chemistry* **11**, 1057-1062, doi:10.1039/b101079o (2001).

39 Marwanta, E., Mizumo, T. & Ohno, H. Improved ionic conductivity of nitrile rubber/Li(CF3SO2)2N composites by adding imidazolium-type zwitterion. *Solid State Ionics* **178**, 227-232, doi:http://dx.doi.org/10.1016/j.ssi.2006.12.022 (2007).

40 Tamada, M., Ueda, S., Hayashi, T. & Ohno, H. Thermally Stable Polymer Gel Electrolytes Composed of Branched Polyimide and Ionic Liquid/Zwitterion Mixture Prepared by In Situ Polycondensation. *Chemistry Letters* **37**, 86-87, doi:10.1246/cl.2008.86 (2008).

41 Soberats, B., Yoshio, M., Ichikawa, T., Ohno, H. & Kato, T. Zwitterionic liquid crystals as 1D and 3D lithium ion transport media. *J. Mater. Chem. A* **3**, 11232-11238, doi:10.1039/c5ta00814j (2015).

42 Díaz, M., Ortiz, A. & Ortiz, I. Progress in the use of ionic liquids as electrolyte membranes in fuel cells. *Journal of Membrane Science* **469**, 379-396, doi:10.1016/j.memsci.2014.06.033 (2014).

43 Wongittharom, N. *et al.* Ionic liquid electrolytes for high-voltage rechargeable Li/LiNi0.5Mn1.5O4 cells. *Journal of Materials Chemistry A* **2**, 3613, doi:10.1039/c3ta14423b (2014).

44 Guyomard-Lack, A. *et al.* Hybrid Silica-Polymer Ionogel Solid Electrolyte with Tunable Properties. *Advanced Energy Materials* **4**, doi:10.1002/aenm.201301570 (2014).

45 Arbizzani, C. *et al.* Safe, high-energy supercapacitors based on solvent-free ionic liquid electrolytes. *Journal of Power Sources* **185**, 1575-1579, doi:10.1016/j.jpowsour.2008.09.016 (2008).

46 Palacin, M. R. & de Guibert, A. Why do batteries fail? *Science* **351**, 1253292, doi:10.1126/science.1253292 (2016).

47 Miller, J. R. & Simon, P. Electrochemical Capacitors for Energy Management. *Science* **321**, 651-652, doi:10.1126/science.1158736 (2008).

48 Winter, M. & Brodd, R. J. What Are Batteries, Fuel Cells, and Supercapacitors? *Chemical Reviews* **104**, 4245-4270, doi:10.1021/cr020730k (2004).

49 Deeley, P. M. *Electrolytic capacitors: the theory, construction, characteristics and application of all types*. (1938).

50 Conway, B. E. *Electrochemical supercapacitors: scientific fundamentals and technological applications*. (Plenum Press, 1999).

51 Chmiola, J. *et al.* Anomalous increase in carbon capacitance at pore sizes less than 1 nanometer. *Science* **313**, 1760-1763, doi:10.1126/science.1132195 (2006).

52 Simon, P. & Gogotsi, Y. Materials for electrochemical capacitors. *Nat Mater* **7**, 845-854 (2008).

53 Freemantle, M. DESIGNER SOLVENTS. *Chemical & Engineering News Archive* **76**, 32-37, doi:10.1021/cen-v076n013.p032 (1998).

54 D'Angelo, A. J., Grimes, J. J. & Panzer, M. J. Deciphering Physical versus Chemical Contributions to the Ionic Conductivity of Functionalized Poly(methacrylate)-Based Ionogel Electrolytes. *J Phys Chem B* **119**, 14959-14969, doi:10.1021/acs.jpcb.5b08250 (2015).

55 Ohno, H., Yoshizawa, M. & Ogihara, W. A new type of polymer gel electrolyte: zwitterionic liquid/polar polymer mixture. *Electrochimica Acta* **48**, 2079-2083, doi:10.1016/s0013-4686(03)00188-9 (2003).

56 Horowitz, A. I., Wang, Y. & Panzer, M. J. Reclamation and reuse of ionic liquids from silica-based ionogels using spontaneous water-driven separation. *Green Chemistry* **15**, 3414, doi:10.1039/c3gc41661e (2013).

57 Bengani, P., Kou, Y. & Asatekin, A. Zwitterionic copolymer self-assembly for fouling resistant, high flux membranes with size-based small molecule selectivity. *Journal of Membrane Science* **493**, 755-765, doi:http://dx.doi.org/10.1016/j.memsci.2015.07.025 (2015).

Chapter 2: Experimental Methods

2.1 Introduction

The work presented in this thesis involves the synthesis of new zwitterion-containing ionogels. This chapter will attempt to outline the synthesis methods used to produce the ionogels and zwitterions of interest, and explain the various characterisation techniques used to assess the performance of the novel zwitterion-containing ionogel materials discussed in the introduction. The methods used can be categorised as mechanical, material, and electrochemical characterisations.

2.2 Materials

Zwitterionic monomers and additives used throughout this thesis were synthesised in the Asatekin lab at Tufts University. The fluorinated monomer used was purchased from Scientific Polymer Products and was passed through an activated alumina column in order to remove the inhibitor. The chemical cross-linker, PETA-4 was purchased from Sigma-Aldrich and used as it was received. Research-grade ionic liquid, EMI TFSI was purchased from EMD Chemicals Inc. and was stored in a nitrogen glove box.

2.2.1 Sulfobetaine Vinylimidazole (SBVI) Synthesis:

The SBVI synthesis was performed by Prity Bengani-Lutz in the Asatekin group at Tufts. 1-vinyl imidazole and 1,3-propanesultone with purities of 99% were purchased from Sigma-Aldrich. SBVI, or 1-ethene-(3-propanesulfonate)-imidazole, was synthesised using a 1.2:1 molar ratio of 1,3 propane sultone to vinyl imidazole in order to account for reaction yields and the reactivity of the starting reagents. To begin, 50 mL of 1-vinylimidazole was added to 250 mL of acetonitrile in a round bottomed flask. Following this, 55 mL of 1,3-propanesultone was added and the reaction mixture was stirred at room temperature. The flask was sealed with a septum and bubbled with nitrogen for twenty minutes in order to remove any reaction inhibitors such as oxygen and water. The reaction was then left to react at room temperature for 24 hours. The product was formed as a white precipitate with a yield of 85% and was then washed in three cycles with 300 mL of diethyl ether. The product was then dried in a vacuum oven held at $50^{\circ}C$ for 24 hours and was subsequently characterised using proton NMR using deuterated dimethyl sulfoxide as a solvent. ^{1}H NMR (DMSO, 500MHz): 9.70 (s, 1H), 8.20 (s, 1H), 7.95 (s, 1H), 7.32 t,1H), 5.95 (d,1H), 5.42 (d,1H), 4.37 (t,2H), 2.62 (t,2H), 2.15 (m, 2H).

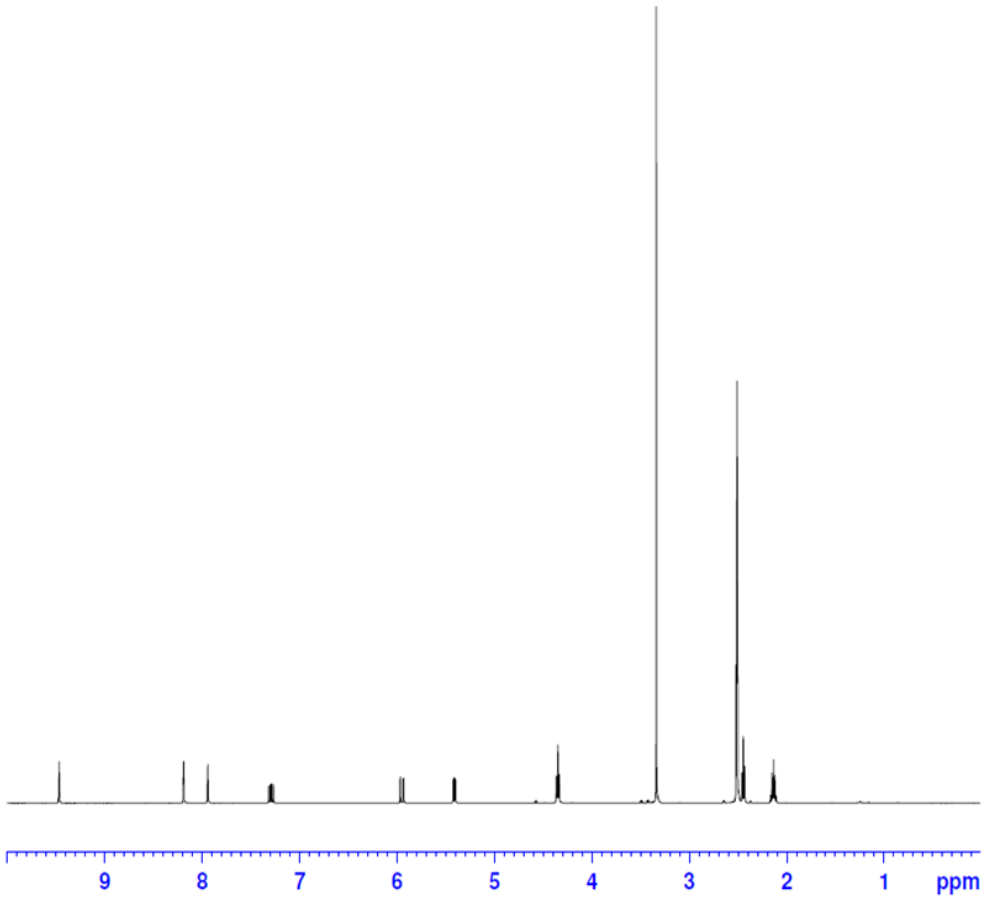

Figure 2.1: ^{1}H NMR spectrum of SBVI monomer in deuterated DMSO. NMR courtesy of Prity Bengani-Lutz.

2.2.2 Sulfobetaine Methylimidazole (SBMI) Synthesis

The SBMI synthesis was performed with the help of Prity Bengani-Lutz in the Asatekin group at Tufts University. 1-methylimidazole and 1,3-propanesultone with purities of 99% were purchased from Sigma-Aldrich. 1-methyl-(3-propanesulfonate)-imidazole (SBMI), was synthesised using a 1.2:1 molar ratio of 1,3 propane sultone to vinyl imidazole with a 20% excess of reagents in order to account for reaction yields and the reactivity of the starting reagents. To begin, 5 mL of 1-methylimidazole was mixed with 50

mL of dichloromethane in a round bottomed flask. Following this, 8 mL of 1,3-propanesultone was added and the reaction mixture was stirred at room temperature. The flask was sealed with a septum and bubbled with nitrogen for twenty minutes in order to remove any reaction inhibitors such as oxygen and water. The reaction was then left at room temperature for 2 hours to allow the reaction to proceed. The product was formed as a white precipitate and was then washed in three cycles with 250 mL of dichloromethane. Each purification step was achieved by vigorously stirring the precipitate in dichloromethane for 24 hours. The product was then filtered and dried in a vacuum oven held at $50^{\circ}C$ for 24 hours. In order to dry the zwitterion further, the product was placed in a vacuum chamber overnight and was subsequently characterised using proton NMR using deuterated water as a solvent. ^{1}H NMR (D_2O, 500MHz): 8.72 (s, 1H), 7.47 (s, 1H), 7.32 (s, 1H), 5.87 (t,1H), 5.38 (d,1H), 4.73 (d,1H), 4.34 (t,2H), 2.72 (t,2H), 2.15 (m, 2H).

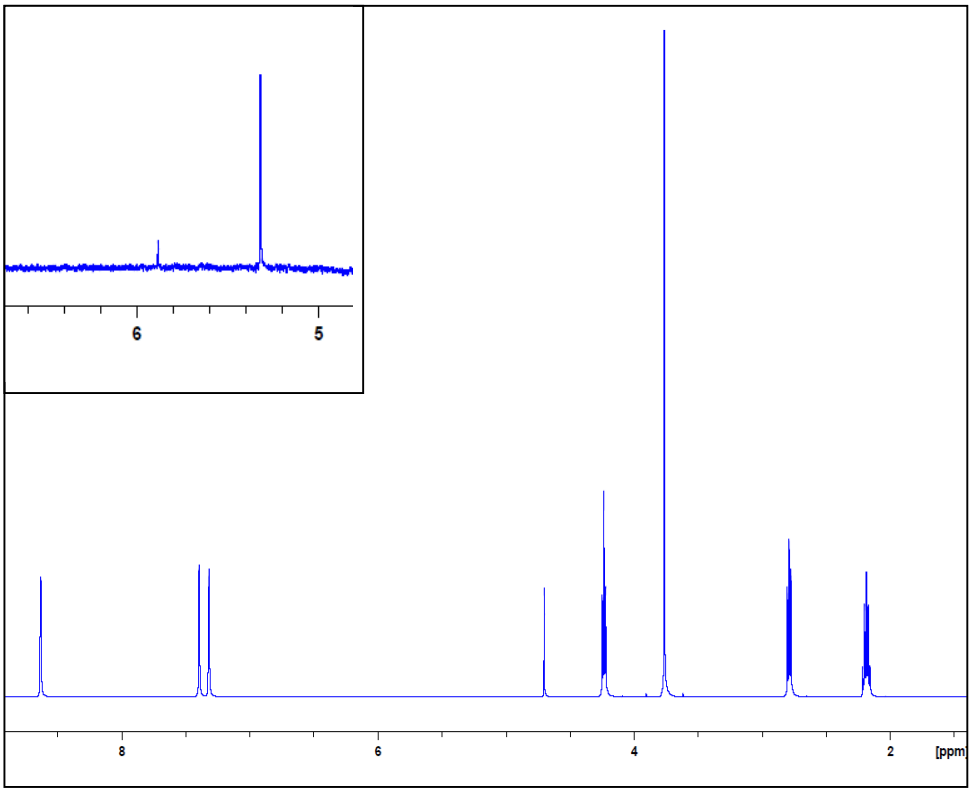

Figure 2.2: ^{1}H NMR spectrum of synthesised sulfobetaine methylimidazole. Inset shows the two peaks at 5.38 and 5.87 ppm.

2.2.3 Zwitterion-Containing Ionogel Synthesis

2,2,2-Trifluoroethyl methacrylate (TFEMA) was purchased from Scientific Polymer Products with a purity of 99%. Pentaerythritol tetraacrylate (PETA-4) and the photoinitiator 2-hydroxy-2-methylpropiophenone (HOMPP) were purchased from Sigma-Aldrich and were used as received. The ionic liquid 1-ethyl-3methylimidazolium bis(trifluoromethylsulfonyl)imide (EMI TFSI) was purchased from EMD Chemicals Inc. and was stored under inert conditions to prevent water absorption. Ionogels were synthesised by polymerising all monomers simultaneously using the ionic liquid as a solvent. Precursor solutions were prepared by adding monomers or zwitterionic additives, along with the

cross-linker, PETA-4, in the desired ratios to EMI TFSI. TFEMA monomer was filtered using a basic activated alumina column to remove the inhibitor prior to its use in zwitterion-containing ionogels. Gel components were then weighed using a digital scale in air. Following this, precursor solutions were mixed using a Fisher Scientific vortex mixer (fixed 2800 rpm, 4.5 mm orbit) for 30 seconds, and placed in a nitrogen glove box. Precursor vials were sealed when placed in the glove box vacuum chamber in order to avoid volatilisation of the TFEMA monomer. Precursor vials were opened inside the glove box in order to exchange the air with nitrogen and were then promptly sealed before heating. The mixtures were stirred and heated in a glove box using hotplate settings of $100^{\circ}C$ and 350 rpm. Typically, solutions were heated and stirred for eight hours in order to allow for the dissolution of the zwitterion. Upon solubilisation of the zwitterion, a photoinitiator, 2-hydroxy-2-methylpropiophenone (HOMPP), was added to the monomer-ionic liquid solution at 2 wt.% of the total monomer content. The solution was then heated and stirred for a few minutes at the same settings mentioned above to ensure that the initiator was well-mixed.

Following this, the solution was injected into pre-assembled devices while still at an elevated temperature. Devices consisted of two indium tin oxide (ITO) coated glass electrodes with a poly(tetrafluoroethylene) (PTFE) spacer of known dimensions in between. The PTFE spacers had a thickness of 1.57 mm, an inner diameter of 6.35 mm, and an outer diameter of 13.2 mm. Once filled, the devices were placed under a long wave UV lamp (365

nm, Spectronic Corp., 8 W) for 7 minutes. Gels were stored under inert conditions for 24 hours prior to testing in order to ensure the termination of the free-radical polymerisation reaction. All gels and ionic liquids were stored under inert conditions, and all electrochemical testing was done in an inert nitrogen glove box environment.

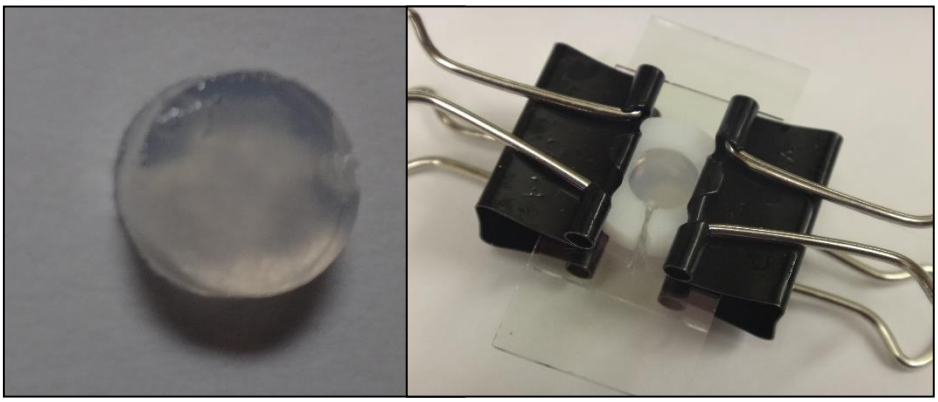

Figure 2.3: 7 mol.% SBVI ionogel with 20 mol.% total polymer content (left). Assembled device with polymerised gel in PTFE spacer between ITO-coated glass slides (right).

2.3 Materials Characterisation

2.3.1 Nuclear Magnetic Resonance

Two types of nuclear magnetic resonance (NMR) spectroscopy techniques were used to characterise materials throughout this thesis: proton NMR (^{1}H NMR), and pulsed-field gradient spin-echo NMR (PGSE NMR). Proton NMR was used to confirm the presence and purity of the synthesised zwitterions, while PGSE NMR was used to empirically determine the diffusion coefficients of the ions in the ionic liquid. ^{1}H and PGSE diffusion

measurements were performed using a Bruker AVANCE III 500 MHz NMR instrument.

Proton NMR takes advantage of the nuclear magnetic moments of various nuclei.[1] The magnetic dipole moments of nuclei arise from the spinning motion of particles. Under the influence of a magnetic field, the magnetic moment that is aligned with the applied field is lower in energy than that of the moment resulting from the opposite spin. The energy difference that results from these different spin states is what leads to the absorption of electromagnetic radiation.[2] Fortunately, the resonance frequencies of different elements and isotopes are sufficiently different, such that NMR may only generate a signal for a specific isotope of an element.

^{1}H NMR is a powerful structural analysis tool as nuclei in molecules are affected by the applied and local magnetic fields, that is to say, the magnetic field induced by the electrons in the molecule. So, resonance positions of nuclei depend on the amount of shielding experienced by the nuclei due to the electron environment in which they are in. Deshielded nuclei absorb radiation at lower magnetic field strengths and exhibit chemical signals or shifts downfield. The opposite is true for more shielded nuclei. So, molecular structures can be gleaned using chemical shifts in NMR spectra.[2]

Zwitterionic purity was ensured after synthesis by dissolving 37.5 mg of the zwitterion in 0.75 mL of a deuterated solvent to give a final

concentration of 50 gZI/L solvent. The solvent used for SBVI was DMSO, while the solvent chosen for SBMI was D_2O.

Pulsed-field gradient spin-echo NMR offers a non-invasive way to measure Brownian or translational motion of the ionic species in the gel. The EMI cation may be tracked by taking a ^{1}H PGSE NMR measurement, while the diffusivity of the TFSI anion may be measured using ^{19}F as the probe nucleus.[3-6] Importantly, the correct gyromagnetic ratio, γ, which is specific to each nucleus, must be used when calculating NMR diffusivities. The gyromagnetic ratios for the two nuclei used, hydrogen and fluorine, are 4257.6 Hz/G and 4005.2 Hz/G, respectively. PGSE NMR measurements employ the use of a modified Hahn spin-echo, invented by Erwin Hahn in 1950, in the form of a rectangular gradient pulse of magnitude g and duration δ.[3, 5-7]

The Hahn echo, g, is a spatially dependent magnetic field gradient. Typically, this spatial gradient is oriented along the *z*-axis, so it is aligned with the static magnetic field, B_0. Gradient pulses impose a phase shift on nuclear spins. To measure the translational motion of nuclei, a $\frac{\pi}{2}$ radiofrequency (rf) pulse is applied in order to rotate the macroscopic magnetisation, or net magnetic moment of all the individual microscopic nuclear spins, into the x-y, or equatorial, plane.[7, 8] This causes the net magnetic moment of the sample to be perpendicular to the spatially homogeneous field, B_0. Following this, a rectangular pulse of magnitude g and

duration δ is applied which causes spin *i* to experience a phase change at the end of the first period, τ.[8]

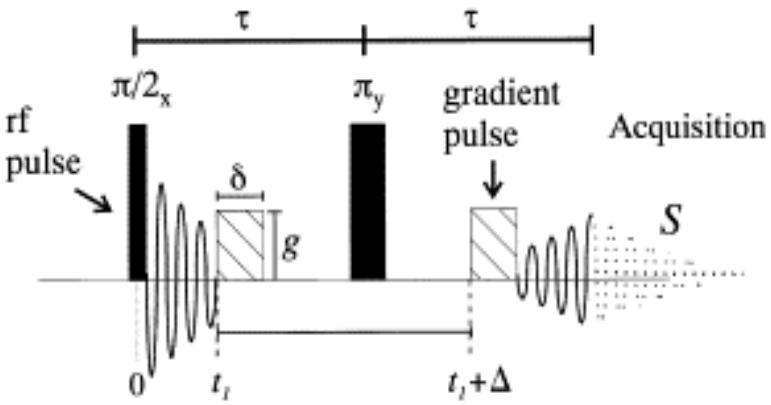

Figure 2.4: Schematic representation of a PGSE NMR modified Hahn-spin echo pulse of magnitude, g, and duration δ, with a period τ. Reproduced from Hayamizu *et al.*[3]

The phase shift of a spin, *i* is given by Equation (2.1), where γ is the gyromagnetic ratio, τ is the period, g is the magnetic gradient strength, and $z_i(t)$ is the displacement of spin *i* along the *z*-axis as a function of time.

$$\phi_i(\tau) = \gamma B_0 \tau + \gamma g \int_{t_1}^{t_1+\delta} z_i(t)\, dt \qquad (2.1)$$

As seen in **Figure 2.4**, at the end of the first period, a π rf pulse is generated, reversing the sign of the pulse and static fields by rotating the magnetic moment vector from the positive *z*-axis to the negative one, creating an effective field gradient.[9, 10] Following this, another Hahn-echo of equivalent duration and magnitude to the first is applied at time $t_1+\Delta$, where Δ is the delay time. In the case where spins have not moved along the *z*-axis between the first and second spin-echo pulses, the effects of the magnetic field gradients cancel out and the nuclei refocus. When the spins undergo

translational motion along the *z*-axis, however, the phase shift, or dephasing, is directly proportional to the displacement in the *z*-direction in the time Δ. The phase shift over a period of 2τ is given by Equation (2.2). In the equation below, γ is the gyromagnetic ratio, g is the gradient strength, and δ and Δ are the length of the gradient, and the diffusion time, respectively. The gyromagnetic ratio is the ratio of the magnetic moment to the angular momentum of the nucleus in question.[9] The functions z(t) and z(t') describe the translational motion of spin *i* along the *z*-axis with respect to time.

$$\phi_i(2\tau) = \gamma g\left[\int_{t_1}^{t_1+\delta} z_i(t)\ dt - \int_{t_1+\Delta}^{t_1+\Delta+\delta} z_i(t')\ dt'\right] \quad (2.2)$$

Comparing Equations (2.1) and (2.2), it can be seen that the phase shift due to the static magnetic field cancels out due to the reversal of the pulse gradients and static field.[8]

In order to account for the different starting and ending spatial positions of the nuclei of concern, the signal attenuation is considered. This, in effect, normalises the intensity of the spin-echo at $t = 2\tau$. The attenuation at 2τ, after much algebraic manipulation, is given by Equation (2.3), where $S(2\tau)_{g=0}$ is the spin-spin relaxation attenuation, *i.e.* the attenuation in the absence of pulse gradients, and the exponential term is the attenuation due to diffusion.[8, 10]

$$S(2\tau) = S(2\tau)_{g=0} \exp\left(-\gamma^2 D g^2 \delta^2 \left(\Delta - \frac{\delta}{3}\right)\right) \quad (2.3)$$

Normalising the attenuation by the relaxation component allows for its elimination, resulting in the diffusion coefficient being the only unknown in the expression give in Equation (2.4). The normalised attenuation, E, is an empirical quantity.[5, 6, 8, 9, 11]

$$\ln(E) = \ln\left(\frac{S(2\tau)}{S(2\tau)_{g=0}}\right) = -\gamma^2 D g^2 \delta^2 \left(\Delta - \frac{\delta}{3}\right) \quad (2.4)$$

To prepare a PGSE NMR sample, ionogel precursors were prepared as in section 2.2.3 and injected into glass capillary tubes with an inner diameter of 1.5 mm. Capillary tubes were filled to an approximate height of 44.0 mm in order to account for the probe height in the NMR spectrometer. At a height of 44.0 mm the sample appears to be an infinite cylinder. Prior to removing gel samples from the glove box, capillary tubes were sealed with Leica Microsystems Critoseal capillary tube sealant in order to prevent water absorption.

Upon gelation, capillary tubes were inserted into 5 mm NMR tubes containing D_2O which was used as the lock solvent. To measure diffusivity, the ledgp2s1d pulse programme was used. The diffusion time, δ and the delay time, Δ were qualitatively adjusted for each gel sample to give an approximate attenuation of 90% when the gradient strength was changed from 2% to 95%. Diffusion time and delay time parameters were in the range of 7-10 ms and 200-500 ms, respectively.

^{1}H PGSE experiments were run to measure the diffusion coefficient of the EMI^{+} cation, and the ^{19}F nucleus was used to measure the diffusivity of the $TFSI^{-}$ anion. The experiment was conducted by taking 16 1-D scans at decreasing gradient strengths until 95% attenuation was reached. A 2-D spectrum was then generated and phase corrected in order to allow for area integration under the peaks. Measured diffusivities were in the range of 2.5-3.0x10^{-11} m^{2} s^{-1} for the gel cations, and approximately 1.5x10^{-11} m^{2} s^{-1} for the $TFSI^{-}$ anions.

2.3.2 Thermogravimetric Analysis

Thermogravimetric analysis (TGA) was run using a TA Instruments Q500 apparatus. These experiments were conducted in order to determine the water content of zwitterion and zwitterion-containing ionogel samples. Samples were loaded in approximately 5 mg quantities into an aluminium pan with a punctured aluminium lid. The pan and lid were used to prevent the samples from blowing off the balance inside the TGA furnace. The sample filled pan and lid were then placed in a platinum basket that had been pre-tared along with the pan and lid combination. The basket and sample were contained in a furnace with continuous nitrogen flow. A temperature ramp programme was run which increased the temperature of the furnace from room temperature to $400^{\circ}C$ at a rate of $3^{\circ}C\ s^{-1}$. The instrument recorded sample weight-loss as a function of temperature, allowing the sample

breakdown temperature and water content on a mass basis to be determined quantitatively.

2.4 Mechanical Characterisation

Ionogel mechanical properties were assessed using a dynamic mechanical analyser (DMA). The elastic modulus was used as an indicator of gel stiffness and was determined by compression testing in free-extension using a TA Instruments RSA3 dynamic mechanical analyser. A strain rate of 0.01 %/s was used up to a maximum strain of 15%. The linear portion of the resulting stress-strain curve generated was used to determine the modulus, E (kPa). The x-axis data range used was 1-10% strain.

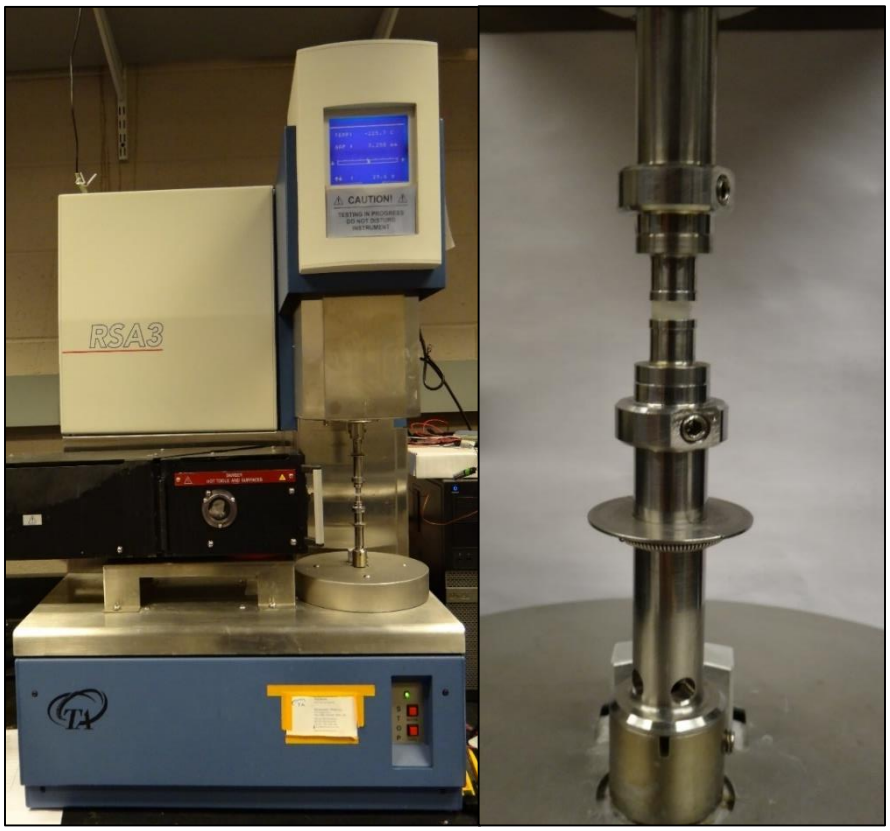

Figure 2.5: TA Instruments RSA3 Dynamic Mechanical Analyser (left). Compressed ionogel (right).

2.5 Electrical Characterisation

2.5.1 Impedance Spectroscopy

AC impedance spectroscopy was used to determine the conductivity values of ionogels and the neat ionic liquid. Tests were performed using a VersaSTAT 3 potentiostat with an integrated frequency response analyser from Princeton Applied Research. Ionogels were polymerised between two ITO-coated glass slides, as shown in **Figure 2.3**. The gel geometry was well-defined due to the known dimensions of the PTFE spacer used. Impedance measurements were taken under inert conditions in a nitrogen-filled glove box over the frequency range of 1 kHz to 100 kHz. A sinusoidal voltage amplitude of 10 mV with a 0 V DC offset was used for all measurements. The high-frequency range was taken to be the resistive response as ions cannot form double-layers, while the low-frequency data is normally used to estimate capacitance, Equation (2.5). In the following equation, f is the frequency and Z" is the imaginary impedance at the chosen frequency.

$$C = \frac{1}{2\pi f Z''} \qquad (2.5)$$

The setup resistance inherent to the ITO plates used as electrodes $(\approx 76\ \Omega)$ was subtracted from the high-frequency series resistance in order to determine the gel resistance. The setup resistance was determined by injecting neat EMI TFSI into ITO devices assembled with PTFE spacers of

various thicknesses and conducting impedance spectroscopy measurements. The magnitude of impedance data were then plotted and the y-intercept was considered to be the resistance associated the test setup. These measurements were recorded in a nitrogen-containing glove box. From the ionogel resistance, ionic conductivity, σ, was calculated, Equation (2.6), where t is the thickness of the gel, A is the cross-sectional area of the gel, and R_{gel} is the gel resistance; $R_{gel} = R_{total} - R_{setup}$. The parameters t and A are known due to the well-defined PTFE spacer geometry.

$$\sigma = \frac{t}{AR_{gel}} \qquad (2.6)$$

2.5.2 Activation Energy of Ionic Conductivity

The activation energy of ionic conductivity is indicative of the relative energetic barrier ions experience as they move through the electrolyte. The activation energy was found by generating an Arrhenius plot from conductivity data at various temperatures. The temperature of the gel was varied by placing the gel on a thermally conductive Molybdenum plate over a Linkam Scientific Instruments LTS 420 platinum temperature controlled microscopy stage (**Figure 2.6**).

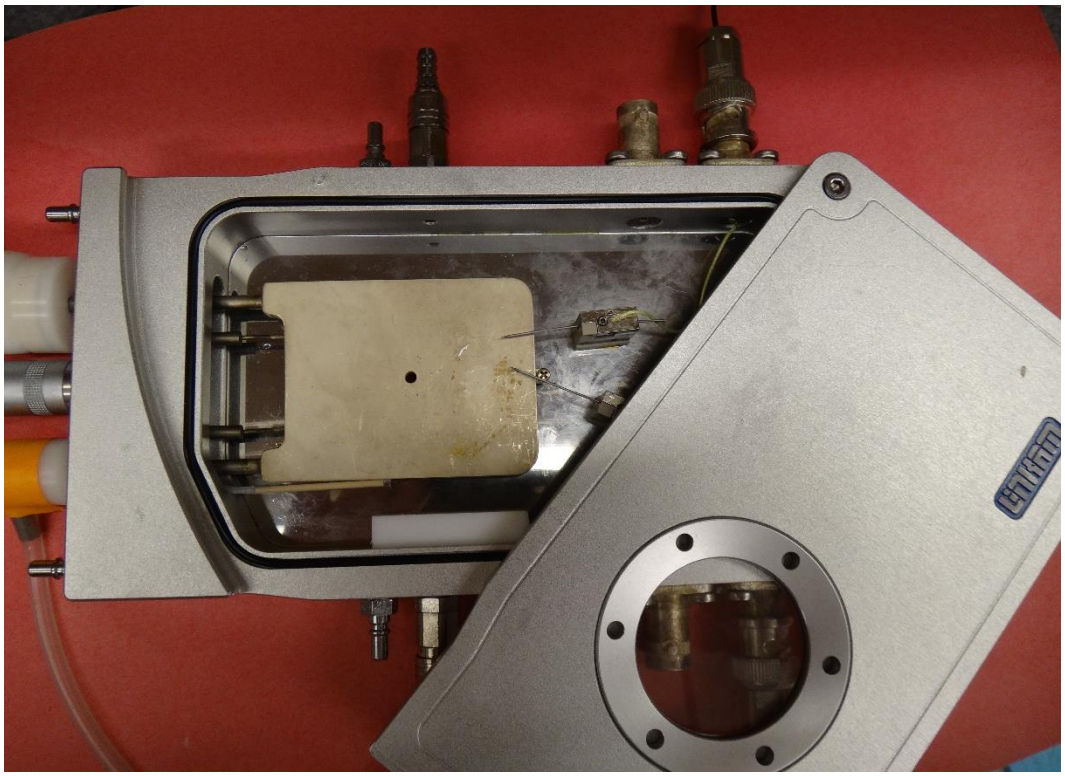

Figure 2.6: Linkam Scientific Instruments LTS 420 temperature stage.

All activation energy impedance measurements were taken using the VersSTAT 3 potentiostat, mentioned above, under continuous nitrogen flow

through the sealed temperature stage. Ionogels were allowed to reach thermal equilibrium before impedance spectra were recorded. To measure gel impedance, two needle electrodes were inserted into a gel with a thickness of 3.14 mm and a diameter of 6.35 mm.

Ionic conductivities were calculated by equating the room temperature conductivities measured in this setup with those measured between ITO at room temperature. From those data, a geometrical correction factor was calculated and applied to all other temperature-controlled resistance data. The natural logarithm of calculated conductivities was then plotted as a function of varying temperature and the Arrhenius relationship was used to find the activation energy of each gel.

$$\sigma = \sigma_0 \exp\left(-\frac{E_A}{RT}\right) \quad (2.7)$$

2.5.3 Cyclic Voltammetry

Cyclic Voltammetry was used to qualitatively determine the stability window of the zwitterion-containing ionogels. Measurements were performed using the VersaSTAT 3 potentiostat. A sweep voltage of $1\ V\ s^{-1}$ was used from a specified minimum voltage to a maximum voltage for several test cycles. Generally, minimum and maximum voltages were symmetric around 0 V. So, when the maximum voltage was set to be 2 V, the minimum was -2 V. From these data, the measured current is plotted versus potential.

Cyclic voltammetry measurements were performed on the symmetric ITO gel devices described in previous sections. The cross-sectional area of the zwitterion-containing ionogels tested was $3.17 \times 10^{-5} m^2$. All measurements were done in a nitrogen-filled glove box.

2.6 References

1 Becker, E. D. in *High Resolution NMR: Theory and Chemical Applications* 13-47 (2000).

2 Carey, F. A. & Giuliano, R. M. *Organic chemistry*. 8th edn, (McGraw-Hill, 2011).

3 Hayamizu, K., Aihara, Y., Arai, S. & Price, W. S. Diffusion, conductivity and DSC studies of a polymer gel electrolyte composed of cross-linked PEO, γ-butyrolactone and LiBF4. *Solid State Ionics* **107**, 1-12, doi:http://dx.doi.org/10.1016/S0167-2738(97)00527-4 (1998).

4 D'Angelo, A. J., Grimes, J. J. & Panzer, M. J. Deciphering Physical versus Chemical Contributions to the Ionic Conductivity of Functionalized Poly(methacrylate)-Based Ionogel Electrolytes. *J Phys Chem B* **119**, 14959-14969, doi:10.1021/acs.jpcb.5b08250 (2015).

5 Noda, A. H., Kikuko; Watanabe, Masayoshi Pulsed-Gradient Spin-Echo 1H and 19F NMR Ionic Diffusion Coefficient, Viscosity, and Ionic Conductivity of Non-Chloroaluminate Room-Temperature Ionic Liquids. *J. Phys. Chem. B* **105**, 4603-4610 (2005).

6 Noda, A., Hayamizu, K. & Watanabe, M. Pulsed-Gradient Spin−Echo 1H and 19F NMR Ionic Diffusion Coefficient, Viscosity, and Ionic Conductivity of Non-Chloroaluminate Room-Temperature Ionic

Liquids. *The Journal of Physical Chemistry B* **105**, 4603-4610, doi:10.1021/jp004132q (2001).

7 Hahn, E. L. Spin Echoes. *Physical Review* **80**, 580-594 (1950).

8 Price, W. S. ChemInform Abstract: Pulsed-Field Gradient Nuclear Magnetic Resonance as a Tool for Studying Translational Diffusion. Part 1. Basic Theory. *CHIN ChemInform* **28**, 299-336 (1997).

9 Carr, H. Y. & Purcell, E. M. Effects of Diffusion on Free Precession in Nuclear Magnetic Resonance Experiments. *Physical Review* **94**, 630-638 (1954).

10 Tanner, J. E. J. *Use of a Pulsed Magnetic-Field Gradient for Measurements of Self-Diffusion by Spin-Echo Nuclear Magnetic Resonance with Applications to Restricted Diffusion in Several Tissues and Emulsions* Doctor of Philosophy thesis, The University of Wisconsin -Madison (1966).

11 Stejskal, E. O. Use of Spin Echoes in a Pulsed Magnetic-Field Gradient to Study Anisotropic, Restricted Diffusion and Flow. *The Journal of Chemical Physics* **43**, 3597, doi:10.1063/1.1696526 (1965).

Chapter 3: Zwitterion-Containing Ionogels as Solid-State Electrolytes

3.1 Introduction

Zwitterion-containing ionogels were produced according to the methods outlined in Section 2.2.3. Chemical and Electrical gel characterisations were conducted under inert nitrogen conditions in order to avoid the plasticisation effects of absorbed water in the gels. This chapter discusses the results and observations gleaned from the various characterisation techniques explained in Chapter 2.

3.2 Ionogel Formulations

Zwitterion-containing ionogels were formulated by pre-determining the desired total polymer mole fraction, then adjusting the ratios of the monomers accordingly. The amount of chemical cross-linker, PETA-4, used was kept approximately constant for the zwitterion-containing ionogels with 20 mol.% polymer, but was scaled linearly when the total polymer content within the ionogel was scaled.

The amount of zwitterion that could be incorporated into the ionogels was limited by the solubility of the zwitterion in the ionic liquid. Due to the hydrophilic nature of zwitterions, and the hydrophobicity of the ionic liquid, TFEMA monomer which is soluble in EMI TFSI was used as a compatibilising

agent to allow the zwitterion to dissolve. The solubility limit of the zwitterions used was found to be approximately 8 mol.% total zwitterion content. At this upper solubility limit, the zwitterion dissolved when a maximum molar ratio of 60:40 TFEMA to SBVI was used. Both SBVI and SBMI exhibited similar solubility limits, likely due to their similar chemical structures.

The bulk of this work concerns ionogels composed of a total copolymer content of 20 mol.%. This corresponds to 10-12 wt.% or 13-15 vol.%, depending on the copolymer ratio. These gels contained ~1-3 mol.% PETA-4 with varying ratios of TFEMA to zwitterion. Zwitterion molar contents were varied from 1 mol.% zwitterion to 7.5 mol.% zwitterion. **Table 3.1** shows the SBVI ionogel formulations that were made for the gels containing 20 mol.% total polymer content.

Ionogel opacity increased with zwitterion content; low zwitterionic contents led to transparent gels, while high zwitterion compositions resulted in translucent gels. This illustrates the favourability of the interactions between zwitterions as the translucence suggests a certain degree of zwitterion aggregation within the gel. Simulation studies have shown that zwitterions in ionic solutions experience competitive association between the charges of the zwitterionic molecules and the free ions in solution.[1] When the zwitterion content is increased, a higher frequency of dipole-dipole interactions between the zwitterionic molecules may cause aggregation.

This effect can be seen in **Figure 3.1** where the ionogel displayed on the left is a transparent 5 mol.% SBVI gel, while the gel shown on the right is a translucent 7 mol.% SBVI gel.

Table 3.1: SBVI ionogel formulations prepared with a total polymer content of 20 mol.%

Total SBVI Mol (%) Mol_{SBVI}/Mol_T	Total TFEMA Mol (%) Mol_{TFEMA}/Mol_T	Total PETA-4 Mol (%) $Mol_{PETA\text{-}4}/Mol_T$	Total Polymer (%) Mol_P/Mol_T
4.29	14.27	0.88	19.44
5.66	12.42	1.02	19.11
2.76	16.79	0.94	20.49
7.72	7.94	3.20	18.86
3.86	14.29	2.47	20.63
7.40	10.76	2.27	20.43
4.93	13.08	2.24	20.25
0.94	16.97	2.60	20.51
0.88	15.51	2.77	19.16
6.85	10.54	2.23	19.62
4.93	13.38	1.78	20.10
4.22	14.20	1.53	19.95
1.08	16.97	1.53	19.58
6.96	11.19	1.67	19.81
3.06	18.32	1.08	22.46
2.50	15.92	1.47	19.89
4.07	14.23	1.50	19.80
5.05	13.25	1.86	20.17
1.41	17.05	1.73	20.19
6.87	11.44	1.36	19.68

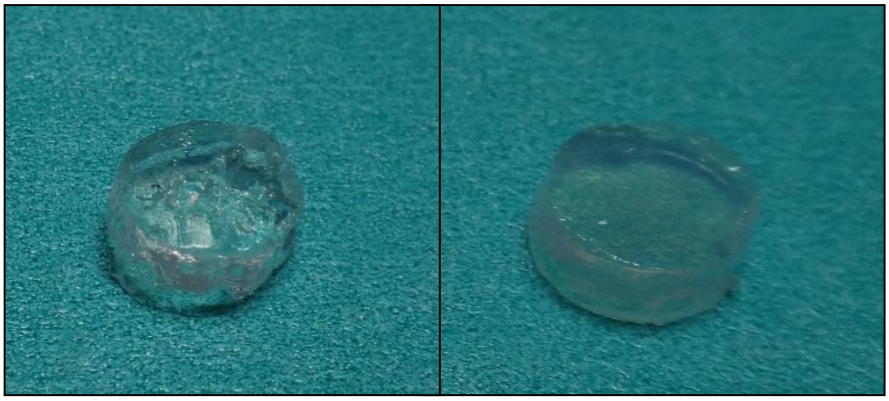

Figure 3.1: Increasing zwitterion content causes a decrease in transparency. A 5 mol.% SBVI gel (left), and a 7 mol.% SBVI ionogel (right).

Similar gel compositions were used for the SBMI-containing gels so as to more effectively compare the effects of the two zwitterions.

Table 3.2: SBMI ionogel formulations prepared with a total non-conducting material content of 20 mol.%.

Total SBMI Mol (%) Mol_{SBMI}/Mol_T	Total TFEMA Mol (%) Mol_{TFEMA}/Mol_T	Total PETA-4 Mol (%) $Mol_{PETA\text{-}4}/Mol_T$	Total Polymer (%) Mol_P/Mol_T
1.03	17.25	2.68	20.96
5.08	13.18	1.61	19.87
6.91	11.33	2.20	20.43
3.21	18.46	1.29	22.96
2.53	15.54	1.40	19.48
7.01	11.45	1.53	20.00
4.01	14.06	1.53	19.60
7.01	11.44	1.60	20.04

A visual comparison of the two different gels led to an immediate qualitative observation: the SBVI gels were significantly more stable than their SBMI counterparts. Evidence of this can be seen in **Figure 3.2** which shows SBVI and SBMI ionogels immediately after polymerisation, and one week later. The zwitterions in the SBMI gels formed clusters and phase

separated as the non-polymerisable zwitterions were free to move within the gel matrix. Over a large enough timescale (in this case, one week) the zwitterions were able to migrate within the gel and aggregate.

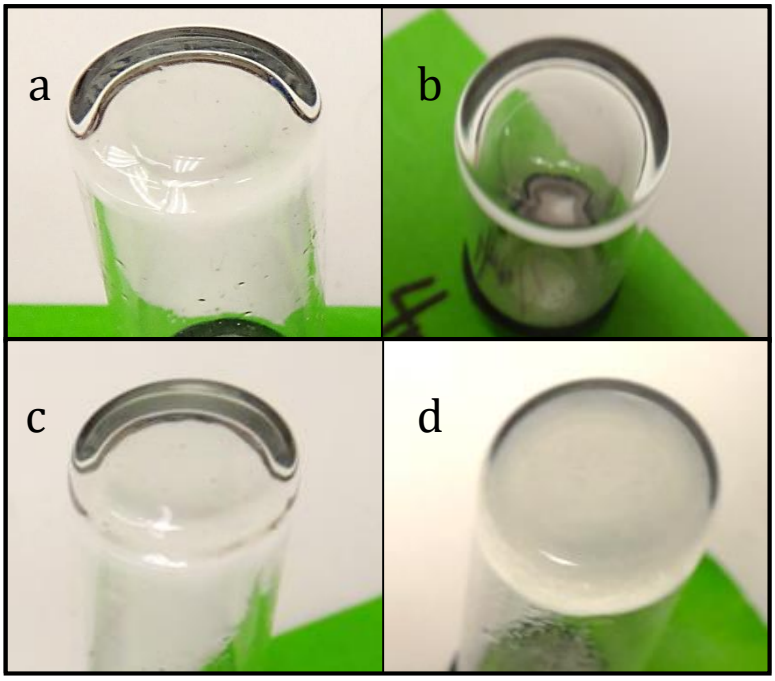

Figure 3.2: SBVI and SBMI ionogels immediately after polymerisation and one week later. (a) SBVI gel upon gelation, (b) SBVI gel after one week. (c) SBMI ionogel immediately after polymerisation, (d) SBMI gel one week later. SBMI gels phase separate, while SBVI gels remain stable.

3.3 Materials Characterisation Results and Discussion

3.3.1 Thermogravimetric Analysis

Thermogravimetric analysis (TGA) was conducted to determine whether there was a substantial amount of water contained within the zwitterionic starting materials and the zwitterion-containing ionogels. Additionally, TGA was used to estimate the degradation temperature of the

samples in order to demonstrate the temperature stability range of the ionogels made.

3.3.1.1 Thermogravimetric Analysis: SBVI Samples

To begin, the synthesised zwitterions were tested for water content as zwitterions are known to be very hygroscopic. Zwitterions were dried in a vacuum oven held at $50^{\circ}C$ subsequent to purification. Following this, they were tested using TGA. Water is an undesirable component of ionogels as it may plasticise ionic liquids by decreasing the viscosity, which could cause measured conductivities to appear higher. While at first glance this may seem to be beneficial, the presence of water decreases the electrochemical

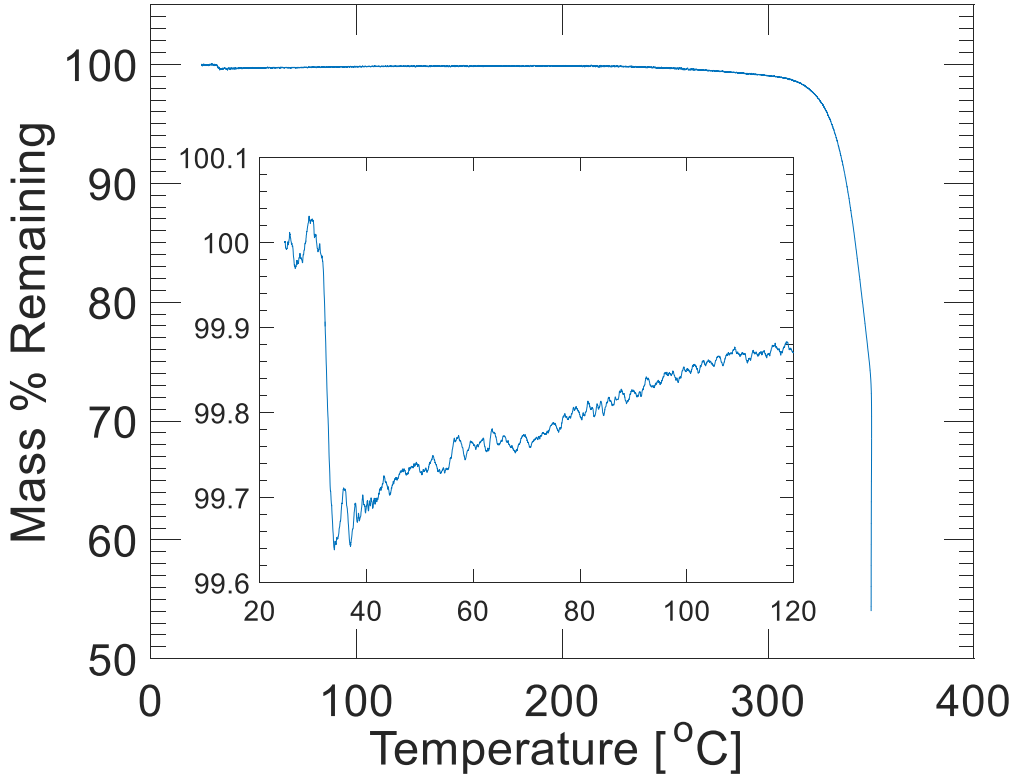

Figure 3.3: TGA thermograph of synthesised SBVI zwitterion. Inset shows the range below $100^{\circ}C$.

potential window of the electrolytic gel -an undesirable effect as it leads to a decrease in energy density. Hence, great care was taken to prevent water absorption within the zwitterions and the ionogels. As such, zwitterions were stored in a nitrogen-filled glove box.

As seen from **Figure 3.3**, synthesised SBVI showed no significant mass loss in the temperature range below $100^{\circ}C$, therefore, it can be concluded that the SBVI synthesised was free of unbound water. Due to the extreme hydrophilicity of the zwitterions, water molecules may still be present in the hydration shell of the zwitterions. Simply heating the sample

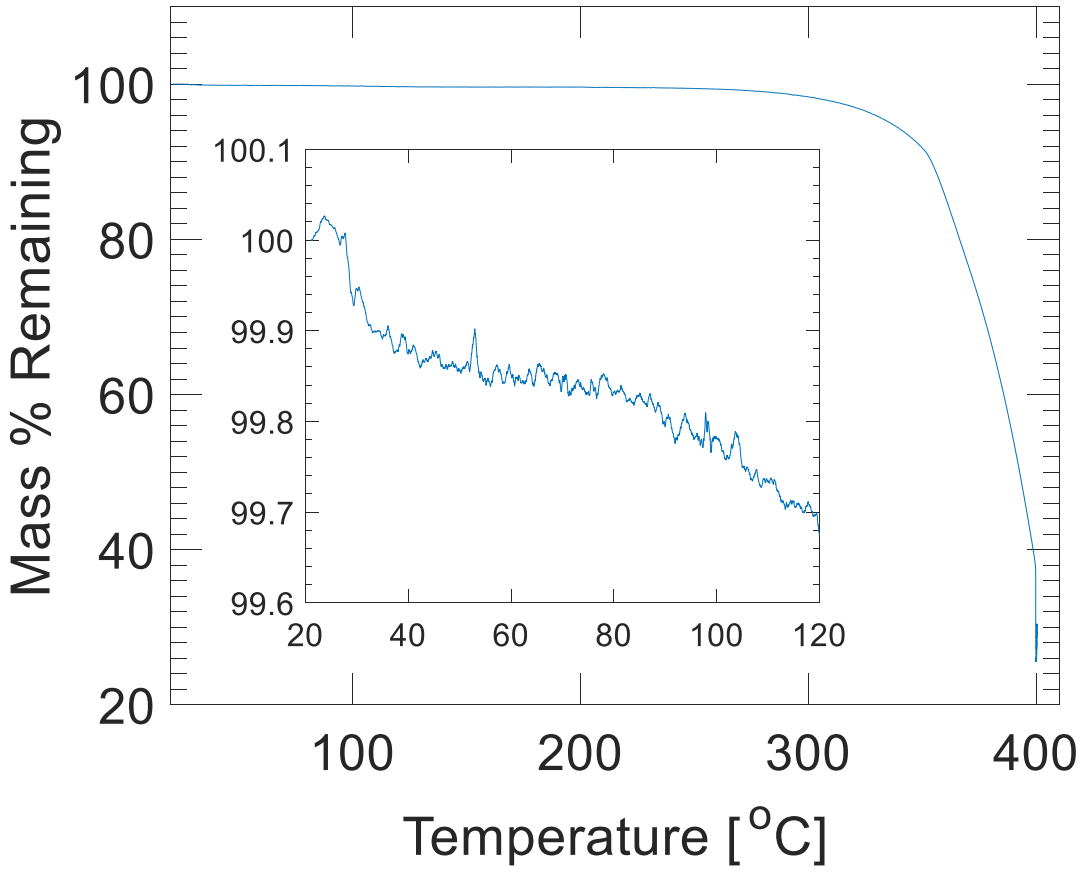

Figure 3.4: 1 mol.% SBVI gel thermograph. Inset shows the region below $100^{\circ}C$.

may not be adequate to release these bound molecules. Another observation from the plot above is that SBVI begins to degrade at approximately $310^{\circ}C$ which is close to the degradation temperature of the EMI TFSI ionic liquid used (over $400^{\circ}C$) relative to the degradation temperature of other ionogels reported [2-4]

Once SBVI ionogels were formulated, gels with a high and low composition of zwitterion were tested using thermogravimetric analysis to ensure the dryness of the gels. This allows the electrochemical data to be better contextualised during analysis.

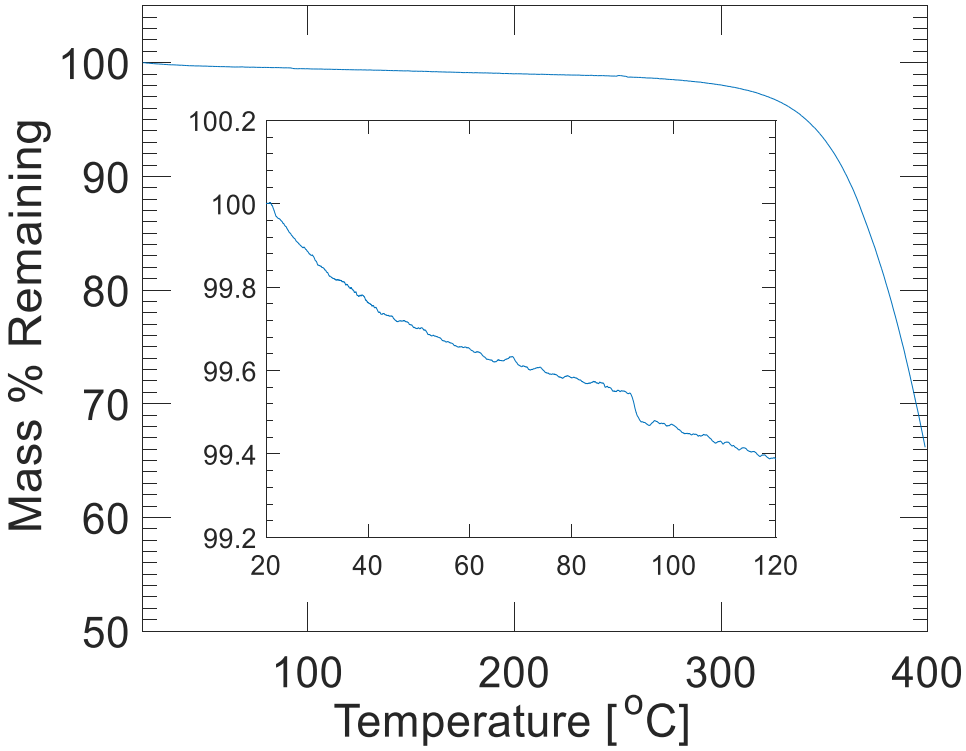

Figure 3.5: TGA thermograph of 7 mol.% SBVI ionogel. Inset enhances the region below $100^{\circ}C$

Looking at the two thermographs above, neither the 1 mol.% SBVI nor the 7 mol.% SBVI ionogels contained a significant amount of water within the gels. As can be seen from **Figure 3.4**, the sample tested displayed a total mass-loss of less than 0.25% below $100^{\circ}C$ with the majority of mass-loss (0.15%) occurring below $40^{\circ}C$. This suggests that there was some unpolymerised TFEMA monomer present in the ionogel as the boiling point of TFEMA monomer, according to Scientific Polymer Products, is $30^{\circ}C$.[5] The remaining mass-loss in this region may be attributed to water evaporation. Thus, the presence of free water can be thought to be negligible when offering analysis for future results, however, the existence of water molecules solvating the zwitterions cannot be discounted. At the beginning of the data collection range, the mass of the sample can be seen to be above 100%. This is attributed to building vibrations that appear as noise on TGA thermographs. Due to the sensitive nature of the balance, slight vibrations may affect the data recorded.

According to **Figure 3.5** the total mass-loss below $100^{\circ}C$ amounts to approximately 0.5% of the sample. Similar to the 1 mol.% sample, 50% of the mass loss can be considered to be due to unreacted TFEMA monomer with the remaining mass decrease due to water loss. This is considered a negligible amount of unbound water present in the sample and alone would not lead to significant plasticisation effects on the ionic liquid. Both the 1

mol.% and the 7 mol.% SBVI begin degrading at $310^{\circ}C$. This gives a large thermal stability range within which gels may be used.

3.3.1.2 Thermogravimetric Analysis: SBMI Samples

In order to ensure that the sulfobetaine methylimidazole (SBMI) synthesised was dry, *i.e.* free of unbound water, thermogravimetric analysis was used on the zwitterionic powder. As can be seen from **Figure 3.6**, the SBMI tested did not contain a significant amount of free water in the sample. All zwitterions were stored in a nitrogen glove box in order to maintain their dryness.

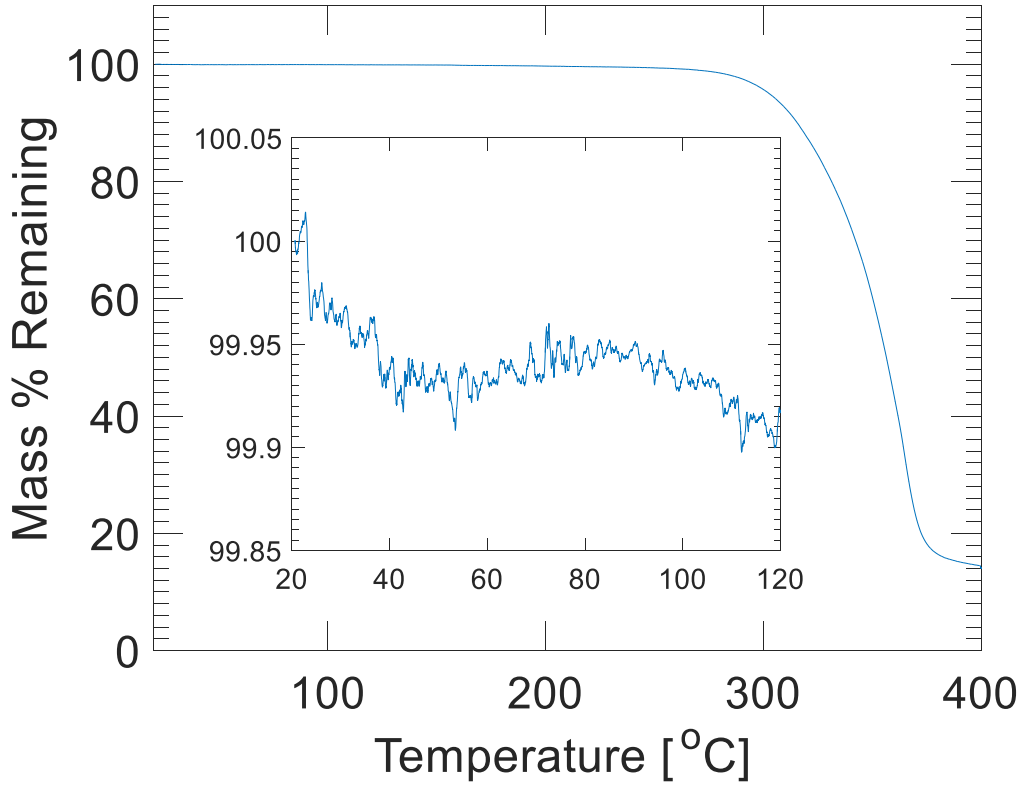

Figure 3.6: TGA thermograph showing pure SBMI additive.

Similar to the SBVI, the SBMI began to degrade at approximately $300^{\circ}C$. Although this is only slightly lower than the degradation temperature of SBVI, the SBVI zwitterion still offers a wider thermal stability window.

In the thermograph shown in **Figure 3.7**, 0.6% mass loss occurs below $60^{\circ}C$ in the 7 mol.% SBMI sample. This suggests that there was some TFEMA monomer present in the sample. Looking at the graph, approximately 50% of the mass loss in the region below $100^{\circ}C$ may be attributed to unreacted TFEMA monomer. The conclusion that arises from this analysis is that the amount of free water in the zwitterion-containing ionogel samples

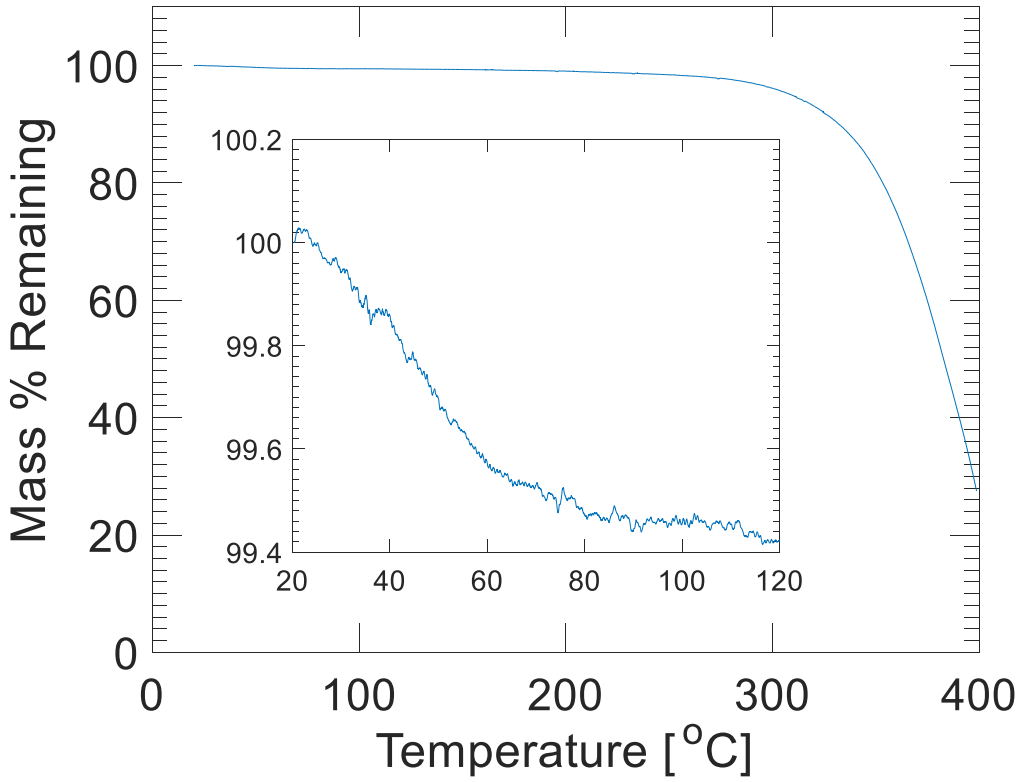

Figure 3.7: 7 mol.% SBMI ionogel. The majority of mass low below $100^{\circ}C$ occurs around $50^{\circ}C$.

produced is insignificant. Bulk sample degradation for the 7 mol.% SBMI ionogel occurred at $300^{\circ}C$.

3.3.2 Pulsed-Field Gradient Spin-Echo Nuclear Magnetic Resonance

Pulsed-field gradient spin-echo nuclear magnetic resonance (PGSE NMR) was used to empirically calculate the diffusion coefficients of the cation and anion in neat EMI TFSI, as well as in zwitterion-containing ionogels. NMR measurements were carried out within the temperature range of $289K - 291K$.

In order to measure the diffusivities, the signal attenuation was qualitatively adjusted to 90% by tuning the parameters δ and Δ; these parameters fell in the range of 7-10 ms and 200-500 ms, respectively. **Figure 3.8** and **Figure 3.9** depict a sample ^{1}H NMR overlay for a 2.5 mol.% SBVI ionogel at full scale and magnified, respectively. Looking at these figures, it can be seen that selecting the correct combination of values for the diffusion time, Δ and the pulse duration, δ yields a large attenuation in signal intensity at 2% and 95% gradient attenuation.

The diffusion coefficient of the ionic liquid cation was found by integrating the peak at 3.7 ppm in the ^{1}H spectrum, although all the protons on the cation resulted in the same diffusivity. The peak at 3.7 ppm is attributed to the methyl protons on the EMI cation.[6, 7]

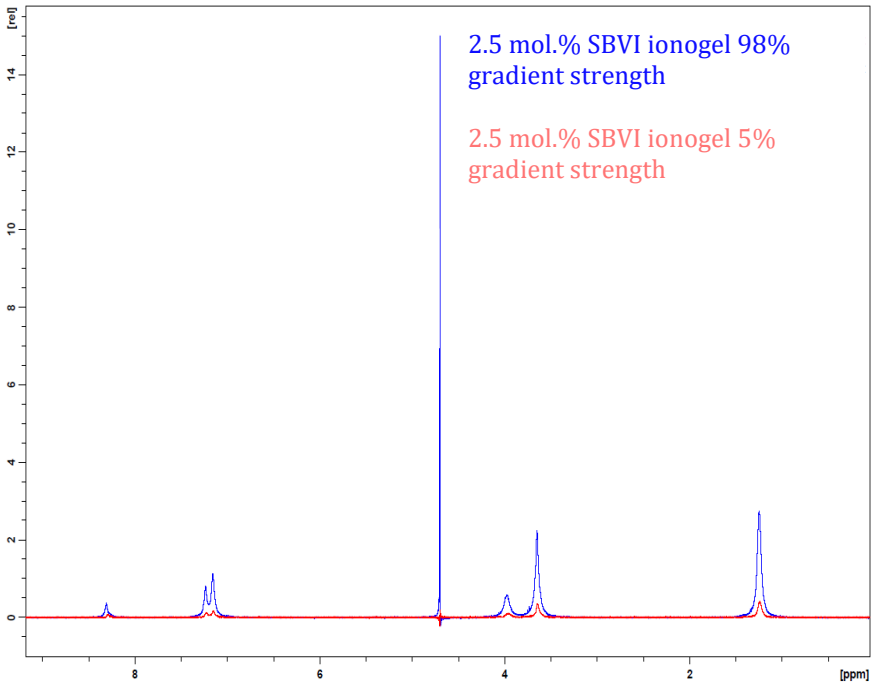

Figure 3.8: ^{1}H NMR overlay showing the 2.5 mol.% SBVI ionogels at 98% of the gradient strength (upper curve), and 5% of the gradient strength (lower curve).

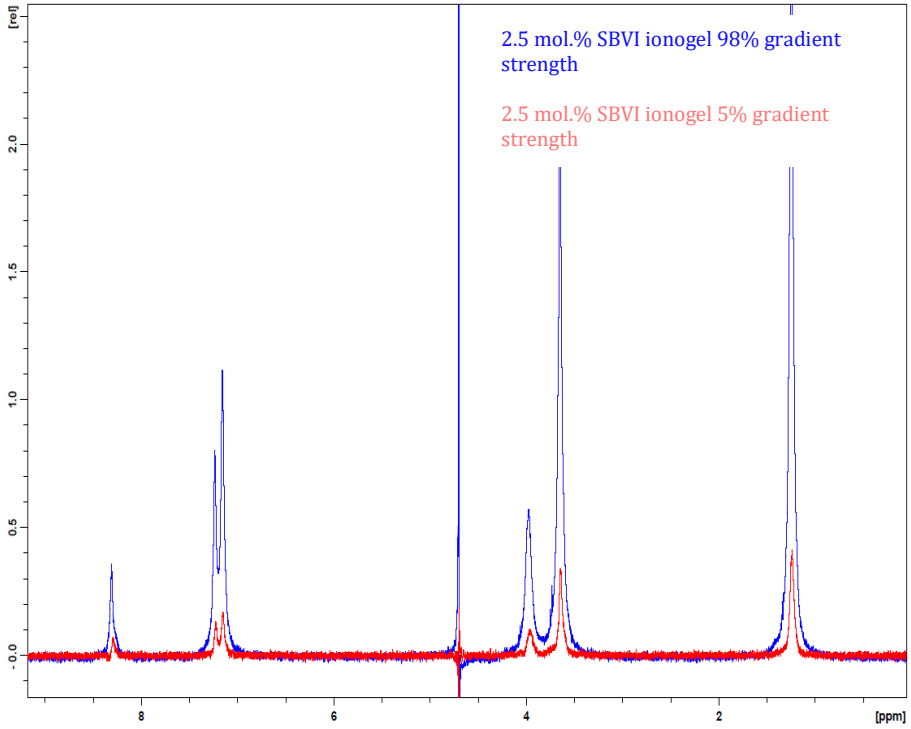

Figure 3.9: Magnified ^{1}H NMR overlay showing the 2.5 mol.% SBVI ionogels at 98% of the gradient strength (upper curve), and 5% of the gradient strength (lower curve).

Similarly, signal attenuation was tuned for each sample when recording ^{19}F NMR spectra. It should be noted that the optimised values found when tuning the proton spectra were not always consistent with those used for the fluorine spectra as different values were often needed to provide adequate signal attenuation. Due to the symmetric structure of the TFSI anion, the ^{19}F NMR spectrum only yielded one peak which accounts for all the fluorine atoms on the molecule.[6]

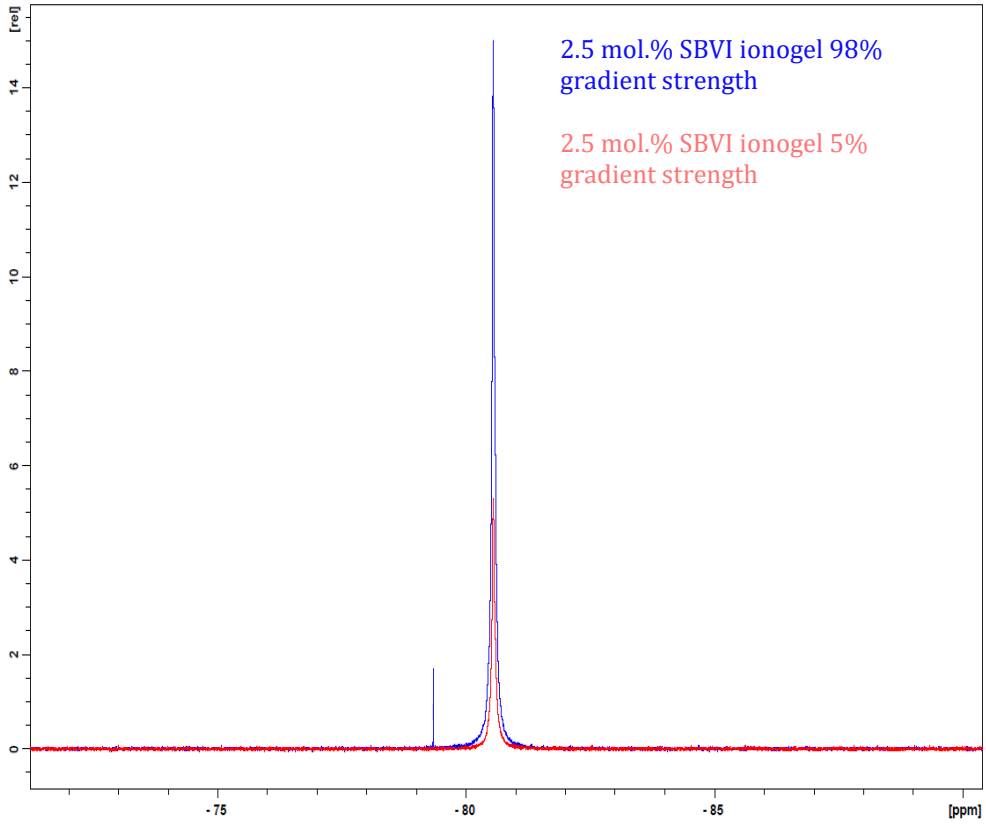

Figure 3.10: ^{19}F NMR overlay showing the 98% gradient strength (upper curve) spectrum and the 5% gradient strength spectrum (lower curve).

Once the diffusion time and pulse duration parameters were optimised in the 1-D spectra, a two-dimensional NMR diffusion programme was used, as outlined in section 2.3.1, and a 2-D dataset was generated. From this, the attenuation in signal intensity is plotted according to Equation (2.4),

repeated here for convenience. In the equation S(2τ) is the attenuation after a 2τ period, $S(2\tau)_{g=0}$ is the attenuation in the absence of pulse gradients, γ is the gyromagnetic ratio, D is the diffusion coefficient, g is the gradient strength, δ is the duration of the magnetic pulse, and Δ is the delay time.

$$\ln(E) = \ln\left(\frac{S(2\tau)}{S(2\tau)_{g=0}}\right) = -\gamma^2 D g^2 \delta^2 \left(\Delta - \frac{\delta}{3}\right) \quad (2.4)$$

The NMR software through the Diffusion Ordered Spectroscopy (DOSY) method generates a curve in the T1/T2 relaxation programme showing intensities against absolute gradient strengths in G/cm. The curve is fitted to the equation above, and diffusivities for all integrated peaks are provided.

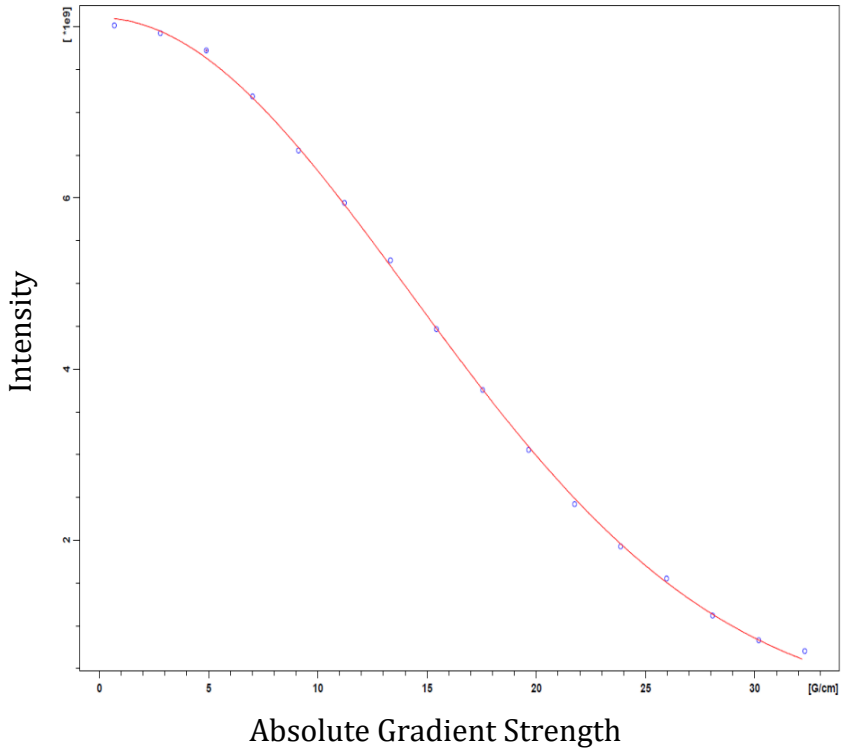

Figure 3.11: DOSY programme-generated curve showing intensities versus absolute gradient strength. These data are fit to give diffusivity values

The diffusivity value obtained from PGSE NMR is an apparent diffusivity; it is a weighted sum of the diffusivities of free ions, as well as paired or clustered entities, as seen in Equations (3.1) and (3.2), where φ is the fraction of ions dissociated and D_i refers to the diffusion coefficient of species *i*.

$$D^{+}_{NMR} = \varphi D^{+}_{free} + \left(1-\varphi\right) D_{pair} \qquad (3.1)$$

$$D^{-}_{NMR} = \varphi D^{-}_{free} + \left(1-\varphi\right) D_{pair} \qquad (3.2)$$

It was previously postulated that zwitterions act as ion-dissociators in ionic liquids which could lead to improved ionic conductivities. This was based on results pioneered by the MacFarlane and Ohno groups where the addition of zwitterions in lithium salt electrolytes led to marginally improved electrochemical properties, including ionic conductivities.[8-14]

Apparent NMR diffusivities of the ionic liquid cation and anion were plotted versus zwitterionic molar percentages in an attempt to determine the effect zwitterions have on the mobility of diffusing species in zwitterion-containing ionogels and their precursors.

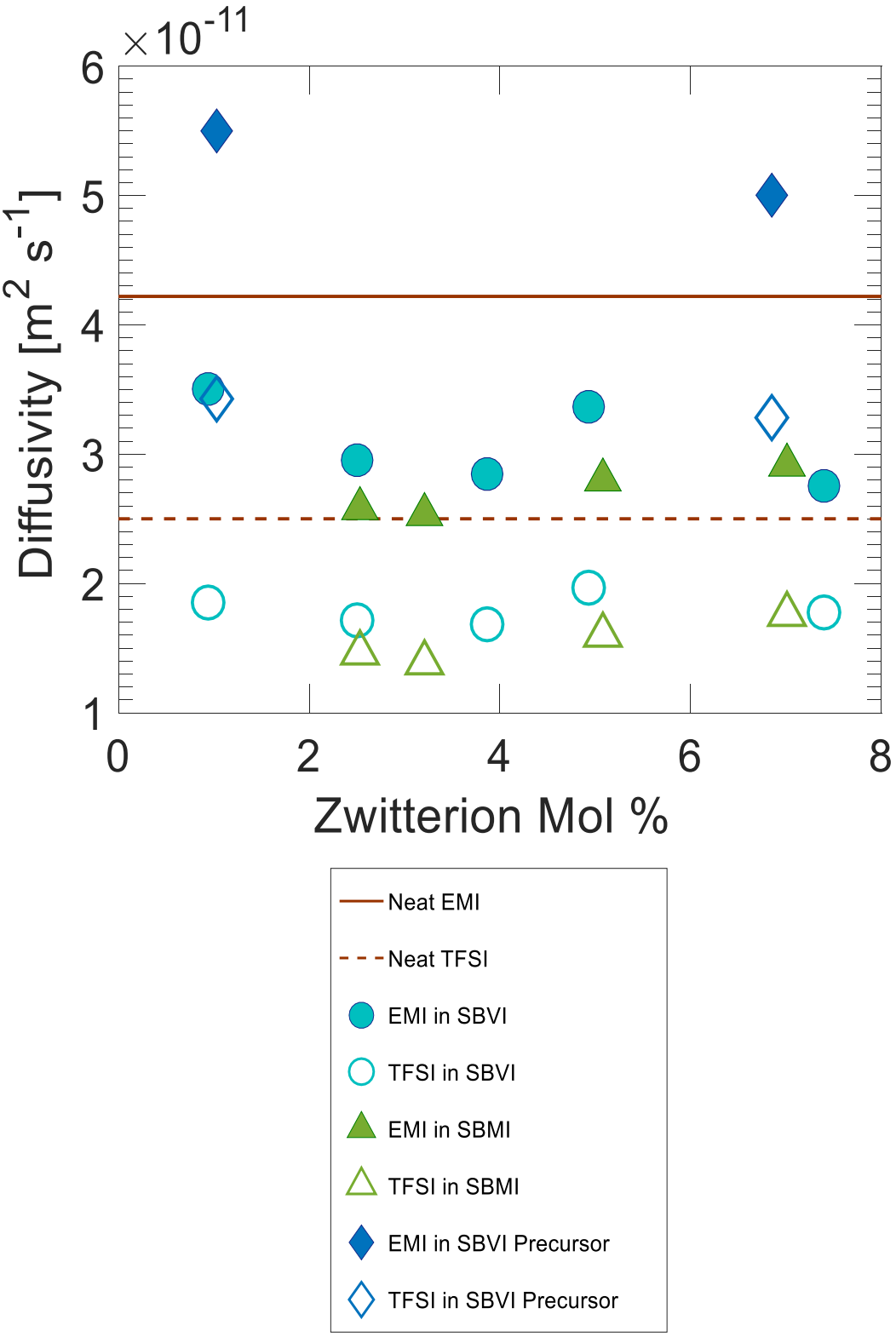

Figure 3.12: Apparent NMR diffusivities for Neat EMI TFSI, SBVI and SBMI ionogels, and SBVI ionogel precursor solutions. The graph legend is shown underneath. The neat EMI and TFSI data are shown as horizontal solid and dashed lines for convenience of comparison.

As can be seen from the above figure, the measured diffusivities of the ionic liquid cation and anion in zwitterion-containing ionogels are lower relative to the neat liquid. This may be attributed to the presence of the cross-linked polymer scaffold causing a decrease in ion mobility in the gels. Equations (3.1) and (3.2) show that the free ion diffusivities may not be de-convoluted from those of the clustered and paired species. It can be assumed, however, that the mobility of the free ions is not significantly affected by the presence of the polymer due to their small sizes. Thus, the diffusivities of the free anion and cation are approximately constant between the neat liquid and the gel. If this is taken to be true, then the addition of zwitterions to the system may likely increase ion dissociation (φ in Equations (3.1) and (3.2)) because gel formation would be expected to decrease the mobility of the larger paired or clustered ions (D_{pair} in Equations (3.1) and (3.2)) and the apparent diffusivities of both the cation and anion are not a function of zwitterion content, **Figure 3.12**. As will be discussed in Section 3.5, the constant apparent diffusivities with increasing zwitterion content are also consistent with the increase in elastic modulus that is observed upon the increase in zwitterion content.

The apparent diffusion coefficient of the cation is always larger than that of the TFSI anion, as shown in **Figure 3.12**. Molecular dynamics have shown that this is due to the structure of the ions -planar EMI cations move faster in the ionic liquid (and gel) than their linear anionic counterparts.[15, 16]

Planar ions are able to glide through the liquid, while linear ions experience more turbulent motion when moving through the liquid.

Comparing the SBVI ionogels with the SBMI ionogels, the diffusion coefficients associated with SBVI ionogels were found to be larger than those for the SBMI gels. Once again, this may be related to the elastic moduli of the respective ionogels. From the elastic modulus data, it was inferred that non-polymerisable SBMI zwitterions acted as nanofillers in the ionogels. This implies the presence of zwitterionic clusters in the ionogels which would cause a decrease in zwitterion-ionic liquid interactions due to the decreased zwitterion accessibility. Therefore, SBMI zwitterion-containing ionogels would have fewer dissociated ions relative to SBVI ionogels with the same zwitterion content.

Precursor solution diffusivities were measured for a 1 mol.% and a 7 mol.% SBVI ionogel. In both cases, cation and anion diffusivities were found to be significantly higher than their respective gel diffusivities, and slightly higher than neat ionic liquid ion diffusivities. This could be because, relative to the neat liquid, the zwitterion-containing ionogel precursor solutions contain a larger proportion of free ions. So, improved ion dissociation in combination with increased mobility, relative to the ion mobility in the gels could lead to increased apparent diffusivities. It is important to note that while precursor ion diffusion coefficients were recorded as higher than neat IL and ionogel diffusivities, these measurements were taken at a slightly

elevated temperature (291K) than ionogel and neat IL measurements (289K) which would have resulted in larger diffusion coefficients. This was done because the temperature of the instrument could not be reliably controlled at temperatures close to room temperature. Using an estimated activation energy of cation diffusivity measured by another group member (Anthony D'Angelo) of 26 kJ/mol, however, the maximum difference in apparent diffusivity was found to be only approximately 7 %. Hence, the apparent diffusivity values of the precursor solutions are still clearly greater than the neat ionic liquid values.

Furthermore, the percentage increase in the apparent diffusion coefficients for the precursor solution cations and anions, relative to neat EMI TFSI, is approximately 30% and 36%. Literature results have indicated that roughly 63% of ions in neat EMI TFSI are dissociated, so an increase in apparent ion mobility may suggest an increase in the presence of free ions. Applying this percentage increase to the assumed percentage of neat free ions, an approximate ion dissociation of 82-86% is calculated. Hence, the increase in apparent diffusivity observed for the precursor solutions is still within the bound of reasonability.

Larger diffusion coefficients observed for the zwitterion-containing ionogel precursor solutions, relative to their gel counterparts, may reflect higher ion mobility as well as an increase in the fraction of ions dissociated. It can be assumed that free ions have higher mobility when compared with

paired or clustered ions due to their smaller size, therefore, a higher proportion of free ions moving faster within the precursor due to the lack of polymer chains leads to a larger apparent diffusion coefficient relative to the gel.

3.4 Mechanical Characterisation Results and Discussion

In order to determine the elastic modulus, E, of the zwitterion-containing ionogels developed, a dynamic mechanical analyser (DMA) was used. Ionogels were polymerised between glass slides in PTFE spacers with a thickness of 3.2 mm, an inner diameter of 6.35 mm, and an outer diameter of 13.2 mm. Once polymerised, gels were carefully removed from the spacers and compression tested in free-extension mode. Since the ionogel dimensions were well-defined, a stress-strain curve was able to be generated. The slope of the linear portion of the stress-strain curve was calculated to yield the elastic modulus.

Figure 3.13 shows a sample stress-strain curve for a 4 mol.% and a 5 mol.% SBVI ionogel. As can be seen from the graph, the 5 mol.% ionogel has a steeper slope, and therefore a higher elastic modulus. Similarly, **Figure 3.14** compares a 4 mol.% SBVI ionogel to a 4 mol.% SBMI ionogel in a stress-strain curve. The SBVI ionogel has a significantly steeper slope when compared with the SBMI gel of the same non-ionic liquid content, indicating that SBVI-containing ionogels were stiffer. When determining the slope to calculate the elastic modulus, only the data between 1 and 10% strain were

used in order to avoid the minor fluctuations that occur at the beginning of the test.

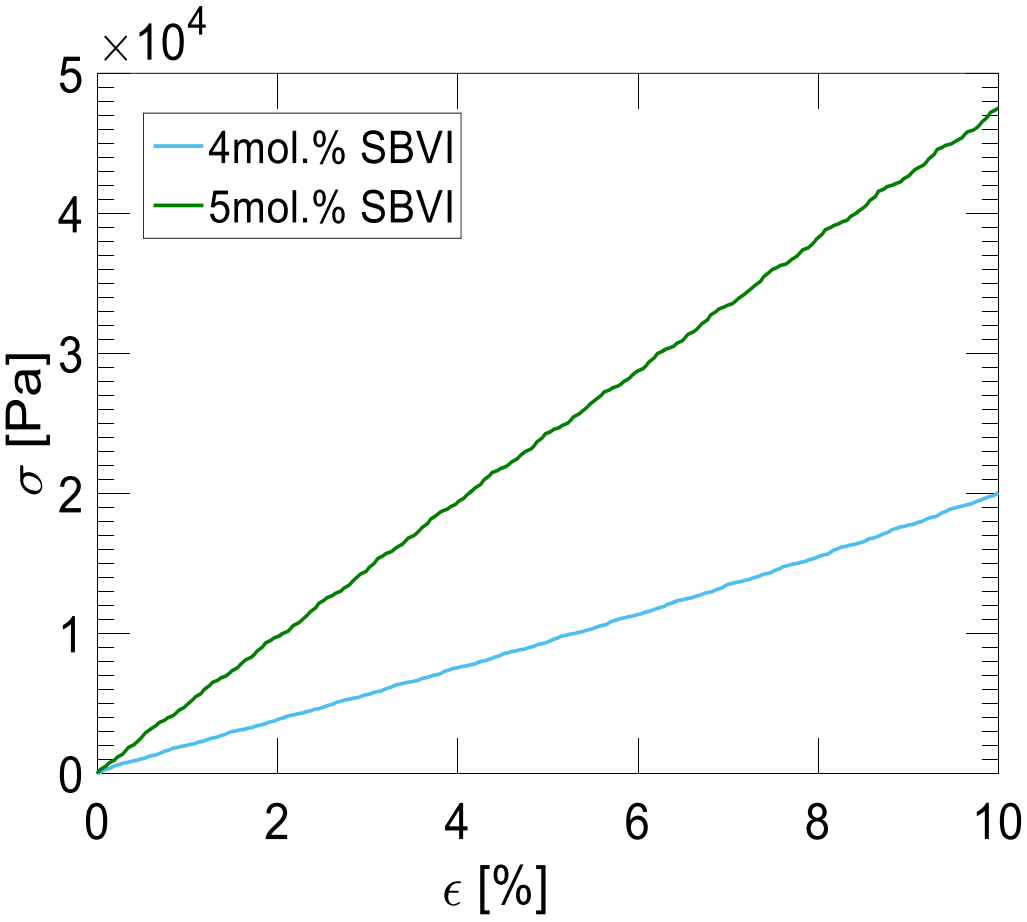

Figure 3.13: Stress-strain curves comparing a 5 mol.% (upper curve) and a 4 mol.% SBVI ionogel (lower curve).

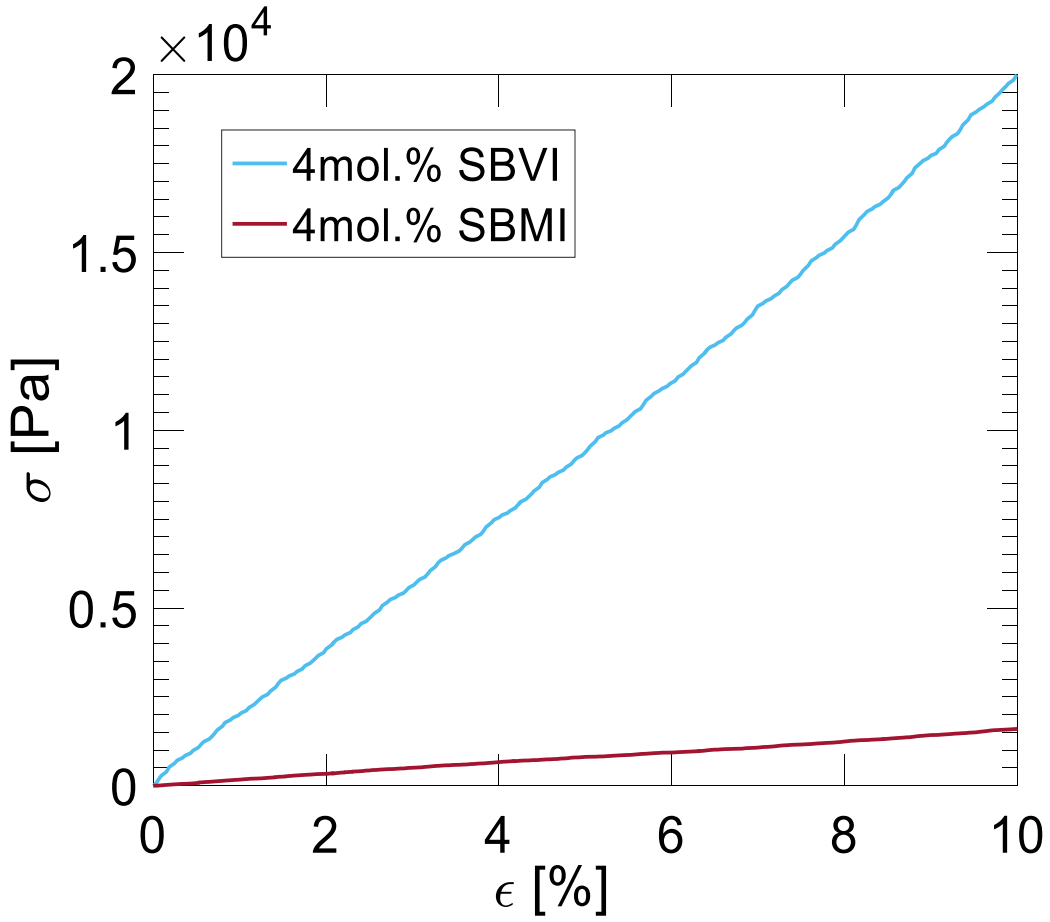

Figure 3.14: Stress-strain curve of a 4 mol.% SBVI ionogel (upper curve) and a 4 mol.% SBMI ionogel (lower curve).

As can be seen from **Figure 3.15** increasing the ratio of SBVI to TFEMA while maintaining the total polymer content at 20% on a mole basis results in a significant increase in the modulus. The 1 mol.% SBVI sample is shown to have a comparable modulus to the sample containing 20mol% of the TFEMA-co-PETA-4 copolymer. This suggests that the increase in modulus is solely due to the increase of the zwitterionic component in the gel. This phenomenon may arise due to the self-assembly of the zwitterionic moieties

within the gel (**Figure 3.16**), caused by attractive dipole-dipole interactions between the zwitterions. Bengani *et al.* proposed a structure for sulfobetaine methacrylate-*co*-trifluoroethyl methacrylate based on zwitterionic self-assembly. It was stated that upon assembling, this copolymer forms bicontinuous hydrophilic zwitterionic channels with approximate pore sizes of 1 nm, and hydrophobic domains occupied by the hydrophobic TFEMA groups.[17] In light of this, one possible architecture for the SBVI-*co*-TFEMA could be ordered nano- to microphase domains of zwitterionic polymer separated from *p*TFEMA. In this way, zwitterions experience increased dipole-dipole interactions which in turn causes an increase in elastic modulus on a macroscopic scale. Previous reports have shown that gelation upon addition of zwitterionic groups is possible via zwitterion-zwitterion interactions.[12, 18]

Although the morphology discussed by Bengani *et al.* is perceived in a hydrophilic aqueous environment, the increase in elastic modulus with increasing zwitterion content indicates some ordering and attractive forces of and between the zwitterions. Due to their hydrophilic nature, it seems apparent that the zwitterions would preferentially interact with one another to minimise their interactions with the hydrophobic ionic liquid. Their confinement to the polymer backbone, however, prevents severe zwitterion migration which would result in smaller ordered domains.

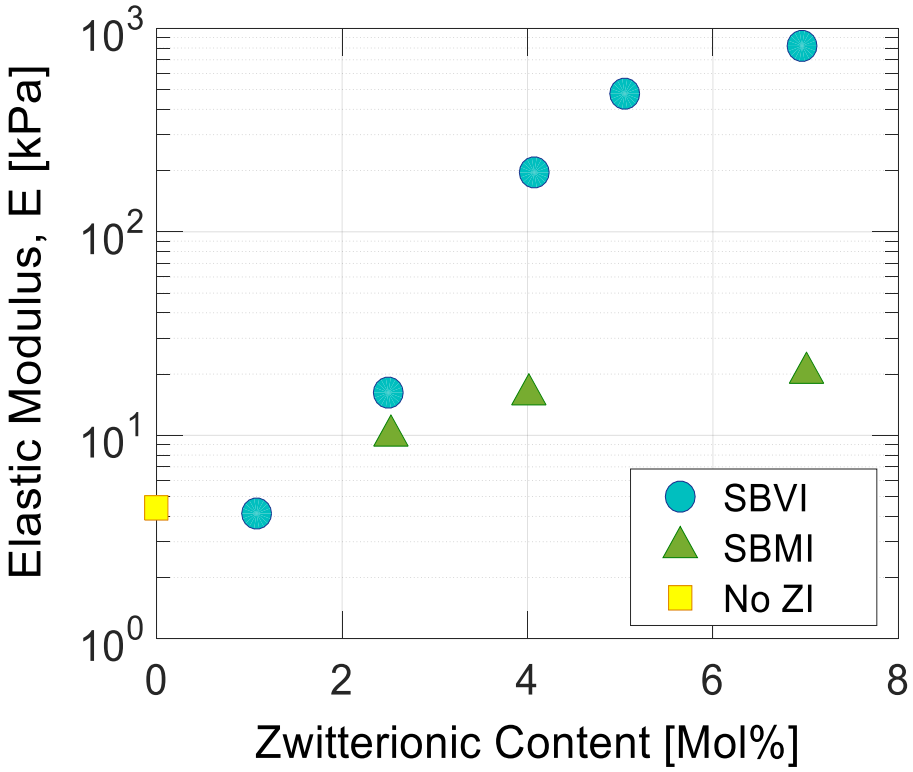

Figure 3.15: Moduli of SBVI ionogels, SBMI ionogels, and an ionogel containing no zwitterion as a function of zwitterion molar content. All ionogels contained 80 mol.% ionic liquid

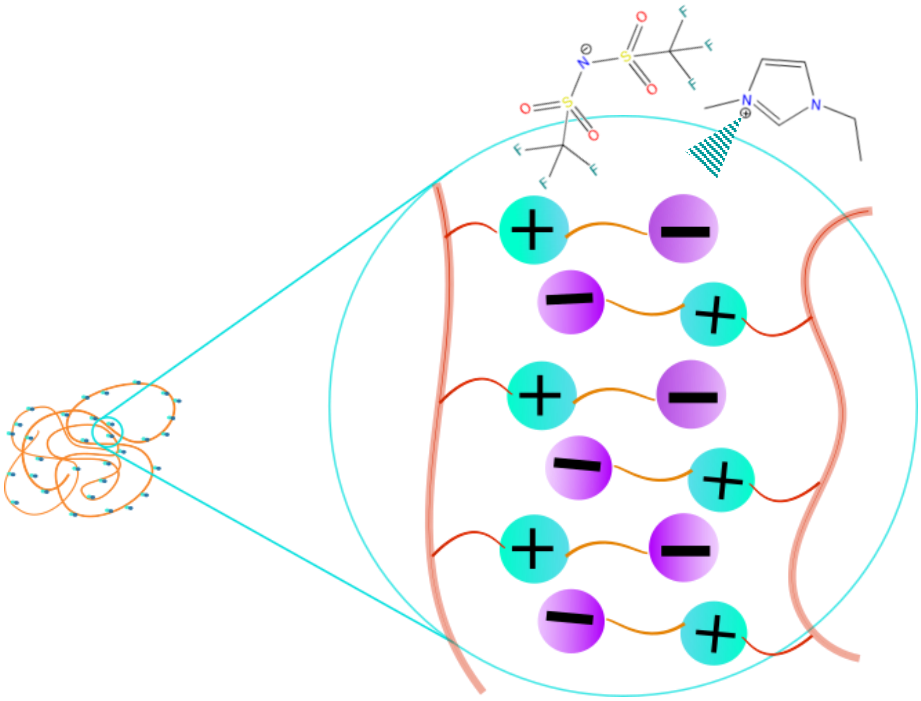

Figure 3.16: Schematic representation of SBVI zwitterionic self-assembly within the zwitterion-containing ionogels.

Although the SBMI ionogels exhibit an increase in elastic modulus with increasing zwitterion content, the increase is not as dramatic as in the case of SBVI. Since the SBMI zwitterionic additive is not polymerisable, it is expected to form nanoclusters or physical crosslinks in the ionogel, as opposed to nanochannels held together through dipole-dipole interactions. This may be akin to adding nanofillers or nanoparticles to ionic liquids where the resulting gels are more like viscous liquids held together through physical interactions than rigid, chemically cross-linked gels. In this particular case, the presence of the zwitterions led to an increase in elastic modulus due to the nanoparticle effect acting in conjunction with the chemically cross-linked TFEMA-*co*-PETA-4 copolymer. In the SBMI zwitterion-containing ionogels, the amount of non-conducting materials that comprised the gel was kept constant on a molar basis. The ratio of TFEMA to SBMI was altered in order for this to remain true, but the total amount of chemical cross-linker used was held at 1.5 mol.%. Thus, since there is an overall decrease in polymer content, the increase in modulus is shown to be solely due to the nanofiller effect observed upon the aggregation of SBMI zwitterions.

SBVI zwitterions were unable to migrate within the gel and cluster as they were tethered to the polymer scaffold. Therefore, it is reasonable to assume that SBVI dipole-dipole interactions led to interdigitation as opposed to clustering. That is, the zwitterions were able to associate their charged moieties complementarily to one another, but only to other charged groups

which were already in close proximity as all zwitterions were largely held in place by the polymer backbone. Comparing the data for both zwitterions, one of which was able to be incorporated into the polymer structure chemically led to the conclusion that containing the zwitterion additives in the polymer scaffold allows for improved mechanical properties and long-term stability.

3.5 Electrochemical Characterisation Results and Discussion

3.5.1 Ionic Conductivities

3.5.1.1 Zwitterion-Containing Ionogels at 80 mol.% Ionic Liquid Loading

Zwitterions have been proposed in this thesis as a means to improve the electrochemical properties of polymer supported ionogels. In order to test this hypothesis, alternating current (AC) impedance spectroscopy measurements were taken in order to quantify the ionic conductivity. This section concerns gels made with a total ionic liquid loading of 80 mol.%.; the SBVI-containing ionogels contained a total polymer content of 20 mol.%, while the SBMI ionogels consisted of a predetermined percentage of SBMI with the remainder of non-ionic liquid materials consisting of a TFEMA-*co*-PETA-4 copolymer. **Figure 3.17** and **Figure 3.18** depict raw impedance data in a magnitude of impedance plot for a representative neat IL, 2.5 mol.% SBMI ionogel, and 2.5 mol.% SBVI ionogel. The magnified impedance plot, **Figure 3.18**, shows the high-frequency portion, which is characteristic of the resistive properties of the materials. It can clearly be seen that the neat IL is

the least resistive, followed by the SBVI ionogel, and the SBMI ionogel. From this, it is inferred that the addition of zwitterions does not negate the effect of replacing some of the ionic liquid in a given ionogel volume with non-conducting materials.

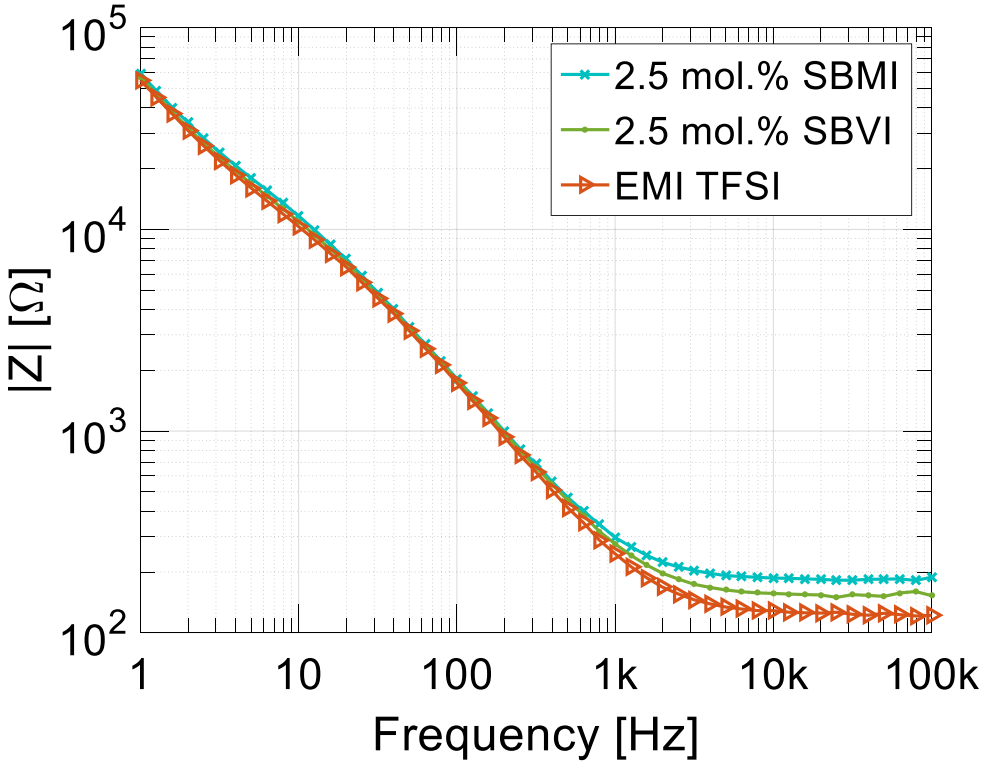

Figure 3.17: Sample raw impedance plot showing data for neat EMI TFSI, a 2.5 mol.% SBMI ionogel, and a 2.5 mol.% SBVI ionogel.

It has been suggested that zwitterions introduce competitive association between ions and zwitterionic charges in aqueous salt solutions due to their high polarity. In a molecular dynamics simulation study conducted by Shao *et al.*, interactions between sulfobetaine groups and cations were found to follow the Hofmeister series; that is to say, sulfobetaines associated more strongly with smaller Li^+ cations and relatively

weakly with larger Cs^+ cations and Br^- anions.[1] Extrapolating this analysis to ionic liquids where the ions are considerably larger than the salts used in the simulation studies, and the electrostatic interactions between the ionic liquid ions are significantly weaker, it may be the case that the presence of zwitterions in ionic liquids promotes a competitive environment in terms of electrostatic interactions where intra ionic liquid interactions are indistinguishable from or outshone by zwitterion-ionic liquid interactions. Due to the presence of the polymer and the reduced concentration of ionic liquid ions, however, an increase in ionic conductivity is not observed.

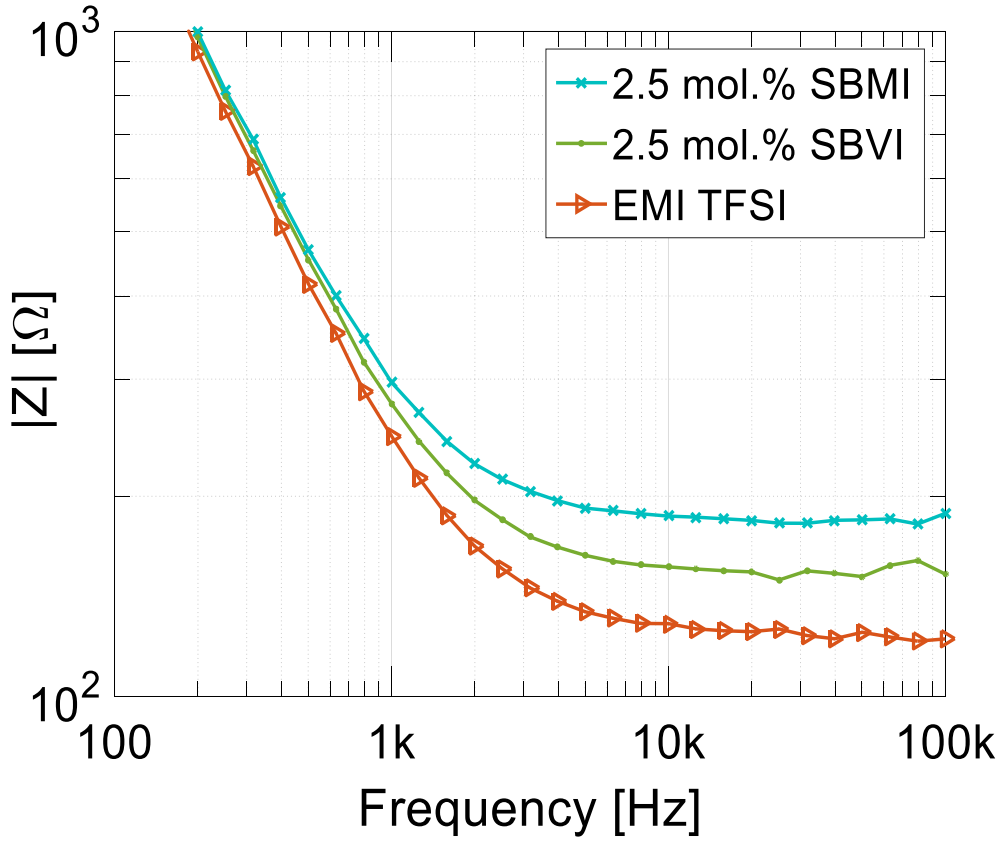

Figure 3.18: Magnified impedance plot of neat EMI TFSI, a 2.5 mol.% SBMI ionogel, and a 2.5 mol.% SBVI ionogel. Neat EMI TFSI is the least resistive, while the SBMI ionogel is the most resistive.

Low zwitterion-content ionogels did not exhibit higher ionic conductivities relative to the neat ionic liquid or a TFEMA-based ionogel at a 20 mol.% polymer loading. However, increasing the zwitterion concentration while maintaining the total polymer content did not result in the lower conductivities one would expect due to increased elastic modulus. In fact, as seen from **Figure 3.19**, the conductivity of zwitterion-containing ionogels at 80 mol.% ionic liquid content is relatively constant with increasing zwitterion content.

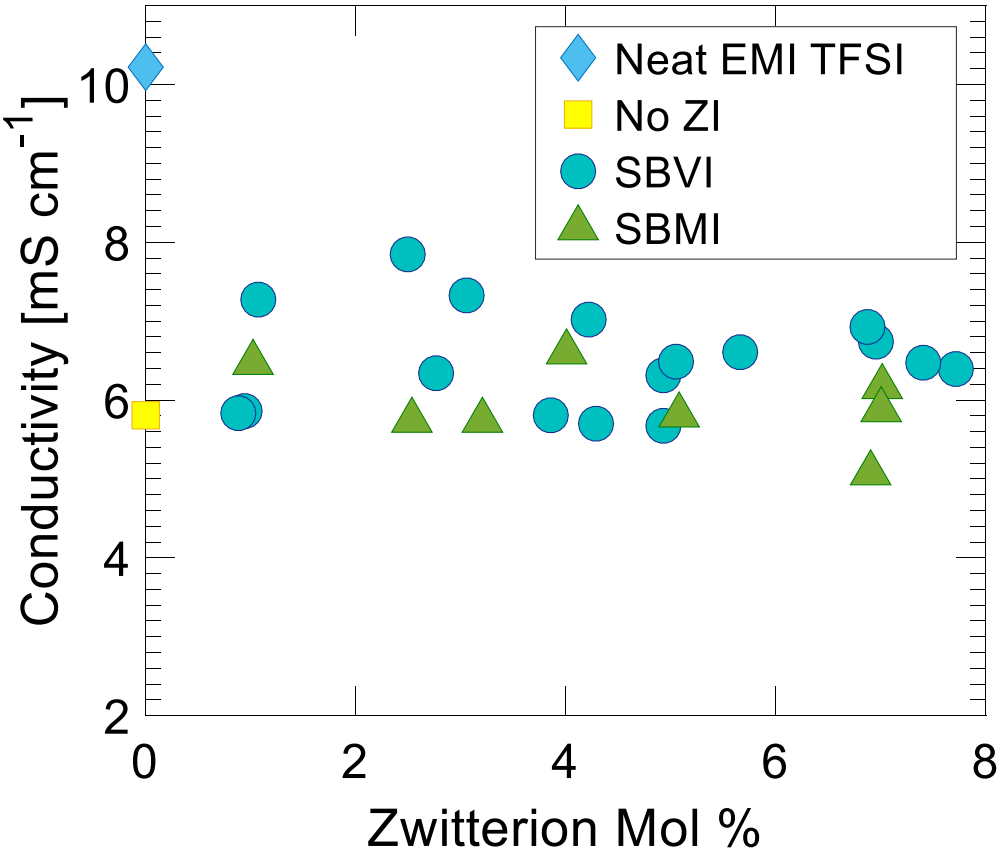

Figure 3.19: Ionic conductivities of zwitterion-containing ionogels relative to neat EMI TFSI and an ionogel containing no zwitterion. All gels contained 80 mol.% IL.

As zwitterions are expected to increase the fraction of ions dissociated, it is expected that increasing the zwitterion loading in the gels would result in higher observed conductivities. Recalling that increasing zwitterion content led to a higher elastic modulus, however, these ionic conductivity results may be better contextualised. The more ordered gels would hinder ion movement, causing a decrease in ion mobility. Accordingly, despite an increase in free ions, overall ion mobility is reduced due to the polymer network, as well as the assembled zwitterion groups.

From the elastic modulus data, it was clear that SBVI ionogels were able to achieve higher moduli for the same zwitterion loading when compared with SBMI ionogels. The explanation given for this observation was that SBVI zwitterions were attached to the scaffold, and were therefore tethered in place, causing them to self-assemble into ordered channels. From the ionic conductivity data shown in **Figure 3.19**, it can be assumed that the self-assembly of the zwitterionic groups decreases ion mobility. The diffusivity data shown in **Figure 3.12** further support this explanation as the diffusion coefficients of the gels were found to be independent of zwitterionic content. In spite of having more free ions contained within the gels, the decrease in mobility caused by the SBVI self-assembly led to lower-than-expected observed conductivities.

In a similar trend, the SBMI ionogel conductivities also did not change with increasing zwitterion content. SBMI ionogel conductivities, however,

were slightly lower than the calculated SBVI ionogel conductivity data. The elastic modulus of SBMI ionogels was consistently lower than that of the SBVI ionogels due to the formation of nano- and microclusters. Non-polymerisable SBMI zwitterions were able to move within the ionogels (evidenced by **Figure 3.2**) and self-aggregate, reducing the ability of the charged moieties of the ionic liquid to interact with the zwitterions within the aggregate. Hence, while zwitterions may increase the fraction of free ions within the ionogel, covalently attaching the zwitterions to the polymer scaffold allows for improved conductivities as zwitterions are prevented from clustering.

Typically, in order to increase the elastic modulus of a polymer-based ionogel system, the ionic liquid must be replaced with increasing amounts of the scaffold material, for a given ionogel volume. This reduction in ionic liquid present within the sample leads to a lower ionic conductivity. Additionally, with increasing polymer content, ion mobility is further impeded which contributes to the lower conductivities observed.

Figure 3.20 compares elastic modulus data as a function of ionic conductivity for crosslinked TFEMA ionogels[7] with SBVI ionogels. In the case of the gels that do not contain zwitterion, the conductivity decreases significantly (approximately 55% over a range of 1MPa). The SBVI ionogels, however, are shown to yield relatively constant conductivity values for the elastic modulus range shown.

This noteworthy result can be attributed to the high ionic liquid content within the zwitterion-containing ionogels. Due to the dipole-dipole crosslinks between the zwitterionic moieties, the elastic modulus may be tuned while allowing for a high concentration of ionic liquid. Conversely, for the TFEMA ionogels shown, the modulus was increased by increasing the polymer content within the ionogels. Thus, in order to create a stiffer gel in this system, a lower ionic liquid loading must be used.

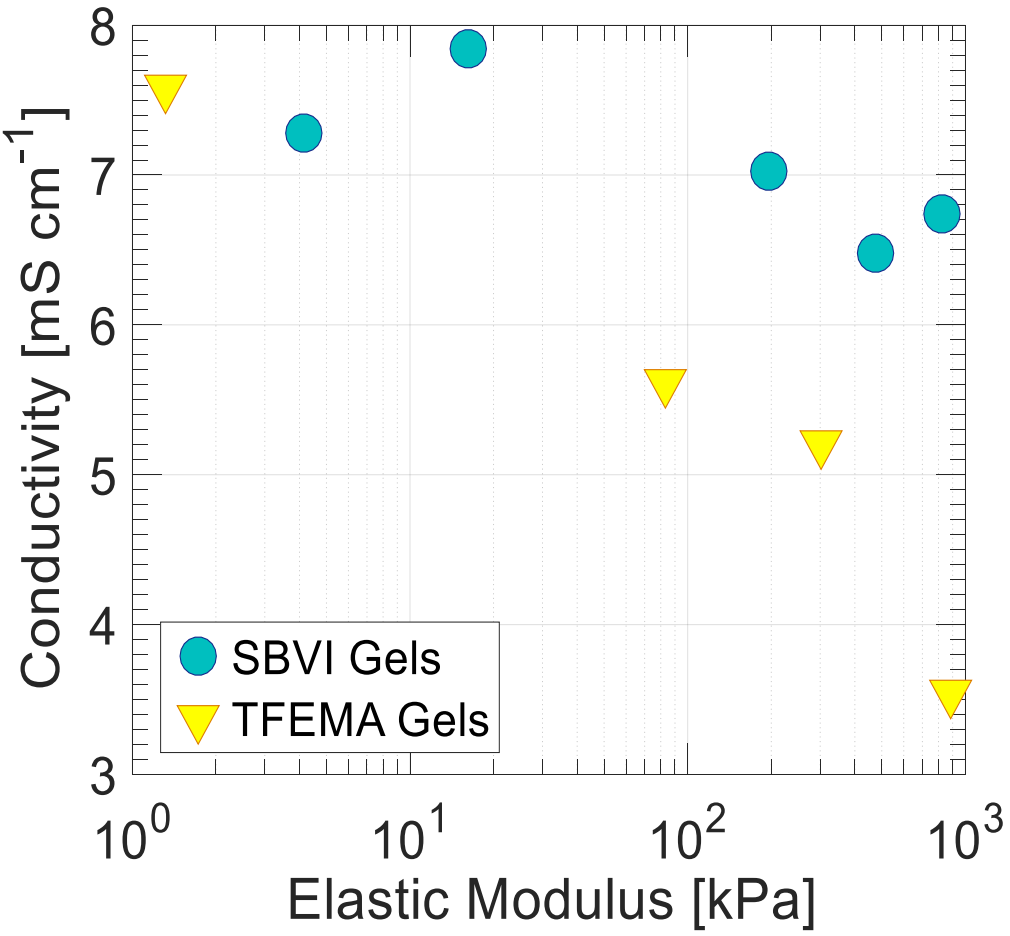

Figure 3.20: Ionic conductivities of SBVI (blue dots) and TFEMA (yellow triangles) ionogels as a function of elastic modulus. A 9.5-10 to 1 molar ratio of monomer to crosslinking PETA-4 was used. The SBVI ionogels contained 80 mol.% ionic liquid. TFEMA data courtesy of Anthony D'Angelo.[7]

Zwitterions have been thought to impart good electrochemical properties by dissociating ions due to their high polarity.[8, 10, 14] To date, however, the ion-zwitterion interactions have not been characterised beyond this analysis. In order to better understand the mechanism by which zwitterions act as ion-dissociating agents, the charge-dipole interaction may be investigated using the expression for angle-averaged free energy.[19]

$$w(r) \approx -\frac{Q^2\mu^2}{6\left(4\pi\varepsilon_0\varepsilon\right)^2 k_B T r^4} \qquad (3.3)$$

Equation (3.3) shows an approximation for the angled-averaged interaction between an ion and a molecule with a dipole moment. In the above equation, w(r) is the free energy as a function of the distance between the two molecules, r. Q is the magnitude of the charge on the ions, and μ is the dipole moment of the interacting molecule. ε_0 and ε are the permittivity of free space, and the dielectric constant of the medium surrounding the ion, respectively. The Boltzmann constant, k_B, temperature, T, and distance between the charge and the dipole moment, r, also factor into this equation. This expression for the free energy of the charge-dipole interaction is relevant only when Equation (3.4) is satisfied. [19]

$$r > \sqrt{\frac{Q\mu}{4\pi\varepsilon_0\varepsilon k_B T}} \qquad (3.4)$$

Considering the two main polymeric constituents here, the dipole moment for TFEMA is approximately 2.35 D[20], while the dipole moment for

sulfobetaine is recorded as being 27.5 D.[21] The disparity between these two values is a factor of ten, which, consulting Equation (3.3), amounts to a 100 fold difference in free interaction energy.

3.5.1.2 Zwitterion-Containing Ionogel Precursor Solutions

In order to assess the influence of the polymer scaffold on the mobility of the ions within the zwitterion-containing ionogels, ionogel precursor solutions were measured using AC impedance for the zwitterion-containing ionogels comprised of 20 mol.% non-conducting materials. Precursor solutions were injected into symmetric ITO devices, according to procedures outlined in section 2.2.3, and were immediately tested in a nitrogen-containing glove box.

Figure 3.21 compares precursor and gel total series resistances for zwitterion-containing ionogels. Total series resistance values were obtained by averaging the plateaued high-frequency resistance data. Recalling Equation (2.6), ionic conductivity is inversely proportional to the precursor or gel resistance. Therefore, lower resistances yield higher conductivities. Looking at the following figure, it can be seen that precursor total series resistances are approximately 20 Ω lower than their respective gel resistances, indicating that precursor solutions are more conductive than the polymerised gels.

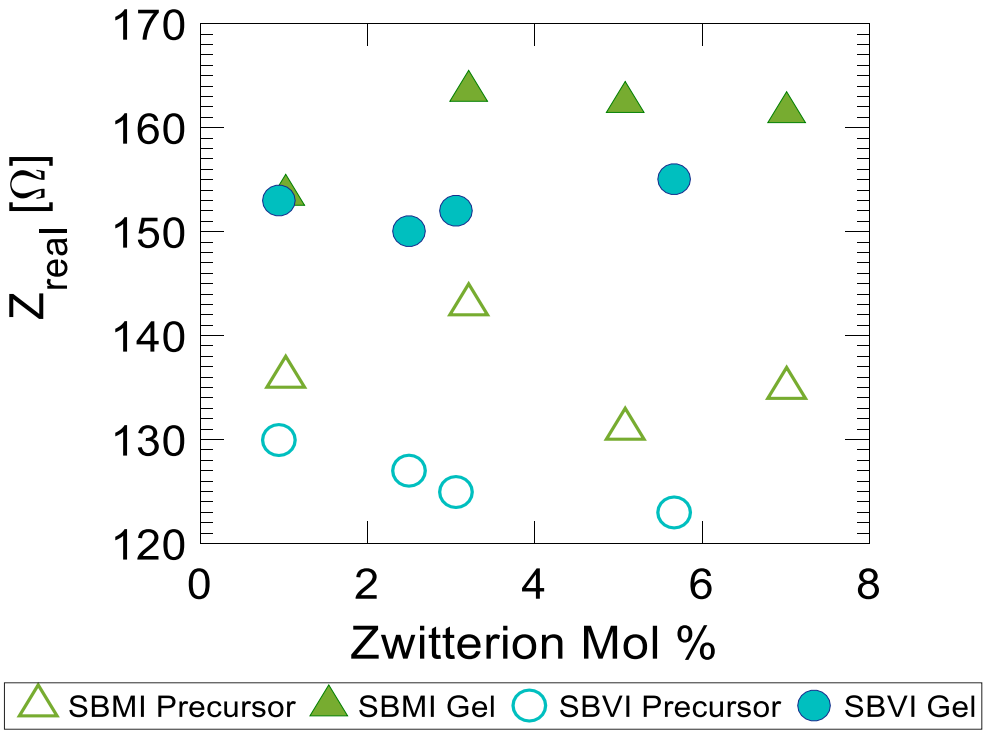

Figure 3.21: Total series resistances of SBVI and SBMI gels relative to their respective precursor solutions. Resistances were obtained by impedance measurements.

The influence of the polymer can be elucidated further by looking at **Figure 3.22**. SBVI ionogel precursor solutions were found to be the most conductive. Moreover, SBVI precursor conductivities were shown to increase with increasing zwitterion content. Higher zwitterion contents led to large conductivity values that were as high or, in some cases, slightly higher relative to the neat ionic liquid conductivity value.

Moreover, precursor conductivities were found to be higher for all the zwitterion-containing ionogel precursor solutions tested. This suggests that zwitterions are inducing more free ions in the solutions, and without the polymer scaffold to contain the ionic liquid, ion mobility is not hindered. While SBMI precursor solutions exhibited conductivities that were larger

than SBMI and SBVI ionogel conductivities, they were still lower than the SBVI precursor conductivities recorded for the same zwitterion loading, and the neat ionic liquid. One possible explanation for this observation is the added potential for steric hindrance afforded by the vinyl group on the SBVI zwitterion. This may prevent zwitterion packing, thus reducing the prevalence of cluster formations in the SBVI precursor solutions. This would, in turn, allow for more zwitterion-ionic liquid interactions which would increase the fraction of ions dissociated, leading to higher conductivities. Following this argument, the SBMI would aggregate more readily due to the smaller methyl group which would decrease the frequency of zwitterion-ionic liquid interactions.

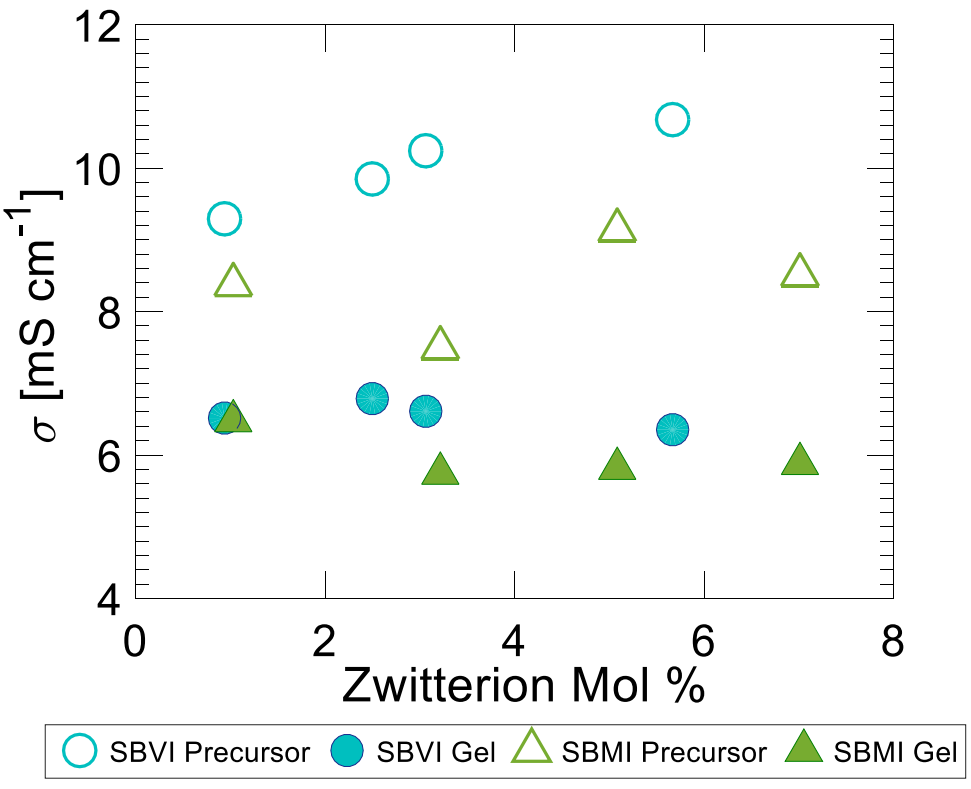

Figure 3.22: Ionic conductivities of SBVI and SBMI ionogels and their respective precursor solutions

3.5.1.3 How Ionic Liquid Loading Affects Ionic Conductivities of Zwitterion-Containing Ionogels

Subsequent to characterising zwitterion-containing ionogels comprised of 20 mol.% of non-conductive materials, the effect of changing the volume fraction of the ionic liquid within the zwitterion-containing ionogels was explored. The strategy of varying volume fraction was chosen as a given volume of ionic liquid contains a constant concentration of ions across samples. It should be noted that volume fraction of ionic liquid was estimated using the densities of the monomers and additives in the precursor solutions. The densities of the synthesised zwitterions were estimated based on visual observations of zwitterion buoyancy in ionic liquid and monomers, as well as the densities of the other monomers in the samples. The densities of zwitterion-containing ionogel materials used for calculating the volume fraction of each component are recorded in **Table 3.3**

Table 3.3: Densities of zwitterion-containing ionogel materials for calculating volume fractions.

Material	Density ($g\ cm^{-3}$)
SBVI/SBMI	1.25
TFEMA	1.18
PETA-4	1.19
EMI TFSI	1.52

To formulate zwitterion-containing ionogels with varying amounts of ionic liquid, a fixed ratio of zwitterion to TFEMA was used and the total

amount of polymer or additive necessary to change the volume fraction of ionic liquid was adjusted accordingly. A ratio of 13:82 percent of zwitterion to TFEMA on a molar basis was used because this ratio yielded stable gels when the ionic liquid volume fraction was varied. At 80 mol.% ionic liquid, this gel corresponded with a total zwitterion content of 3 mol.%. Importantly, at an 80 mol.% ionic liquid loading, the volume fraction of ionic liquid was 0.87 for this copolymer system.

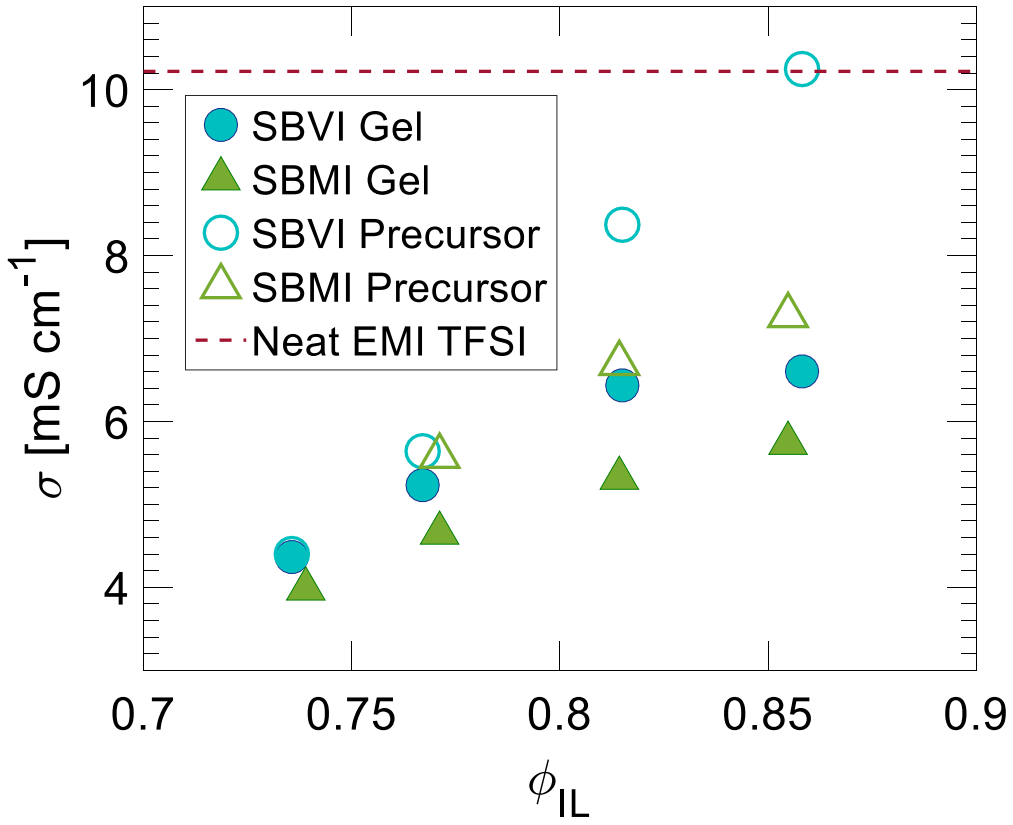

Figure 3.23: Ionic conductivity of SBVI and SBMI ionogels and their respective precursor solutions as a function of volume fraction of ionic liquid.

The above figure indicates that for the SBVI and SBMI ionogels, decreasing the volume fraction of ionic liquid in the ionogels leads to reduced conductivities. Despite this, even at high mass fractions of polymer,

moderate ionic conductivities may be obtained. So, if desired, the mechanical stability of the gels could be further improved by increasing the polymer content while maintaining conductivities relatively close to that of the neat IL. The trend observed in **Figure 3.23** is expected as increasing the polymer loading would encumber ion movement within the gel. Additionally, a smaller volume fraction of IL would result in a lower concentration of ions, so there would not be as many conductive charge carriers present per volume of ionogel. The increase in zwitterion content as the total additive amount is increased could lead to an increase in free ions present. It is conceivable, however, that beyond a certain zwitterion loading, the electrochemical properties of the zwitterion-containing ionogels would have a diminishing return. That is to say, once all the ions in the ionic liquid are dissociated, any further zwitterionic additions would act as obstacles for the ions and would hinder ion movement. Currently, the fraction of free ions is unquantifiable, so it is unclear whether the zwitterionic loading in the formulated gels is adequate to ensure complete ion dissociation.

Ionic conductivities of zwitterion-containing ionogel precursor solutions were measured for both the SBVI and SBMI ionogels. The data show higher conductivity values relative to their respective gels which are indicative of unencumbered ion mobility. At the highest IL volume fraction, the SBVI precursor solution conductivity is as high as the neat ionic liquid. This implies an increased fraction of dissociated ions contained within the

sample as the ionogel samples contain fewer charge carriers relative to the neat liquid.

3.5.2 Activation Energy of Ionic Conductivity

The activation energy of ionic conductivity is correlated with the energy barrier that must be overcome to elicit ion movement in an electric field. High activation energies are often associated with lower conductivity electrolytes, while the opposite is true for low activation energy values. In order to determine the activation energy of a zwitterion-containing ionogel, ionic conductivity measurements were taken at various temperatures and were plotted according to the Arrhenius relationship in Equation (3.5).

$$\ln(\sigma) = \ln(\sigma_0) - \frac{E_A}{RT} \quad (3.5)$$

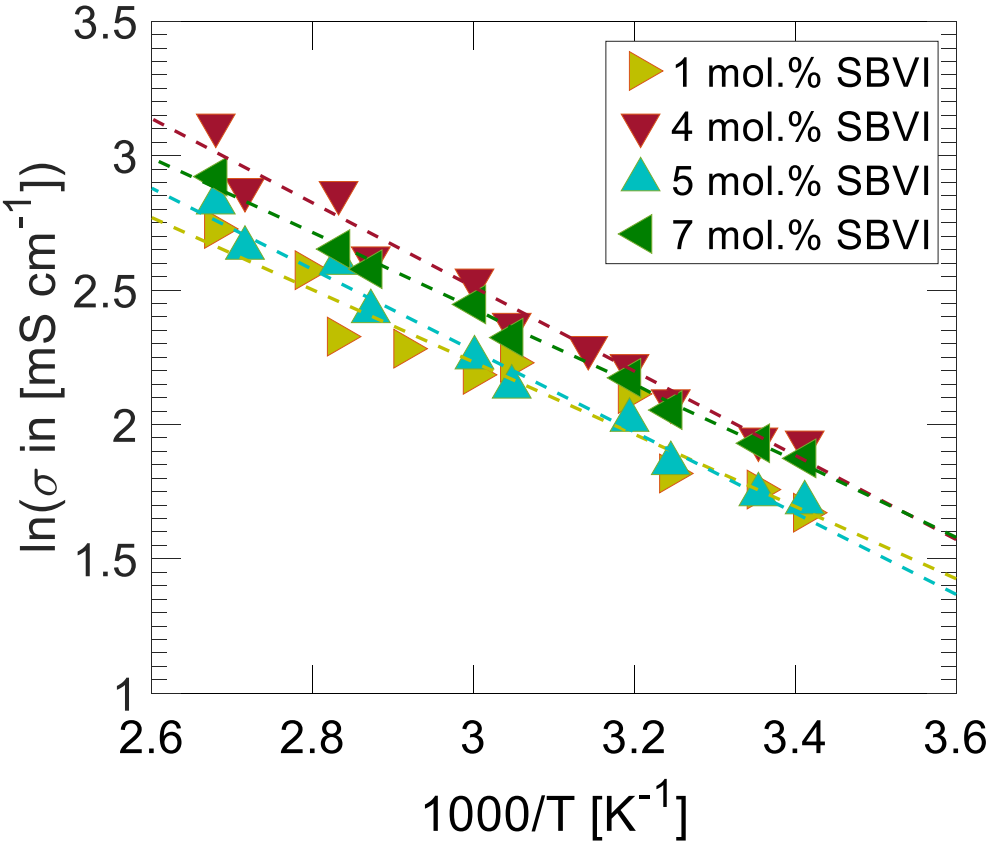

Figure 3.24: Representative Arrhenius plot of select SBVI ionogels. Conductivities used were in mS cm^{-1}.

The Arrhenius plot in **Figure 3.24** depicts several zwitterion-containing ionogels consisting of 20 mol.% polymer at different concentrations of SBVI. Looking at the plot, the data appear to be linear, justifying the use of the Arrhenius model to calculate activation energy. The coefficient of determination, R^2 values for the Arrhenius data ranged from 0.972 to 0.993. The ionic conductivity data were obtained by decreasing the temperature from $100^{o}C$ to room temperature in increments of $20^{o}C$ and then increasing the temperature to find data points in between.

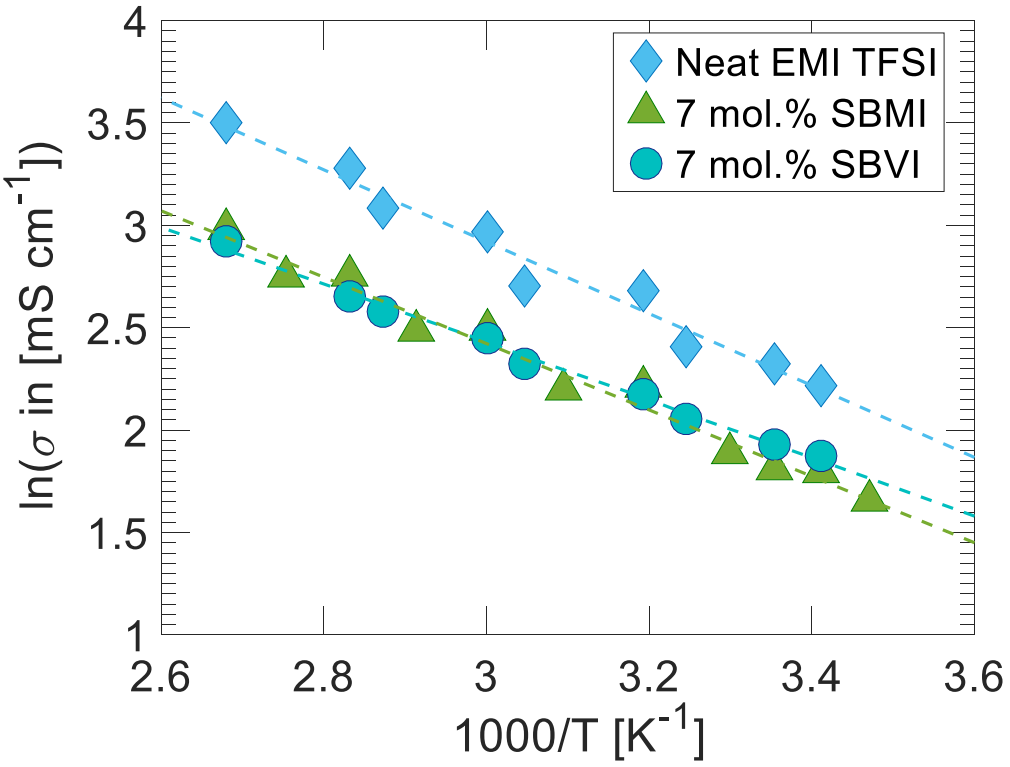

Figure 3.25: Arrhenius plot comparing SBVI and SBMI ionogels to neat EMI TFSI. Conductivities used were in mS cm^{-1}

The slope for the representative compositions appears to be constant, suggesting that the activation energy of the SBVI ionogels does not change with ionogel composition. Comparing these data with those shown in **Figure 3.25**, the SBMI ionogel and the neat EMI TFSI also follow a linear relationship between the natural logarithm of conductivity and scaled absolute temperature. Thus, the Arrhenius model may be used as a tool to compare all the zwitterion-containing ionogels formulated to neat ionic liquid. For ease of assessment, the calculated activation energies for SBVI and SBMI ionogels, as well as neat ionic liquid and a 20 mol.% TFEMA ionogel are shown in **Table 3.4**.

Table 3.4 Calculated activation energies of ionic conductivity for neat EMI TFSI, a 20 mol.% TFEMA ionogel, 20 mol.% polymer SBVI-containing ionogels with varying concentrations of SBVI zwitterion, and SBMI ionogels with 80 mol.% ionic liquid.

	Mol zwitterion (%)	E_A (kJ/mol)
Neat EMI TFSI	0	14.6
20 mol.% TFEMA	0	15.5
20 mol.% copolymer SBVI Ionogels	0.89	11.2
	4.22	12.8
	4.93	12.6
	6.85	11.7
SBMI Ionogels	2.53	12.7
	7.01	13.5

The SBVI ionogels are shown to have activation energies lower than that of neat EMI TFSI. Although this is consistent with high-conductivity gels, the conductivity data do not reflect this. Similarly, the SBMI gels display activation energies that are lower than the neat ionic liquid. The standard deviation between SBVI activation energies was found to be 0.65 kJ/mol, so the activation energies of the SBVI-containing ionogels can be said to be independent of the concentration of zwitterion within the gel. This finding is also consistent with the diffusion coefficient data reported, as well as the ionic conductivity data pertaining to the 20 mol.% polymer ionogels. Analogously, similar conclusions may be drawn for elastic modulus: the increase in elastic modulus, which was assumed to hinder ion movement such that ionic conductivity and ion mobility did not increase with increasing zwitterionic content, could be the cause for the observed constant activation energies. Considering that ionic conductivity remained unchanged due to the increased dipole-dipole interactions within the zwitterion-containing

ionogels, it is imaginable that the activation energies associated with these zwitterion-containing ionogels would also remain constant.

The SBMI-containing ionogel activation energies are also shown to be lower than that recorded for neat EMI TFSI. For the SBMI-containing ionogels consisting of 20 mol.% of non-conducting materials, the ionic conductivities were found to be higher than those recorded for neat ionic liquid, but lower than the ionic conductivities measured for SBVI ionogels. The calculated activation energies for SBMI ionogels are consistent with these data.

Since the activation energies of the zwitterion-containing ionogels were found to be lower than the activation energy recorded for neat EMI TFSI, it may be inferred that the zwitterions decrease the energy barrier associated with ionic motion within the ionogels. The combination of encumbered ion movement and fewer charge carriers, however, results in conductivities lower than the neat IL.

3.5.3 Cyclic Voltammetry

Cyclic voltammetry (CV) tests were done in order to determine the effect of the zwitterionic copolymer on the electrochemical window of the composite zwitterion-containing ionogel material. The electrochemical window of EMI TFSI is understood to be slightly larger than 4 V.[22] Additives such as water which may be contained in the zwitterions, however, have the

potential to reduce the electrochemical window.[23, 24] This is undesirable as the wide voltage window associated with ionic liquids is important to ensure a high energy density when producing electrochemical energy storage devices.

CV testing was done on the symmetric ITO-zwitterion-containing ionogel devices used for ionic conductivity testing. The spacers used were 1.57 mm thick and had an inner diameter of 6.35 mm. The cross-sectional area of the zwitterion-containing ionogels was $3.17\times10^{-5}m^2$.

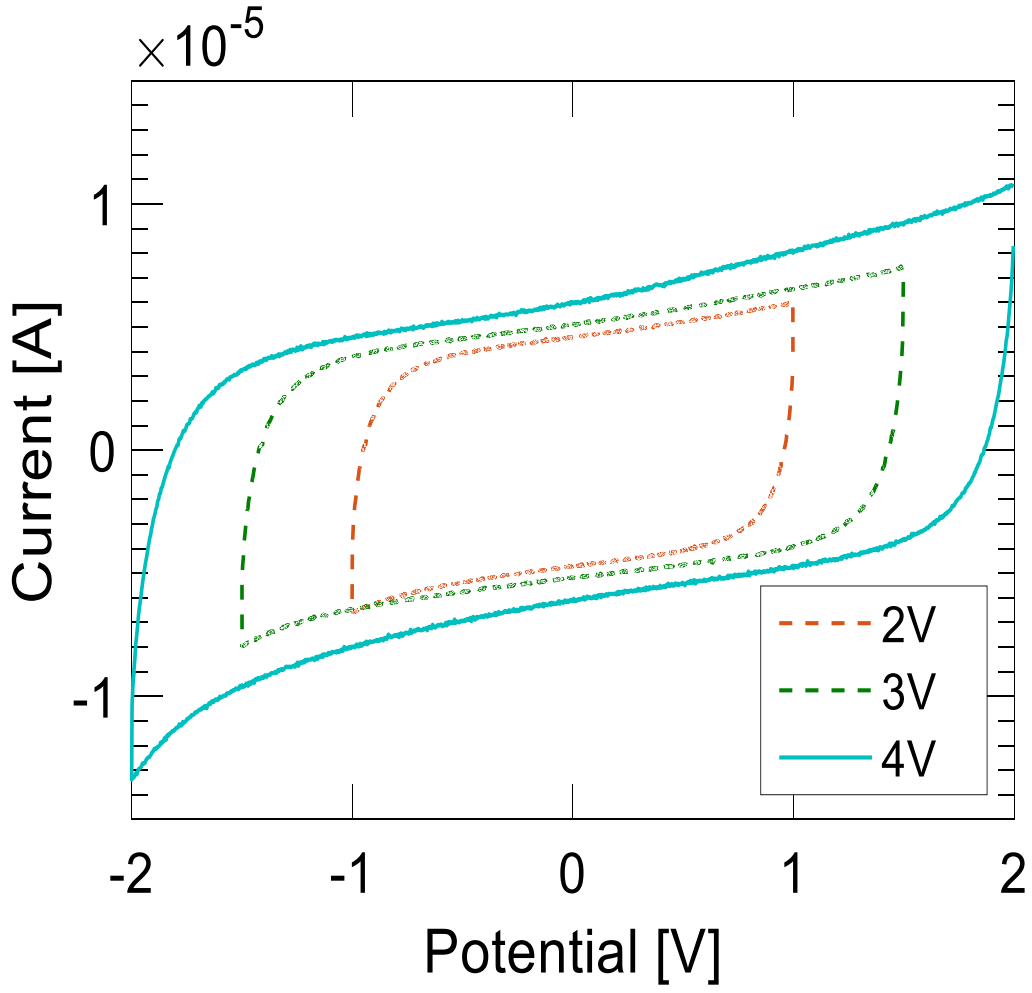

Figure 3.26: Cyclic Voltammogram of a 1 mol.% SBVI ionogel at various voltages. A scan rate of 1 V/s was used

To begin, a low zwitterion-loading ionogel was tested with a scan rate of 1 V/s. The 1 mol.% SBVI zwitterion-containing ionogel shown in **Figure 3.26** was tested at different voltage windows to determine whether or not reduction/oxidation (redox) reactions occur. As can be seen from the plot above, the zwitterion-containing ionogels were stable up to 4 V, suggesting that the presence of the zwitterionic copolymer does not significantly affect the electrochemical stability.

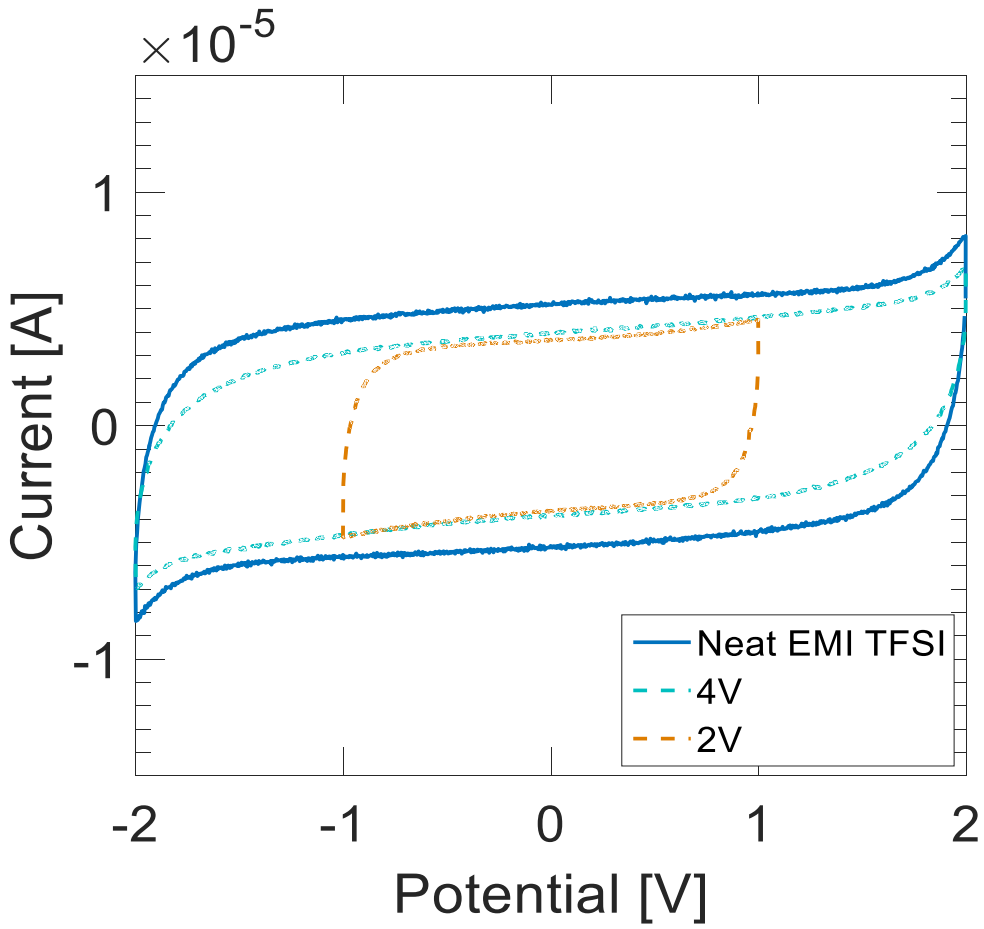

Figure 3.27: Cyclic Voltammogram for neat EMI TFSI (blue solid), a 7 mol.% SBVI ionogel and 2 V (orange dashes) and 4 V (green dots). A scan rate of 1 V/s was used.

In order to ensure that this was the case, a high zwitterion-content ionogel was tested at the same scan rate. **Figure 3.27** shows the results of that test where the electrochemical stability of a 7 mol.% SBVI-containing

ionogel was measured. The saw-tooth effect observed here is common to most ionogel systems due to the inherent gel resistance. Despite this effect, even at high zwitterion concentrations, the SBVI zwitterion-containing ionogels appear to be electrochemically stable up to 4 V for the high zwitterion loading. For comparison, a neat EMI TFSI cyclic voltammogram is shown for a 4 V window. Hence, the incorporation of zwitterions does not significantly reduce the electrochemical stability of the ionogel system.

Considering the similarities in structure between SBMI and SBVI, SBMI is not expected to have a significant impact on the voltage window of the ionogels. This is evidenced by **Figure 3.28** where a 1 mol.% and a 7 mol.% SBMI-containing ionogel was tested at a window of 4 V at a scan rate of 1 V/s. The cyclic voltammogram appears to be stable with no large saw-tooth or aberrations visible.

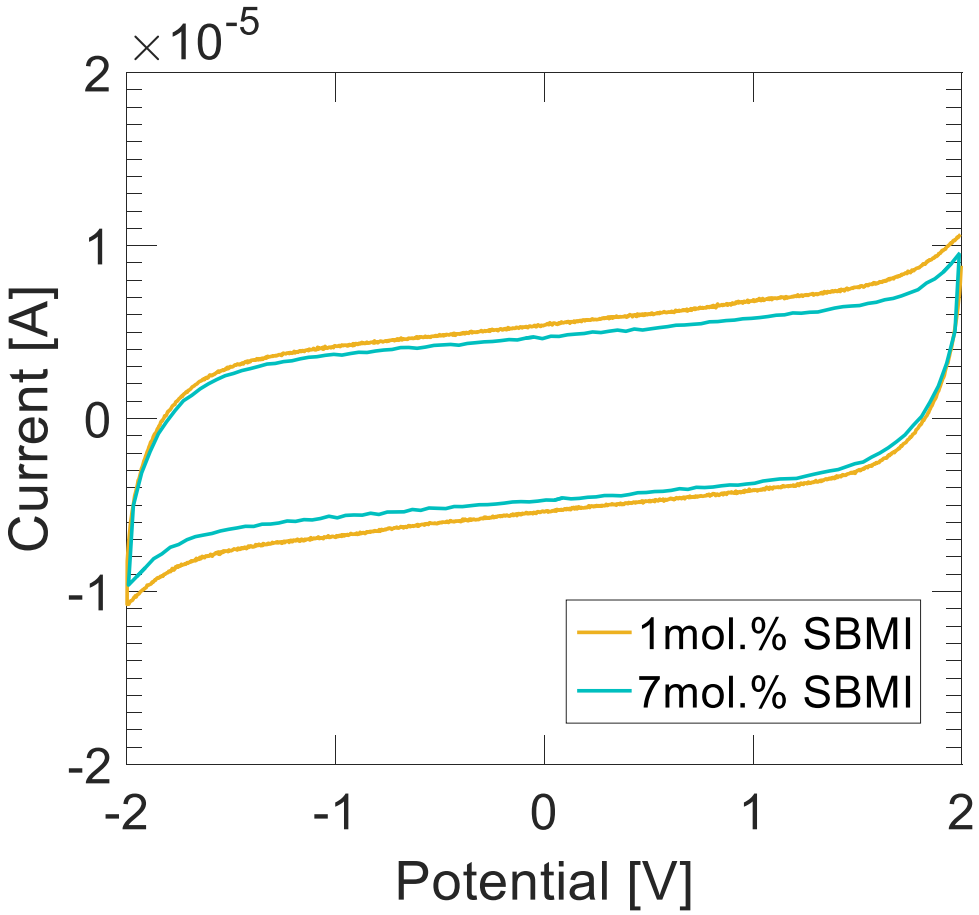

Figure 3.28: Cyclic voltammogram showing 1 mol.% (outer curve) and 7 mol.% (inner curve) SBMI-containing ionogels at a 4 V window. The scan rate used was 1 V/s.

Thus it may be concluded that zwitterion-containing ionogels have a large electrochemical stability and that the presence of the zwitterionic copolymer does not affect the voltage window within which zwitterion-containing ionogel electrolytes may be operated safely.

3.6 References

1 Shao, Q., He, Y. & Jiang, S. Molecular dynamics simulation study of ion interactions with zwitterions. *Journal of Physical Chemistry B* **115**, 8358-8363, doi:10.1021/jp204046f (2011).

2 McEwen, A. B., Ngo, H. L., LeCompte, K. & Goldman, J. L. Electrochemical Properties of Imidazolium Salt Electrolytes for Electrochemical Capacitor Applications. *Journal of The Electrochemical Society* **146**, 1687-1695, doi:10.1149/1.1391827 (1999).

3 Garcia, B., Lavallée, S., Perron, G., Michot, C. & Armand, M. Room temperature molten salts as lithium battery electrolyte. *Electrochimica Acta* **49**, 4583-4588, doi:10.1016/j.electacta.2004.04.041 (2004).

4 Xuan, F. & Liu, J. Preparation, characterization and application of zwitterionic polymers and membranes: current developments and perspective. *Polymer International* **58**, 1350-1361, doi:10.1002/pi.2679 (2009).

5 Scientific Polymer Products, I. *2,2,2-Trifluoroethyl methacrylate*, Safety Data Sheet, Catalogue No. M-284. (www.scipoly.com, 2015).

6 Noda, A., Hayamizu, K. & Watanabe, M. Pulsed-Gradient Spin−Echo 1H and 19F NMR Ionic Diffusion Coefficient, Viscosity, and Ionic Conductivity of Non-Chloroaluminate Room-Temperature Ionic Liquids. *The Journal of Physical Chemistry B* **105**, 4603-4610, doi:10.1021/jp004132q (2001).

7 D'Angelo, A. J., Grimes, J. J. & Panzer, M. J. Deciphering Physical versus Chemical Contributions to the Ionic Conductivity of Functionalized Poly(methacrylate)-Based Ionogel Electrolytes. *J Phys Chem B* **119**, 14959-14969, doi:10.1021/acs.jpcb.5b08250 (2015).

8 Byrne, N., MacFarlane, D. R. & Forsyth, M. Composition effects on ion transport in a polyelectrolyte gel with the addition of ion dissociators. *Electrochimica Acta* **50**, 3917-3921, doi:10.1016/j.electacta.2005.02.068 (2005).

9 Byrne, N. *et al.* Effect of zwitterion on the lithium solid electrolyte interphase in ionic liquid electrolytes. *Journal of Power Sources* **184**, 288-296, doi:10.1016/j.jpowsour.2008.04.094 (2008).

10 Tiyapiboonchaiya, C. *et al.* The zwitterion effect in high-conductivity polyelectrolyte materials. *Nat Mater* **3**, 29-32, doi:10.1038/nmat1044 (2004).

11 Byrne, N., Howlett, P. C., MacFarlane, D. R. & Forsyth, M. The Zwitterion Effect in Ionic Liquids: Towards Practical Rechargeable

Lithium-Metal Batteries. *Advanced Materials* **17**, 2497-2501, doi:10.1002/adma.200500595 (2005).

12 Taguchi, S., Matsumoto, T., Ichikawa, T., Kato, T. & Ohno, H. Gelation of an amino acid ionic liquid by the addition of a phosphonium-type zwitterion. *Chem Commun (Camb)* **47**, 11342-11344, doi:10.1039/c1cc14455c (2011).

13 Marwanta, E., Mizumo, T. & Ohno, H. Improved ionic conductivity of nitrile rubber/Li(CF3SO2)2N composites by adding imidazolium-type zwitterion. *Solid State Ionics* **178**, 227-232, doi:http://dx.doi.org/10.1016/j.ssi.2006.12.022 (2007).

14 Soberats, B., Yoshio, M., Ichikawa, T., Ohno, H. & Kato, T. Zwitterionic liquid crystals as 1D and 3D lithium ion transport media. *J. Mater. Chem. A* **3**, 11232-11238, doi:10.1039/c5ta00814j (2015).

15 Zhang, Y. & Maginn, E. J. Direct Correlation between Ionic Liquid Transport Properties and Ion Pair Lifetimes: A Molecular Dynamics Study. *The Journal of Physical Chemistry Letters* **6**, 700-705, doi:10.1021/acs.jpclett.5b00003 (2015).

16 Liu, H. & Maginn, E. Effect of ion structure on conductivity in lithium-doped ionic liquid electrolytes: a molecular dynamics study. *J Chem Phys* **139**, 114508, doi:10.1063/1.4821155 (2013).

17 Bengani, P., Kou, Y. & Asatekin, A. Zwitterionic copolymer self-assembly for fouling resistant, high flux membranes with size-based small molecule selectivity. *Journal of Membrane Science* **493**, 755-765, doi:http://dx.doi.org/10.1016/j.memsci.2015.07.025 (2015).

18 Peng, X. *et al.* A zwitterionic gel electrolyte for efficient solid-state supercapacitors. *Nat Commun* **7**, 11782, doi:10.1038/ncomms11782 (2016).

19 Israelachvili, J. N. *Intermolecular and surface forces*. Vol. 3rd (Academic Press, 2011).

20 Haynes, W. M. *CRC Handbook of Chemistry and Physics: A Ready-Reference Book of Chemical and Physical Data, 96th Edition (Internet Version 2016)*. (CRC Press/Taylor and Francis, 2015).

21 Galin, M., Chapoton, A. & Galin, J.-C. Dielectric increments, intercharge distances and conformation of quaternary ammonioalkylsulfonates and alkoxydicyanoethenolates in aqueous and tirfluoroethanol solutions. *Journal of the Chemical Society, Perkin Transactions 2*, 545-553, doi:10.1039/P29930000545 (1993).

22 Bonhôte, P., Dias, A.-P., Papageorgiou, N., Kalyanasundaram, K. & Grätzel, M. Hydrophobic, Highly Conductive Ambient-Temperature Molten Salts. *Inorganic Chemistry* **35**, 1168-1178, doi:10.1021/ic951325x (1996).

23 Armand, M., Endres, F., MacFarlane, D. R., Ohno, H. & Scrosati, B. Ionic-liquid materials for the electrochemical challenges of the future. *Nat Mater* **8**, 621-629, doi:10.1038/nmat2448 (2009).

24 O'Mahony, A. M., Silvester, D. S., Aldous, L., Hardacre, C. & Compton, R. G. Effect of Water on the Electrochemical Window and Potential Limits of Room-Temperature Ionic Liquids. *Journal of Chemical & Engineering Data* **53**, 2884-2891, doi:10.1021/je800678e (2008).

Chapter 4: Conclusions and Future Works

4.1 Conclusions

Zwitterion-containing ionogels were successfully synthesised incorporating both polymerisable (SBVI) and non-polymerisable (SBMI) zwitterions. TGA data showed that the presence of free unbound water molecules in the zwitterion-containing ionogels was negligible and that these ionogels displayed high degradation temperatures, above $300^{o}C$.

For the zwitterion-containing ionogels with an 80 mol.% ionic liquid loading, the elastic modulus was shown to increase with increasing zwitterion content for both the SBVI and the SBMI ionogels. The increase in modulus was not as dramatic for the SBMI gels, relative to their SBVI counterparts. The increase in elastic modulus was attributed to the zwitterion's ability to self-assemble within the ionogel. The SBMI zwitterions were able to migrate and aggregate within the gel, acting as nanoparticle fillers, while the SBVI zwitterions that were confined to the polymer backbone created dipole-dipole cross-links and/or ordered domains due to zwitterionic self-assembly.

Relating these findings to the ionic conductivity and diffusivity data at fixed ionic liquid loading, it may be concluded that the zwitterions caused an increase in free ionic liquid ions present within the gel. This was achieved via charge-dipole interactions and the competitive association between the

charges in the ionic liquid and the zwitterionic moieties. The moderate values of ionic conductivity that were approximately constant with increasing zwitterion content could be attributed to the increase in elastic modulus; the self-assembled domains hindered ion movement within the gel. This led to an effective cancellation of the benefits associated with increased presence of free ions due to their reduced mobility.

The ionic conductivities of the SBMI-containing ionogels were consistently lower than those for the SBVI ionogels. The explanation provided pertained to the clustering effect seen in the SBMI ionogels. SBMI zwitterions, being able to move within the gel, were able to aggregate and effectively reduce the number of charge-dipole interactions which would have reduced the fraction of ions dissociated.

The apparent diffusivities for SBVI and SBMI ionogels followed the same trend as the ionic conductivity data. Once again these results were ascribed to the increase in elastic modulus, causing a reduction in ion mobility, despite an increased presence of faster free ions, relative to the paired and clustered entities.

Zwitterion-containing ionogel precursor solutions were also examined. The increase in ion dissociation, combined with the lack of polymer network resulted in improved ion mobility which manifested as an even greater increase in measured diffusivity and conductivity values that were comparable to the neat ionic liquid.

Cyclic voltammetry results showed that the electrochemical stability remained unchanged from that of the neat ionic liquid. Thus, zwitterion-containing ionogels synthesised with both types of zwitterion showed moderate conductivity values, good mechanical properties, as well as high thermal and electrochemical stability.

4.2 Future Directions

The results presented in this thesis offer an exciting platform to leap from when conducting future studies involving zwitterion-containing ionogels. Firstly, the copolymer morphology must be characterised more fully as, from the elastic modulus data, the polymer architecture appears to have a great impact on the mobility of the ions within the gel. To achieve this, X-ray scattering or electron cryomicroscopy may be employed. In this way, the copolymer that is synthesised in the ionic liquid may be examined and the specific morphology may shed further light on the nature of the zwitterion-ionic liquid interactions.

In the work presented, the SBVI zwitterions used were tethered at the cationic imidazolium portion of the molecule, a potential source of steric hindrance for TFSI-zwitterionic imidazolium interactions. Hence, another potential route for exploration involves tethering the zwitterion to the polymeric backbone at the anionic end of the monomer. With this change, different results may be obtained for the ion diffusivities, as well as the electrochemical properties. Additionally, the alkyl chain length between the

charges on the zwitterion may be varied in order to potentially allow both ionic liquid ions to interact with the zwitterionic portions of the copolymer. Longer carbon spacers may lead to increased zwitterion-ionic liquid interactions which could result in the presence of even more dissociated ionic liquid ions.

Along this vein, the synthesis and implementation of a hydrophobic zwitterion would be of significant interest as its behaviour in the hydrophobic ionogel system may be quite different from the hydrophilic zwitterion used in this study. In this way, solubility limitations arising from the hydrophilicity of zwitterions may be avoided. Furthermore, increased ion-dipole interactions with a hydrophobic zwitterion have the potential to further increase the fraction of dissociated ions within the zwitterion-containing ionogels, leading to a potential increase in ionic conductivity. A hydrophobic zwitterion may exist in the form of a long alkyl chain separating the two charges on the zwitterionic molecule. An extension of this may be to include hydrophobic functional groups on the alkyl separator or as side chains on the molecule, which would deter water molecules from solvating the zwitterions.

A longer alkyl spacer chain populated with hydrophobic functional groups, such as fluorine, would also cause an increase in the molecular dipole moment. This may, in turn, affect the free energy of interaction between the

ions in the ionic liquid and the zwitterionic moieties. Increase charge-dipole interactions may lead to a further increase in ionic conductivities.

Finally, these findings must be validated across different zwitterion-ionic liquid systems in order for their applicability to be extended over a wide range of fields. With this, the implementation of zwitterion-containing ionogels may be advanced into the field of lithium ion and metal batteries, as well as proton exchange membranes for fuel cell applications.

Appendix A: Experimental Data

A.1 Elastic Modulus Data

Table A.1: Elastic moduli of a 20 mol.% TFEMA ionogel, and zwitterion-containing ionogels with 80 mol.% ionic liquid loading.

	Total Moles Zwitterion (mol.%)	E (kPa)
20mol.% TFEMA	0.00	4.41
SBVI Ionogels 80 mol.% IL	1.08	4.13
	6.96	820.20
	2.50	16.24
	4.07	195.60
	5.05	476.30
SBMI Ionogels 80 mol.% IL	2.53	10.00
	7.01	20.33
	4.01	15.80

A.2 Apparent Diffusivity Data

Table A.2: Apparent PGSE NMR diffusivity values for the EMI cation and the TFSI anion in neat ionic liquid, and in zwitterion-containing ionogels with 80 mol.% IL.

	Total Moles Zwitterion (mol.%)	D_+^{NMR} $x10^{11}$ m^2/s	D_-^{NMR} $x10^{11}$ m^2/s
Neat EMI TFSI	0	4.22	2.50
SBVI Ionogels 80 mol.% IL	3.86	2.85	1.69
	7.40	2.75	1.78
	4.93	3.37	1.97
	0.94	3.51	1.85
	2.50	2.95	1.72
SBMI Ionogels 80 mol.% IL	5.08	2.80	1.60
	3.21	2.53	1.39
	2.53	2.58	1.47
	7.01	2.91	1.76

Table A.3: Apparent PGSE NMR diffusivity values for SBVI-containing ionogel precursor solutions with 80 mol.% ionic liquid loading.

SBVI-Containing Ionogel Precursor Solution		
Total Moles SBVI (mol.%)	D_+^{NMR} $x10^{11}$ m^2/s	D_-^{NMR} $x10^{11}$ m^2/s
6.85	5.01	3.29
1.03	5.50	3.42

A.3 Ionic Conductivity Data

Table A.4: Reproduced ionic conductivities and standard deviations of neat EMI TFSI and 20 mol.% polymer TFEMA ionogels.

	Conductivity (mS cm^{-1})	Standard Deviation (mS cm^{-1})
Neat EMI TFSI	10.22 10.45 10.68	0.19
20 mol.% TFEMA ionogel	5.80 5.27	--

Table A.5: Reproduced ionic conductivities and standard deviations of SBVI-containing ionogels with 80 mol.% ionic liquid loading.

Total Moles SBVI (mol.%)	Conductivity (mS cm^{-1})	Standard Deviation (mS cm^{-1})
0.88	5.84	0.54
0.94	5.86	
1.08	7.28	
2.50	7.84	
2.76	6.34	
3.06	7.33	
3.86	5.81	0.28
4.22	7.02	
4.29	5.70	
4.93	6.32	
4.93	5.67	
5.05	6.48	
5.66	6.61	
6.87	6.92	--
6.96	6.74	
7.40	6.47	
7.72	6.39	

Table A.6: Reproduced ionic conductivities and standard deviations of SBMI-containing ionogels with 80 mol.% IL.

Total Moles SBMI (mol.%)	Conductivity (mS cm^{-1})	Standard Deviation (mS cm^{-1})
1.03	6.48	
2.53	5.74	
3.21	5.74	
4.01	6.61	
5.08	5.80	
6.91	5.07	0.45
7.01	5.87	
7.01	6.16	

Table A.7: Total impedance resistances and ionic conductivity values for zwitterion-containing ionogels with 80 mol.% IL and their precursor solutions.

	Total Moles Zwitterion (mol.%)	Precursor Resistance (Ω)	Precursor Conductivity (mS cm^{-1})	Gel Resistance (Ω)	Gel Conductivity (mS cm^{-1})
SBVI Ionogels with 80 mol.% IL	0.94	130	9.30	153	6.52
	2.50	127	9.84	150	6.78
	3.06	125	10.25	152	6.61
	5.66	123	10.68	155	6.36
SBMI Ionogels with 80 mol.% IL	1.03	136	8.37	154	6.48
	3.21	143	7.49	164	5.74
	5.08	131	9.13	163	5.80
	7.01	135	8.51	162	5.87

Table A.8: Ionic conductivities of zwitterion-containing ionogels with varying ionic liquid volume fractions.

	Volume Fraction EMI TFSI $\phi_{EMI\ TFSI}$	Conductivity (mS cm^{-1})
SBVI Ionogels	0.86	6.61
	0.81	6.44
	0.77	5.23
	0.74	4.37
SBMI Ionogels	0.85	5.74
	0.81	5.31
	0.77	4.65
	0.74	3.98

Appendix B: Arrhenius Data

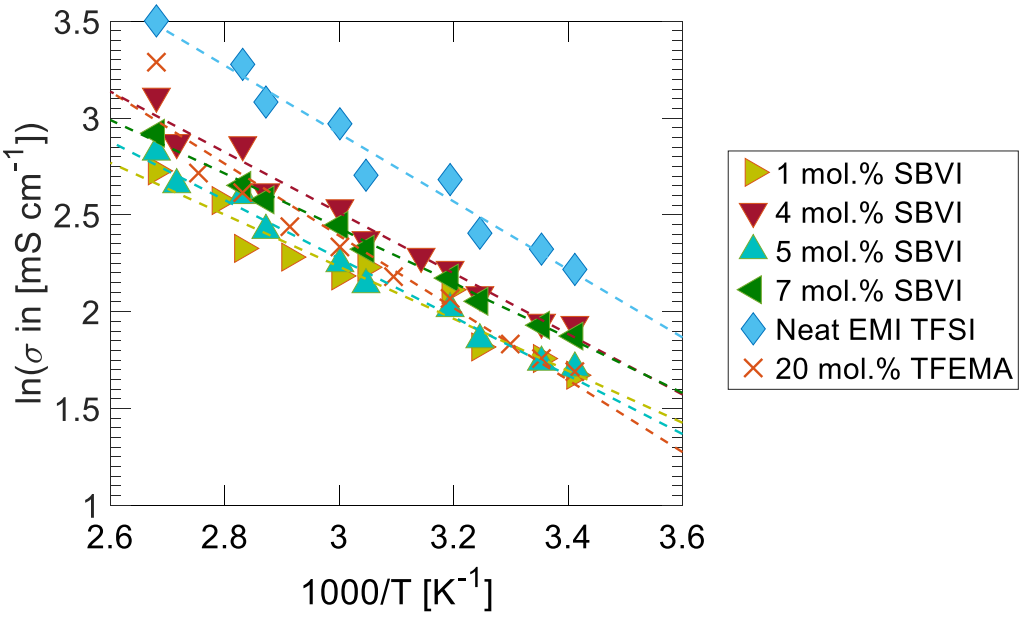

Figure B.1: Arrhenius plot of neat EMI TFSI, a 20 mol.% TFEMA ionogel, and SBVI-containing ionogels with 80 mol.% IL.

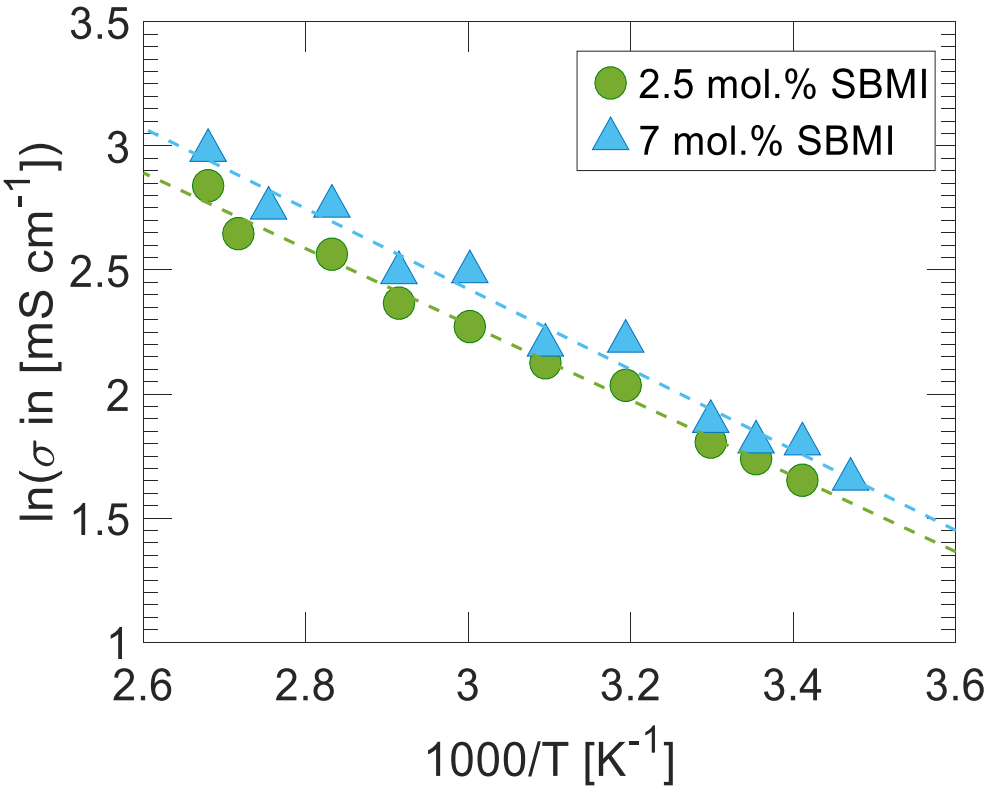

Figure B.2: Arrhenius plot of SBMI ionogels with 80 mol.% IL.